12-2010

Pin-Wise Loading Optimization and Lattice–to-Core Coupling for Isotopic Management in Light Water Reactors

Hermilo Hernandez Noyola
University of Tennessee - Knoxville, hhernand@utk.edu

To the Graduate Council:

I am submitting herewith a dissertation written by Hermilo Hernandez Noyola entitled "Pin-Wise Loading Optimization and Lattice–to-Core Coupling for Isotopic Management in Light Water Reactors." I have examined the final electronic copy of this dissertation for form and content and recommend that it be accepted in partial fulfillment of the requirements for the degree of Doctor of Philosophy, with a major in Nuclear Engineering.

G. Ivan Maldonado, Major Professor

We have read this dissertation and recommend its acceptance:

Kevin T. Clarno, Thomas Papenbrock, Lawrence H. Heilbronn

Accepted for the Council:

Carolyn R. Hodges

Vice Provost and Dean of the Graduate School

(Original signatures are on file with official student records.)

To the Graduate Council:

I am submitting herewith a thesis written by Hermilo Hernandez Noyola entitled "Pin-Wise Loading Optimization and Lattice to Core Coupling for Isotopic Management in Light Water Reactors." I have examined the final electronic copy of this thesis for form and content and recommend that it be accepted in partial fulfillment of the requirements for the degree of Doctor of Philosophy, with a major in Nuclear Engineering.

G. Ivan Maldonado, Major Professor

We have read this thesis
and recommend its acceptance:

Kevin T. Clarno

Thomas Papenbrock

Lawrence H. Heilbronn

Accepted for the Council:

Carolyn R. Hodges
Vice Provost and Dean of the Graduate School

(Original signatures are on file with official student records.)

PIN-WISE LOADING OPTIMIZATION AND LATTICE–TO-CORE COUPLING FOR ISOTOPIC MANAGEMENT IN LIGHT WATER REACTORS

A Thesis Presented for the
Doctor of Philosophy
Degree
The University of Tennessee, Knoxville

Hermilo Hernandez Noyola
December 2010

To my wife

Nayeli Benavides Castillo

my daughter

Daniela Hernandez

my mother

Faustina Noyola Aguilar

my father

Hermilo Hernandez Avila

and my siblings

Fernando, Luis, Carlos†, Veronica, Alba, Viatriz, Eva and Faustina.

Acknowledgements

I would like to express my sincere gratitude to my research advisor: Dr. G. Ivan Maldonado for his support and guidance during my graduate studies abroad. Perceptive observations to the work here presented came also from the members of my dissertation committee: Dr. Lawrence H. Heilbronn, Dr. Kevin T. Clarno, and Dr. Thomas Papenbrock.

I am grateful to the professors of the Nuclear Engineering Department at the University of Tennessee for their contribution to my formation. A special appreciation to the Nuclear Science and Technology Division group at Oak Ridge National Laboratory (ORNL) for their assistance in my research, particularly to Dr. Jess C. Gehin for becoming my mentor during my first summer internship at ORNL; important to mention are Dr. Mark De Hart, Dr. Matthew Jesse and Dr. Mark Williams for their support and advice with the SCALE package and the NESTLE code.

Thanks to my classmates for their team work: Jonathan Chavers, David Dixon, Jack Galloway, Shane Hart, Mark Massie and the rest of the excellent members of the Nuclear Reactor Physics group lead by Dr. Ivan Maldonado at the University of Tennessee, for their comradeship and technical feedback: James Banfield, David Chandler, Susan Hogle, Oscar Lastres and Brenden Mervin.

Let me express my gratitude to Dr. Juan Luis Francois Lacouture for being my former advisor at the National University Autonomous of Mexico (UNAM) and for encouraging me to have a higher education.

Thank you to my wife Nayeli Benavides for her valuable support and company, I appreciate the amity and advice with Linux clusters of Daniel Lucio as well as the friendship and encouragement of Deytcia Limas, Carlos Pinilla and Anabel Lino.

Finally, my appreciation to the U.S. Department of Energy trough the Nuclear Energy Research Initiative grant DE-FC07-05ID14653, the Oak Ridge National Laboratory Reactor Physics group, the North Carolina State University and the Westinghouse Electric Company for funding and software tools to my work here presented. I would like to acknowledge the National Council of Science and Technology (Mexico) for its economical support during part of my studies and a special gratitude to the Mechanical and Nuclear Engineering Department of the University of Cincinnati, where I initialized the project.

Abstract

A generalized software capability has been developed for the pin-wise loading optimization of light water reactor (LWR) fuel lattices with the enhanced flexibility of control variables that characterize heterogeneous or blended target pins loaded with non-standard compositions, such as minor actinides (MAs). Furthermore, this study has developed the software coupling to evaluate the performance of optimized lattices outside their reflective boundary conditions and within the realistic three-dimensional core-wide environment of a LWR.

The illustration of the methodologies and software tools developed helps provide a deeper understanding of the behavior of optimized lattices within a full core environment. The practical applications include the evaluation of the recycling (destruction) of "undesirable" minor actinides from spent nuclear fuel such as Am-241 in a thermal reactor environment, as well as the timely study of planting Np-237 (blended NpO_2 + UO_2) targets in the guide tubes of typical commercial pressurized water reactor (PWR) bundles for the production of Pu-238, a highly "desirable" radioisotope used as a heat source in radioisotope thermoelectric generators (RTGs). Both of these applications creatively stretch the potential utility of existing commercial nuclear reactors into areas historically reserved to research or hypothetical next-generation facilities.

In an optimization sense, control variables include the loadings and placements of materials; U-235, burnable absorbers, and MAs (Am-241 or Np-237), while the objective functions are either the destruction (minimization) of Am-241 or the production (maximization) of Pu-238. The constraints include the standard reactivity and thermal operational margins of a commercial nuclear reactor. Aspects of the optimization, lattice-to-core coupling, and tools herein developed were tested in a concurrent study (Galloway, 2010) in which heterogeneous lattices developed by this study were coupled to three-dimensional boiling water reactor (BWR) core simulations and showed incineration rates of Am-241 targets of around 90%. This study focused primarily upon PWR demonstrations, whereby a benchmarked reference equilibrium core was used as a test bed for MA-spiked lattices and was shown to satisfy standard PWR reactivity and thermal operational margins while exhibiting consistently high destruction rates of Am-241 and Np to Pu conversion rates of approximately 30% for the production of Pu-238.

Preface

The work in this thesis includes advances to the lattice optimization code named FORMOSA-L, which is a multi-objective optimization computer program based on the simulated annealing technique which was originally designed to optimize pin-by-pin loadings and spatial arrangement of standard LWR fuel lattices. Some of the new adaptations to FORMOSA-L include its coupling to the commercial-grade lattice physics code named PHOENIX-4 from the Westinghouse Electric Co., as well as the inclusion of minor actinides within the objective function to maximize incineration or production of specific isotopes during the irradiation fuel cycle. Likewise, a Message Passage Interface (MPI) implementation of the Linear Superposition Model (LSM) of FORMOSA-L was also developed to help eliminate 90% of the computational effort when running on 7 or more processors, and to help speedup further analysis of core-to-lattice feedback information in the pursuit of optimal fuel loading patterns. A 10x10 BWR lattice with americium content was analyzed with FORMOSA-L as well as a 17x17 PWR lattice with americium and Np-237 preloaded at the beginning of the fuel irradiation cycle.

To couple optimized PWR lattices to the three dimensional core-wide environment. The software infrastructure was developed to link the SCALE/TRITON lattice physics sequence to the NESTLE three-dimensional core simulator. This coupling code was named TRITON-TO-NESTLE or T2N for short. Furthermore, to validate this coupling, a well known OECD PWR full-core 3D benchmark was evaluated, which includes a 1/3 loading of mixed-oxide (MOX) fuel. For this validation, the lattice-homogenized and energy-collapsed two-group cross-sections were generated by the module TRITON, which effectively couples the ORIGEN depletion capabilities to the generalized-geometry discrete-ordinates transport code NEWT. Other modifications to the NESTLE code included the implementation of thermodynamic tables for its hydrodynamic model. The developed software and modifications have been carried out in an open and collaborative environment that has included contributions from NCSU, ORNL, and UT, with the aim to ultimately release a validated and first of its kind open-source end-to-end lattice to core LWR design capability to support research and education.

Specific lattice-to-bundle-to-core designs were studied using the FORMOSA-L, TRITON/NEWT, and NESTLE approach above described. These designs were developed to try to maximize the incineration of Am-241 and/or the production of Pu-238 (from blended Am-241 as well as from heterogeneous Np-237 targets). To help confirm the viability of the core designs herein studied, key assessments of core-wide safety parameters were performed for the reference benchmark as well as for the cores loaded with minor actinides to ensure that these studies were as realistic as possible.

Table of Contents

List of Tables

List of Figures

1 Introduction

An important aspect of the nuclear fuel cycle is the planning of the fuel reload. Reactivity, power, and burnup distributions vary spatially as does thermal-hydraulic feedback. The material properties of the core are constrained by performance limits, and the aim of nuclear fuel management generally targets to maximize the thermal output as a function of time while minimizing cost (or enrichment) of fuel, while satisfying all reactivity, thermal, and mechanical (safety related) constraints.

This thesis describes the development of a variety of software tools that support the optimization of light water reactor fuel lattices with the inclusion of minor actinide compositions (targets) as control variables, while minimizing the maximum power peaking factor and maintaining a prescribed/constrained reactivity profile as a function of burnup. Furthermore, among the tools developed is the capability to test and evaluate optimized lattices in realistic (and benchmarked) three-dimensional full core environments. In this study, optimized lattices loaded with Am-241 and Np-237 are evaluated within boiling water reactor (BWR) and pressurized water reactor (PWR) environments. The results obtained indicate that the rate of incineration of Am-241 (a highly undesired component of spent nuclear waste) is higher than 90% at the end of cycle (EOC) for BWRs and PWRs, both. Concurrently, the conversion rate of Np-237 targets into Pu-238 (a highly desirable isotope that is a thermal source for space applications) is of the order of 30%. In other words, roughly 30% of the initial mass of planted Np-237 can be converted into Pu-238. The inclusion of Np-237 has the principal objective of producing Pu-238, a radioisotope

that can be used in Radioisotope Power Sources (RPSs) or Radioisotope Thermoelectric Generators (RTGs) in space exploration.

In principle, the general idea is to design a realistic and believable nuclear reactor fuel bundle and core design; therefore, to know whether a design is suitable, the following sequence of nuclear fuel design steps should be followed:

- Design an initial fuel lattice; loadings of fuel, enrichments, burnable absorbers, location of pins.
- Evaluate reactivity and power distribution attributes for the fuel lattice; k-infinity versus burnup, maximum power peaking factor. Note that at this stage, boundary conditions on lattice reflect "infinite or reflective boundary conditions."
- Apply constraints; cycle length, maximum power peaking, maximum enrichment or concentration of burnable absorbers. If unacceptable, change lattice design.
- Load lattice into the core: evaluate core-wide attributes (k-effective or boron dilution ppm level versus burnup, local three-dimensional power peaking, thermal margins such as the Moderator Temperature Coefficient (MTC) and Doppler Temperature Coefficient. This step reflects appropriate boundary conditions upon lattice design that are representative of a real core.
- If core-wide metrics are unacceptable, modify lattice loadings to satisfy core-wide attributes. Repeat process.

2 Minor Actinide Recycling in Light Water Reactors

During the irradiation of uranium dioxide (UO_2) in Light Water Reactors (LWRs), transuranic elements as americium, curium and neptunium are built through neutron capture and subsequent decay. As a consequence, at the end of an irradiation cycle, nuclear fuel has a variety of Minor Actinides (MAs) and fission products (FPs); this mixture of elements is enclosed within the ceramic UO_2 pellets and within an outer layer (tubing) of Zircaloy cladding. After a fuel element can no longer support full rated power operation following the significant loss of the primary fissile isotopes (U-235 and Pu-239), it is ultimately removed from the reactor and colloquially referred to as "spent nuclear fuel." It should be noted, however, that spent fuel is actually a highly valuable resource, in fact, as it contains a large majority of benign elements and a small minority of highly radiotoxic isotopes. Therefore, carefully understanding the nature of what elements can be produced and which ones can be destroyed is an important area of what some may call "waste management," assuming that the appropriate chemical separation technology is viable.

Transmutation systems are typically distinguished by their neutron energy spectrum; in particular, whether they are fast or thermal. Although a fast reactor spectrum is desirable (the ratio of fission to capture in the MAs is greater), the vast availability of LWRs around the world has given some interest in the study of recycling transuranics as americium, neptunium and curium in thermal reactors (a.k.a., "minor actinides").

2.1 Minor Actinide Transmutation in Thermal Reactors

The potential of thermal reactors to incinerate Am-241 was investigated in Pressurized Water Reactor (PWR) fuel cells (*Takeda et al., 1997).* It was found that the effect of moderation in the

fuel cell by changing the proportion between volumes of moderator with respect to fuel is almost negligible and that the overall transmutation rate is governed by capture reactions. Thus, an accurate knowledge of the transmutation path and the time-dependent MA concentrations is essential for a practical nuclear waste management. The growing demand for Pu-238 as a heat source in isolated environments, such as in NASA missions, also suggests another viable path for its production; that is, by Am-241 transmutation, since its incineration has a path leading to Pu-238. Likewise, for higher production yields, a thermal core with heterogeneous pins of neptunium-237 dioxide (NpO_2) could be another suitable strategy, whereby the oxide form could facilitate the separation process following irradiation.

Considering the design of a long-term nuclear waste repository and accounting for non-proliferation issues, the recycling of transuranics is one of the best options available for the post-processing of the spent nuclear fuel compared to a direct disposal of once-through irradiated fuel. However, this option is also the most problematic due to fuel handling, fabrication, and transportation issues that are a result of the very high spontaneous fission neutron emission rates, as well as high volatility of some of the MAs. Nevertheless, assuming that the above-noted issues are ultimately managed, the possibility of recycling americium in a mixed oxide (MOX) fuel form promises to be of significant benefit to repository performance over those obtained with plutonium-only recycling. Furthermore, coupling americium recycling in the fuel cycle alongside storage of curium is an option that appears promising if an appropriate solution for the curium storage is found (*Taiwo et al., 2006*). Note in Figure 2.1 the overwhelming contribution from Am-241 to the total decay heat in spent LWR fuel, in particular between 100 and 1000 years after discharge.

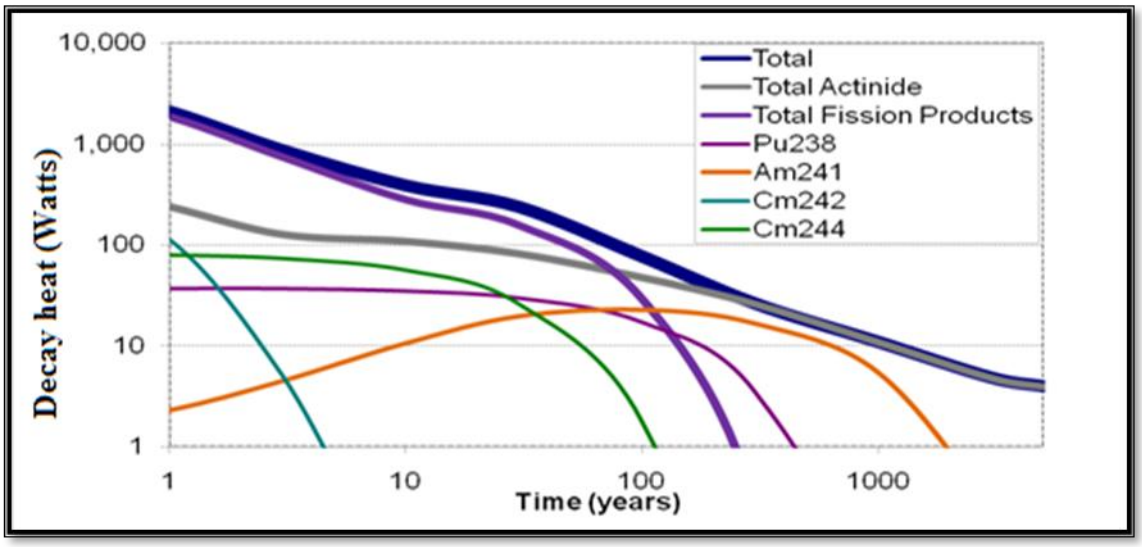

Figure 2:1 Decay heat load contributors from LWR discharged fuel

Due to its short half-life ($T_{1/2}$ = 162.8 days) Cm-242 outbalances the global alpha activity in every scenario at the end of irradiation. However, the Cm-242 daughter, Pu-238, also represents a key "nuisance" that limits repository performance and sizing, with Cm-244 not far behind in terms of having a similar impact. In fact, curium isotopes in spent fuel are generally considered problematic due to their high neutron emission rates. This is of particular importance when considering target manufacturing in a multi-reprocessing environment. In addition, as previously discussed, Pu-238 is also a long-term neutron emitter (*Bringer et al. 2008*), but it is useful as a radioisotope heat source in isolated environments.

An important fact to consider is that MA recycling in LWRs reduces the initial reactivity excess and can be used for longer cycles, achieving higher fuel discharge burnup. Nevertheless the introduction of high concentrations of fissile plutonium and MAs can lead to positive void reactivity coefficients, limiting the amount of MAs that can be loaded in the fuel (*François and Guzman, 2007*). Therefore, an optimization technique to maximize the MA content at the

Beginning of Cycle (BOC) has to consider carefully any positive reactivity inserted in the reactor core.

The neutronic performance when americium and neptunium are co-inserted in the UO_2 fuel was evaluated using a UO_2 type "C" fuel from ANGRA-I Nuclear Plant (*Lombardi and Pereira, 2002*) with 3.1 wt. % of initial U-235 enrichment and simulated using the code WIMS-D5 (*Santos, 1994; Aldama et al., 2000*). The transmutation potential of americium was about 80% and for neptunium about 45% at approximately 33 GWd/MTHM. All fuels analyzed were compared to a standard UO_2 core and exhibited similar performance and safety margins.

2.2 Use of Pu-238 as a Heat Source for Space Exploration

There exists a long history of the use of Radioisotope Power Sources (RPS's) and Radioisotope Thermoelectric Generators (RTG's) in space exploration (*Rankin, et al, 2000*). These were first launched in 1961 and have been used safely and reliably in National Aeronautics and Space Administration (NASA) missions for over 40 years; including 5 on the Moon (1960s – 1970s), 8 in Earth orbit (1960s – 1970s), 2 on Mars (1970s and two heater units 1996, 2003), and 8 to outer planets and the Sun (1970s through 2006). The heat source program at the Savannah River Site (SRS) had been providing the raw material, Plutonium-238, until the K Reactor at SRS was shutdown in the late 1980's. Pu-238 has been the primary heat source used in these applications and it offers an ideal combination of a long half-life (~88 years) and lower shielding requirements relative to other potential isotopes for RPS/RTG applications such as Sr-90, Cm-242, Po-210, and Am-241.

In April of 2008, during a briefing to the US Department of Energy's Nuclear Energy Advisory

Committee (NEAC), Dennis Miotla, Deputy Assistant Secretary for Nuclear Power Deployment, highlighted that procurement of Pu-238 from Russia started in the early 1990's (which by agreement cannot be used for national security applications) and will conclude in 2010. Moreover, Russia has also lost its capability to produce additional Pu-238. Preliminary cost estimates indicate that restoring the infrastructure to support domestic production of Pu-238 will cost several hundreds of millions of dollars. Accordingly, Figure 2.2, a key slide from Miotla's presentation to the NEAC, illustrates the projected state of the Pu-238 inventory through 2028.

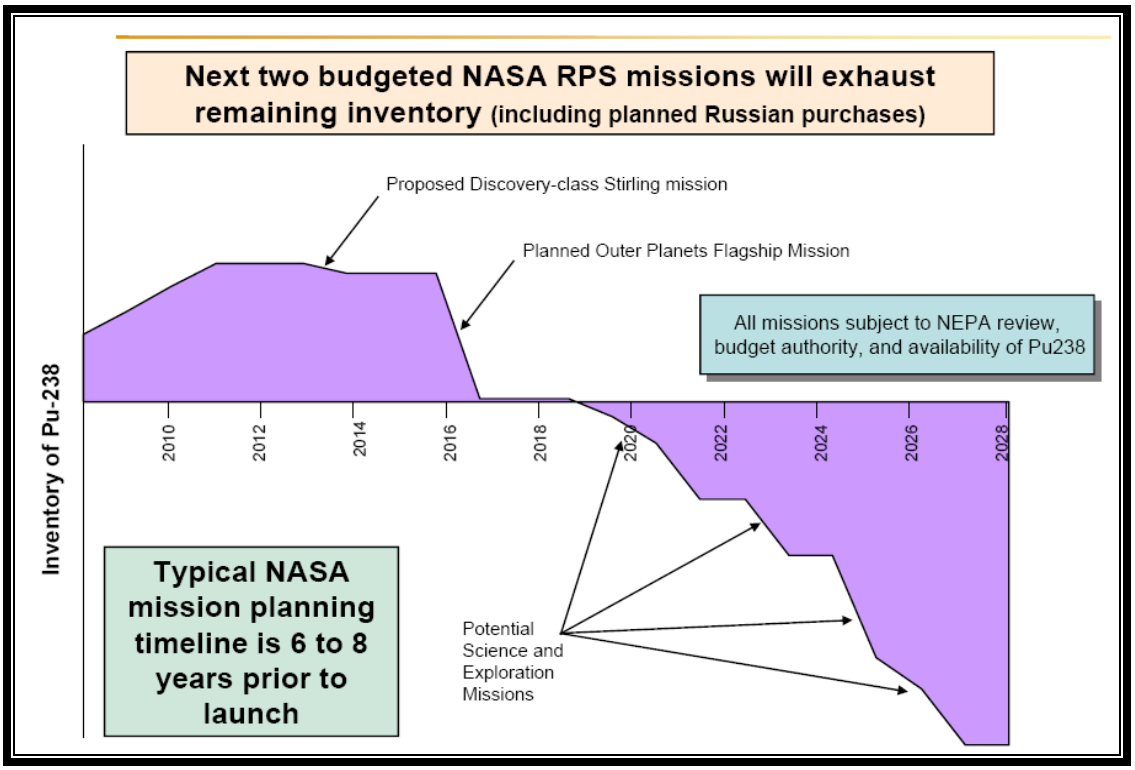

Figure 2:2 Projected inventory of Pu-238 to support NASA missions (Miotla, 2008)

Striking to realize; the next two budgeted NASA missions are projected to exhaust the remaining supply of Pu-238, a steady demand for approximately 5 kg of Pu-238 per year will persist, and not much seems to be in the works to address this serious problem that has the potential to be a show stopper to future NASA missions.

Interestingly enough, in the world of nuclear reactors, whether of a commercial or research nature, isotopes such as Pu-238, Sr-90, Cm-242, Po-210, and Am-241, are integrally created within the nuclear fuel elements as byproducts of the fission process, via transmutations, or by decay reactions normally occurring as part of the operational and discharge facets of the nuclear fuel cycle. However and ironically, many of these and other valuable isotopes produced are often rolled into a term known to most as "nuclear waste."

The projected increased demand for Pu-238 has opened the possibility to use commercial powers reactors, such as Pressurized Water Reactors (PWRs) to produce this radioisotope by transmutation of Np-237 targets. In fact, Np-237 is still currently in abundant supply at SRS and incidentally is also an integral component of "nuclear waste" or *spent fuel*, as we prefer to call it. Early calculations have shown a maximum conversion of Np-237 to Pu-238 within a single exposure cycle is about 20% and an overall conversion of 50% to 60% for a neptunium recycling strategy. In a typical 1000 MW nuclear power plant with a lower than typical 80% capacity factor, the Np-237 production averages about 3 kg per year (*Roggenkamp, 1987*).

2.2.1 Production of Pu-238 at the Savannah River Site

The process of production and irradiation of NpO_2 has been proven and carried out at the Savannah River Plant (research type) reactor with an annual production yield of up to 50 kg/year of Pu-238. Pu-238 as a heat source emits 5.4 MeV alpha particles and has a half life of

approximately 88 years; Figure 2.3 shows a simplified nuclear reaction chain as to illustrate how this isotope is produced from natural radioisotopes as U-235 in a Light Water Reactor (LWR).

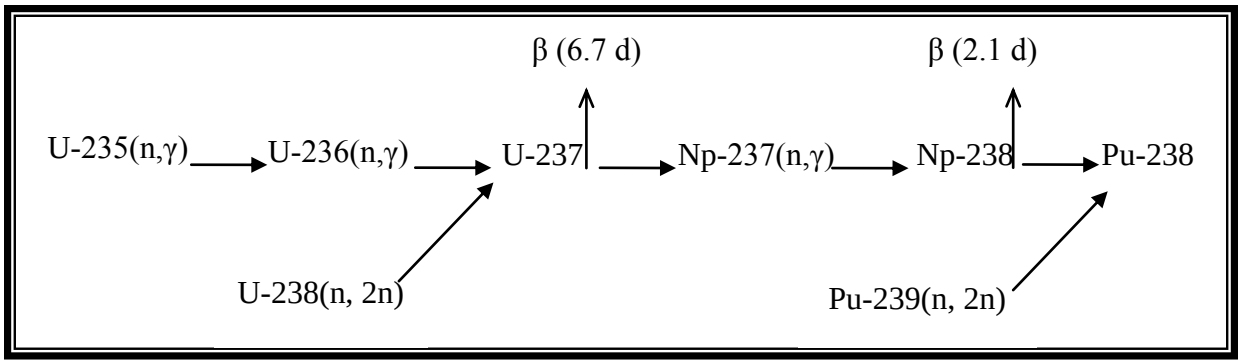

Figure 2:3 Simplified nuclear reaction chain for Pu-238

The use of heavy water as a moderator and highly enriched uranium as a fuel made the Savannah River Site reactors particularly suitable for Pu-238 production. Target elements to produce radioisotopes of Pu-238, Pu-239 and tritium products are deposited in the reactor separated from the UO_2 rods to facilitate the recovery process (*Roggenkamp, 1987*). To produce Pu-238, the target nuclide is Np-237. To fabricate neptunium targets, NpO_2 is compacted with aluminum powder to form a billet core to be assembled with aluminum components into a composite billet. The composite billet is extruded into a target tube having the NpO_2-Al cermet core and aluminum cladding. The target tube is irradiated in the production reactor lattice where it displaces one of the depleted uranium target assemblies used for Pu-239 production. Up to one fourth of the depleted uranium target assemblies may be replaced at any specific time. After a cooling period, the target elements are deposited in a nitric acid solution. Plutonium, neptunium, fission products (FP's) and aluminum are partitioned by ion exchange. The plutonium and neptunium nitrates are converted to oxides, while neptunium is recycled in the reactor. Plutonium is fabricated as a heat source, forming spheres enclosed within an iridium shell, each containing a nominal 112 grams of Pu-238. This multi-decade experience easily validates the feasibility of manufacturing targets and the availability of processes and techniques to post-process these for the extraction of Pu-238.

3 Lattice Optimization Adaptations for Minor Actinide Handling

In order to carry out lattice optimization studies with MAs recycling, the FORMOSA-L code (Electric *Power Research Center, NC State University and Iowa State University, 1999*) was used and updated considerably. FORMOSA-L employs an optimization algorithm based on the Simulated Annealing (SA) technique for pin placement and loading decisions. This code was first coupled to a modern lattice cell code simulator, the PHOENIX-4 from Westinghouse Electric Co, to maximize the loading and optimize the placement of MA heterogeneous pins while constraining reactivity requirements and pin power factors in the assembly as a function of burnup; furthermore, this code was also more recently adapted to multiprocessor environments (*Hernandez, et al., 2009*).

3.1 Overview of the Simulated Annealing Technique in FORMOSA-L

The advantage of the Simulated Annealing (SA) technique is its proficiency for seeking a global optimum within a large numbers of local extrema during a combinatorial optimization. The implementation of the Metropolis algorithm (*Metropolis N.*, et al., 1953) is a probabilistic technique appropriate for large-scale combinatorial optimization problems with nonlinear objectives and constraints. One useful illustration has been its application to the in-core nuclear fuel management of PWRs (Kropaczek and Turinsky, 1991), and given that the lattice optimization problem has similar properties, SA is employed in FORMOSA-L for the pin-by-pin lattice loading and placement optimization.

The Metropolis algorithm was originally applied to determine the equilibrium state of atomic configurations in an annealing solid. A simulated annealing (SA) minimization problem implements the Metropolis algorithm and can be explained as follows: First, randomly generated

solutions that *increase* the objective function (being *minimized*) by a value ΔF_O can be conditionally accepted with a probability P defined as:

$$P = \exp(-\Delta F_O / kT) \tag{3.1}$$

where the control parameter T is analogous to the original Metropolis absolute temperature application and the coefficient k is like the Boltzmann constant. The kT values are adjusted from high to low during an optimization cycle (referred to as a "cooling schedule") in order to accept a large number of solutions at the beginning of the cooling cycle but being more restrictive toward the end of the search. More randomly generated domains are explored by carrying out several "re-heatings" of kT and applying multiple cooling schedules during the optima search.

The annealing schedule in FORMOSA-L is determined by the total number of single assembly perturbations (N_{chng}) which is calculated according to the total possible available perturbations for the problem in question as a user-defined input. Via a built-in fraction B_0, the number of attempts for calculating the initial temperature is confined to $B_0 \times N_{chng}$. The code will perturb the initial reference configuration, calculating the initial temperature after each perturbation, according to Equation 3.2.

$$T_{init} = \frac{-\Delta}{\ln(\Theta)} \tag{3.2}$$

FORMOSA-L was coupled originally to the lattice physics codes CPM-2 and CASMO-3 to produce a within-bundle optimization code named FORMOSA-L (Version 1.0) to perform two dimensional (radial) loading optimizations of Light Water Reactors (LWR) assemblies (*Zheng, 1999*)

3.1.1 Coupling the Lattice Physics Code PHOENIX-4 to FORMOSA-L

Via collaboration with the Westinghouse Electric Company, this project was able to include the coupling of PHOENIX-4 (*Yin, et al., 2006*) to the SA algorithm in FORMOSA-L. The coupling between PHOENIX-4 and FORMOSA-L enabled the modeling of 10x10 BWR and 17x17 PWR lattice configurations and the use of a more modern and well established code system of industrial grade/quality, which is able to simulate MOX fuels with a 33 energy group library. Initially, a simple strategy applied to study the impact of MA loadings was to replace gadolinium pins in a BWR lattice with americium pins which could be modeled with PHOENIX-4 and optimized with FORMOSA-L.

The recycling of Am and Np in a heterogeneous PWR assembly by loading/replacing two water channel rods with Np-237 blended with Zr in a 20:80 volume ratio was a strategy specifically explored with FORMOSA-L in this study, which required a number of software upgrades, modifications, and developments herein described.

3.2 Overview of options in FORMOSA-L

As previously noted, the FORMOSA-L code can perform a two-dimensional loading optimization for LWR lattices using the Simulated Annealing (SA) technique. The manner in which the designer interacts with FORMOSA-L is as follows: First, an initial lattice loading pattern (LLP) is specified at the beginning of each optimization. The code then generates new LLP stochastically by randomly perturbing the initial LPP and carries out the SA scheme. Exclusion rules can be applied, such as ”freezing locations” or “freezing compositions”, that is, during the optimization the code may not permit a specific pin to change in composition or location within the initial LLP.

In this section the FORMOSA-L features and main modifications to the original code are described; among them, the use of a Linear Superposition Model (LSM), which was well-suited to an MPI implementation for parallel and multiprocessor environments. In fact, as part of the overhaul of Version 1.0, the entire FORMOSA-L code was first translated from FORTRAN 77 and converted to FORTRAN 90. Furthermore, following recent adaptations, the FORMOSA-L code includes the following updated list of objective functions:

- Minimization of power peaking
- Minimization of average enrichment
- Minimization of uranium cost
- Minimization of power peaking and average enrichment (combined)
- Maximization of the end-of-cycle (EOC) k_∞
- Maximization of minor actinide (MA) BOC concentration (e.g., Am-241)

Likewise, the constraints that can be applied to the optimization via penalty functions are:

- Burnup-dependent upper and lower bounds on assembly-average k_∞
- Maximum pin power peaking
- Maximum assembly-average enrichment.
- Maximum assembly-average minor actinide (MA) content.

Table 3.1 summarizes the combinations of objectives and penalty-based constraints presently available in FORMOSA-L.

Table 3:1 Penalty-based constraints and objective functions in FORMOSA-L.

Penalty-based Constraints	**Objective Functions**
Average enrichment and k_∞ bounds	Power peaking minimization
Power peaking and k_∞ bounds	Average enrichment minimization
Power peaking and k_∞ bounds	Uranium cost minimization
k_∞ bounds	Dual objective power peaking and enrichment
Power peaking and avg. enrichment	EOC k_∞ maximization
Avg. minor actinide concentration	Maximize BOC minor actinide loading

The decision variables in the classical FORMOSA-L optimization process are the pin distribution, individual pin enrichments and burnable poison (BP) concentrations. Because a transuranic element such as americium or neptunium in the form of AmO_2 or NpO_2 can act as a burnable absorber, in this most recent version of the code a new variable was added to substitute the BP concentration in minor actinides recycling studies (*Hernandez H., et al.,* 2007). Mathematically, the variables are described by the binary values of $p_{l,m}$, $e_{l,m,n}$ and $b_{m,k}$ respectively for fresh fuel analysis and $p_{l,m}$, $e_{l,m,n}$ and $t_{m,k}$ for a recycling strategy.

$$p_{l,m} = \begin{cases} 1 \text{ fuel pin type } m \text{ in location } l \\ 0 \text{ otherwise} \end{cases} \tag{3.3}$$

$$e_{m,n} = \begin{cases} 1 \text{ enrichment candidate } n \text{ for pin type } m \\ 0 \text{ otherwise} \end{cases} \tag{3.4}$$

$$b_{m,k} = \begin{cases} 1 \text{ BP concentration candidate } k \text{ for pin type } m \\ 0 \text{ otherwise} \end{cases} \tag{3.5}$$

$$t_{m,k} = \begin{cases} 1 \text{ transuranic concentration candidate } k \text{ for pin type } m \\ 0 \text{ otherwise} \end{cases} \tag{3.6}$$

The pin type *m* refers to a certain number of pins with the same enrichment value and the same burnable poison or transuranic concentration. Constraints include; maximum power peaking at each burnup step,

$$P(i) < P_{max}(i) \text{ for all burnup steps } i, \tag{3.7}$$

minimum and maximum assembly averaged multiplication factors at each burnup step,

$$k_{\infty}^{\min}(i) \le k_{\infty}(i) \le k_{\infty}^{\max}(i) \tag{3.8}$$

and the maximum assembly averaged U-235 fuel enrichment at BOC,

$$E \le E_{max} \tag{3.9}$$

3.2.1 The Multi-Level Superposition Model in FORMOSA-L Version 2.0

A lattice-physics calculation can be thought of as an arbitrary function whose independent variables are the design parameters which describe the fuel assembly (i.e. code input), and whose dependent variables include attributes such as the assembly-average k_{∞} profile and/or relative pin power distribution versus burnup (i.e. code output). Accordingly, the basic principle behind the multi-level superposition model (MLSM) is based upon casting the above-noted function into a Taylor's series expansion about a selected reference assembly, where the truncation of second and higher-order terms constitutes the main approximation which makes this a first-order accurate model. Assume an LWR fuel assembly contains *N* pins and *M* types of pins, where type

refers to pure fuel, fuel with integral burnable poison, discrete burnable poison pins, water hole, etc., then the following vectors are defined:

P: Pin Power Distribution (N-vector);

L: Pin Type Spatial Distribution, where L_i denotes the pin type at assembly spatial position I (N-vector);

E: Pin Material Distribution, where E_j denotes the material composition (e.g. fuel and/or burnable poison concentration) for the jth pin type (M-vector).

Two functions are defined: f and g, to represent the relationship between the dependent variables (P and k_∞) and the independent variables (L, E, etc.). Accordingly, a Taylor's Series functionality is assumed for an assembly's power distribution and its average k_∞. The first-order approximation manifests itself when the second and higher-order terms are neglected, as show below where the subscript ``0'' denotes a reference (unperturbed) condition, and the superscript ``*'' denotes the estimated quantities.

$$\mathbf{P} \approx \mathbf{P}^* = \mathbf{P}_0 + \left[\frac{\partial \mathrm{f}}{\partial \mathbf{L}}\right]_0 \Delta\mathbf{L} + \left[\frac{\partial \mathrm{f}}{\partial \mathbf{E}}\right]_0 \Delta\mathbf{E} \tag{3.10}$$

$$k_\infty \approx k_\infty^* = k_{\infty,0} + \left[\frac{\partial \mathrm{g}}{\partial \mathbf{L}}\right]_0 \Delta\mathbf{L} + \left[\frac{\partial \mathrm{g}}{\partial \mathbf{E}}\right]_0 \Delta\mathbf{E} \tag{3.11}$$

When combined perturbations are made to a reference assembly, the changes of relative power distribution and the multiplication factor can be approximately estimated by summing up the changes due to all involved single basic perturbations. A second-order cross-term compensation for material perturbation was added to FORMOSA-L[5] under the assumption that for all the models, the MLSM with second order interpolation improves accuracy by refining the algorithm for material perturbations (material perturbations include U-235 enrichment, BA and transuranics). The Taylor's series expansion after truncating of the third and higher terms is:

$$\mathbf{P} \approx \mathbf{P}^{*} = \mathbf{P}_0 + \left[\frac{\partial f}{d\mathbf{E}}\right]_0 \Delta\mathbf{E} + \frac{1}{2}\begin{bmatrix} \Delta\mathbf{E}'.\left[\frac{\partial^2 f_1}{\partial\mathbf{E}^2}\right]_0.\Delta\mathbf{E} \\ \vdots \\ \Delta\mathbf{E}'.\left[\frac{\partial^2 f_N}{\partial\mathbf{E}^2}\right]_0.\Delta\mathbf{E} \end{bmatrix} \tag{3.12}$$

$$k_\infty \approx k_\infty^{*} = k_{\infty,0} + \left[\frac{\partial g}{d\mathbf{E}}\right]_0 \Delta\mathbf{E} + \frac{1}{2}\Delta\mathbf{E}'.\left[\frac{\partial^2 g}{\partial\mathbf{E}^2}\right]_0.\Delta\mathbf{E} \tag{3.13}$$

The second-order terms include not only the second-order derivatives of each pin type but also the cross terms presenting the interactive effect between any two pin types. Extensive computational experiments have been conducted with the MLSM. Several approaches to create a library have been implemented into FORMOSA-L code, including separated libraries (spatial and material), combined library and simplified library. The first key aspect of the MLSM methodology is the construction of the appropriate linear superposition libraries, which are

developed with respect to a reference (unperturbed) lattice physics calculation. One type of linear superposition library can be created during a simulated annealing cooling cycle; namely, a library involving only spatial perturbations, or a library involving only material perturbations, or a library involving both of them. The emphasis was placed upon the separated library.

It has been concluded by observation that to maintain an acceptable level of accuracy, the material perturbations (i.e. enrichment or burnable absorber changes) and the spatial re-arrangements (i.e. pin shuffling) should be best performed independently of each other during an optimization. Fortunately, the simulated annealing strategy is well-suited to handle the material and spatial changes in alternating cooling cycles. In other words, when evaluating changes due to spatial perturbations, the material properties are not perturbed ($\Delta\mathbf{E} = 0$). Likewise, when evaluating changes due to material perturbations, the spatial arrangement of the pins remains unperturbed ($\Delta\mathbf{L} = 0$). This separability assumption during optimizations was deemed appropriate to employ because of the considerable improvements in error performance produced relative to treating both types of perturbations simultaneously (Maldonado and Zheng, 1998). Although the concern of this approach is that trapping in local minima may occur, so far, no measurable degradation in optimization fidelity has been observed as a consequence of this assumption. An additional not-so-obvious drawback is that at least twice as many SA cooling cycles are generally required during the optimization process if material and spatial perturbations are to be performed independently of each other. Furthermore, it could be reasonably expected that carrying out material and spatial perturbations simultaneously ought to lead to a more thorough global sweeping of the search space.

3.3 New features of FORMOSA-L

As previously noted, the latest version of FORMOSA-L includes the coupling to a new lattice physics code as an option, namely, the PHOENIX-4 code from Westinghouse. Also, it now has the ability to handle MA contents as constraints or objective functions, and the code has been updated from FORTRAN 77 to FORTRAN 90 and can work with the GFORTRAN or the IFORT compilers.

More recently, a master-slave implementation (*Gropp et al., 1999*) based in message passing interface (MPI) was coded into FORMOSA-L. In the master-slave scheme a task is divided up into subtasks, this philosophy is well-suited for this specific case in which the head node carries out the division of the material library according to the number of worker nodes desired, each of these nodes executes PHOENIX-4; once each slave obtains a vector of values in k_∞ and a 2D matrix of maximum power peaking factor for each task assigned, the result is sent back to the head node with non blocking communication. The extreme values ([s,e]) for each library subdivision assigned to each slave processor and are given by:

$$s = \begin{cases} (id-1)*(nlocal) + \mathrm{mod}(n, nprocs) + 1 & \text{if id>1} \\ 1 & \text{if id=1} \end{cases} \tag{3.14}$$

$$e = id * nlocal + \mathrm{mod}(n, nprocs) + 1 \tag{3.15}$$

where:

nprocs = number of processors

my_id= integer number assigned to each processor, my_id = 1,2,3,…,nprocs

n = number of cases in the library

nlocal = n/nprocs

The MPI material library creation is carried out in two basic steps; first, k_∞ and max power peaking factors are used to obtain 1st order derivatives, then used to obtain second-order terms with cross terms included. In contrast, for the spatial library, only first-order terms are considered. The general idea being with the use of parallel processing is that the data stored in the material or spatial sensitivity libraries can be independently collected, thus, the process is inherently parallel. In fact, library creation is the portion of the code which requires the majority of its CPU time.

Figure 3.1 shows the time spent for a cooling cycle in FORMOSA-L using MPI as a function of the number of processors. This parallel implementation is well suited to 7 processors.

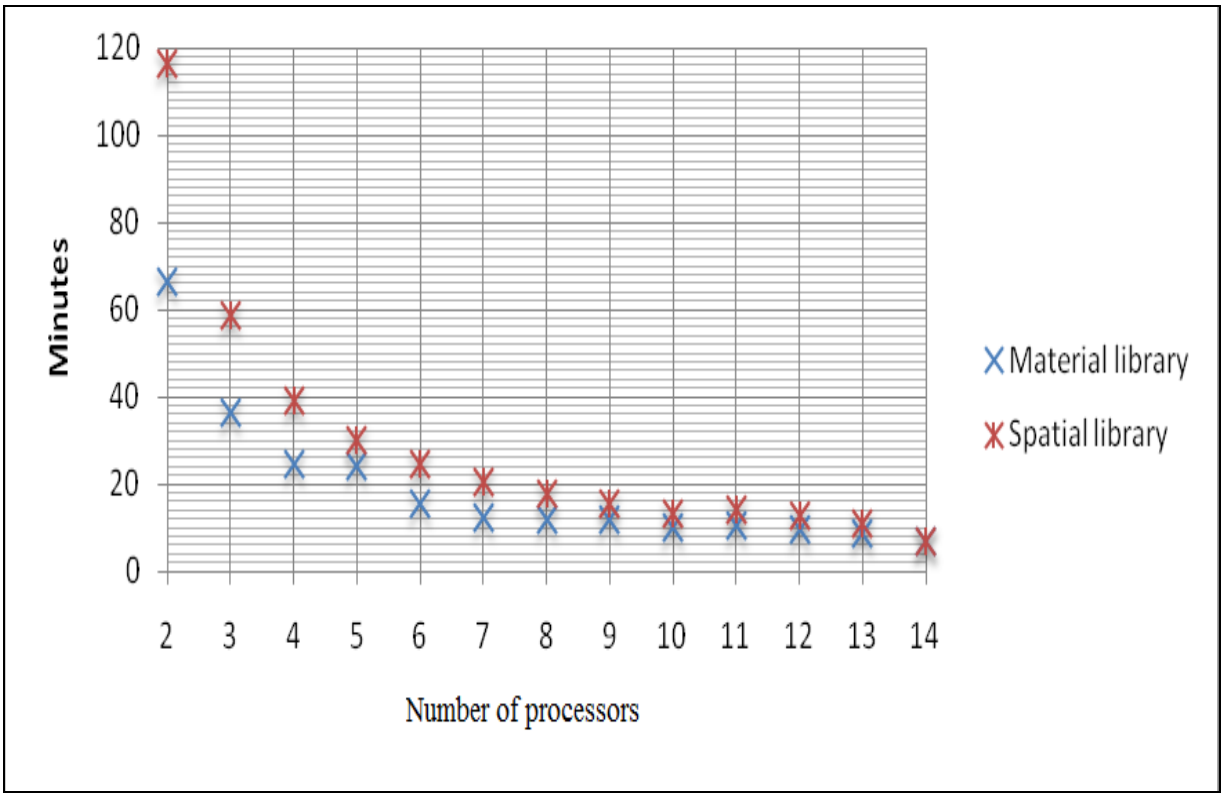

Figure 3:1 Calculation Time per Cooling Cycle as a function of number of processors

The error of MLSM is defined as the difference between pin power and k_∞ obtained via linear superposition model (LSM) and those values obtained using CPM-2, CASMO-3 or PHOENIX 4 for a specified fuel assembly loading and pin arrangement. Thus, the error can be expressed as:

$$PE = P^{LSM} - P^{exact} \tag{3.16}$$

$$KE = k_\infty^{LSM} - k_\infty^{exact} \tag{3.17}$$

where PE and KE define the errors in pin power and k_∞, respectively. P and $k_\infty$are the pin power and infinite multiplication factor. The superscripts "LSM" and "exact" indicate the values obtained by LSM or by direct (exact) evaluations. Also other types of error functions can be defined based on the above error definition, such as maximum pin power error (MPE), average pin power error (APE), maximum k_∞ error (MKE) and average k_∞ error (AKE).

$$MPE = \max(PE[i, j]) \tag{3.18}$$

$$APE = \frac{\sum_{i,j} PE[i, j]}{N \times M} \tag{3.19}$$

$$MKE = \max(KE[j]) \tag{3.20}$$

$$AKE = \frac{\sum_{j} KE[j]}{M} \tag{3.21}$$

where I denotes the pin position in an assembly, from1to N; and j denotes the burnup steps, from

1 to M. Figure 3.2 shows how the maximum absolute error using the MLSM is reduced when more than one cooling cycle is performed in FORMOSA-L.

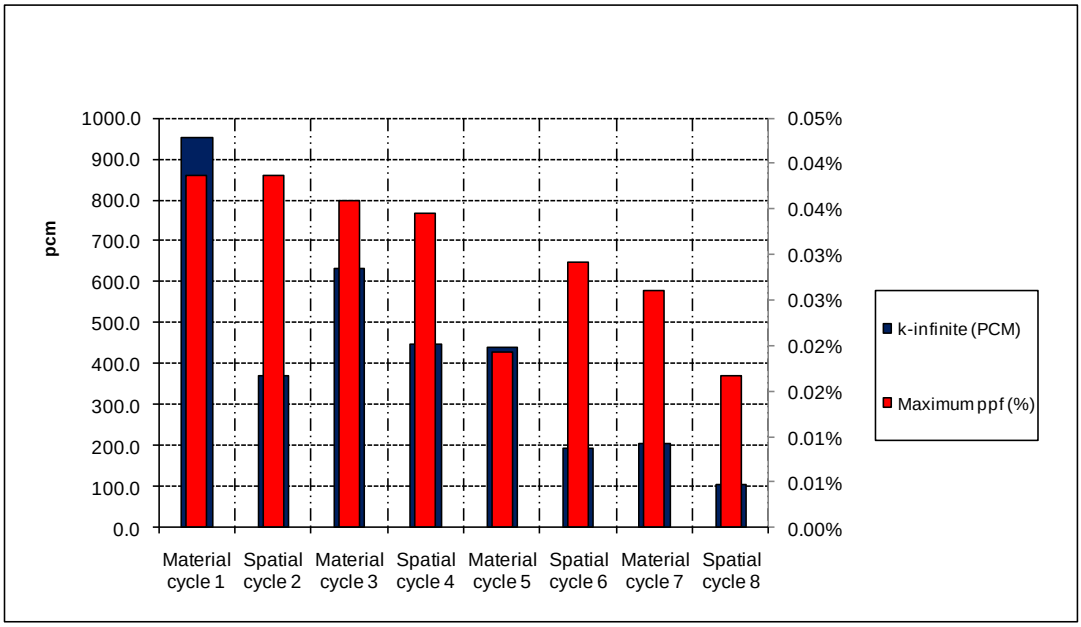

Figure 3:2 Average Errors with Multiple Cooling Cycles

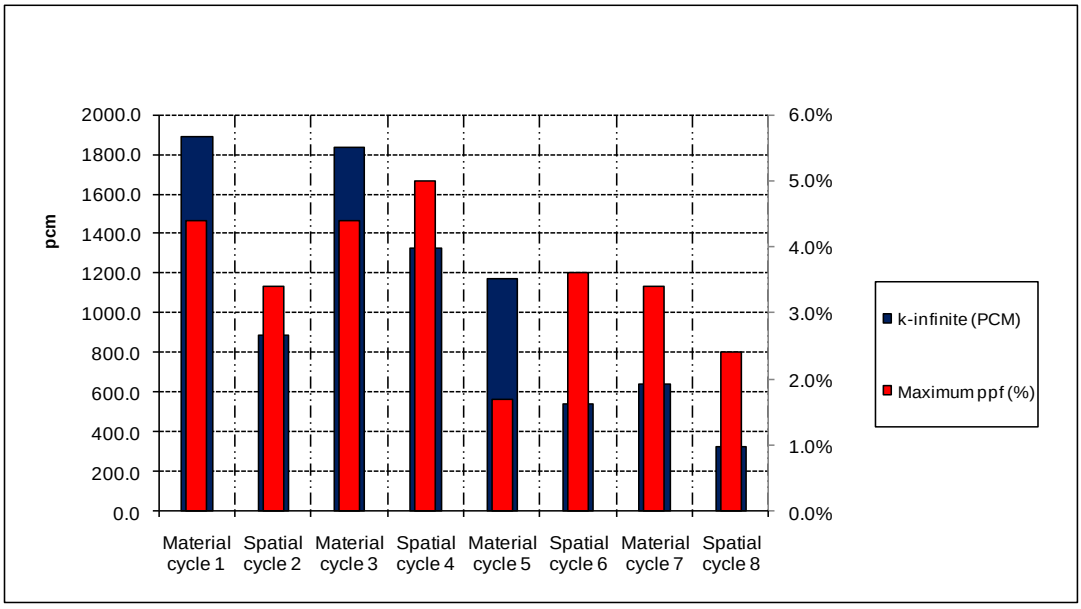

Figure 3:3 Maximum Errors with Multiple Cooling Cycles

4 LWR Lattice Optimization with the FORMOSA-L Code

In this chapter, the upgraded version of FORMOSA-L is employed to optimize LWR lattices loaded with MAs. A Boiling Water Reactor (BWR) lattice was loaded with americium by substituting the pins with gadolinium with pins of $AmO_2 + UO_2$ while maximizing the percent in weight of Am at the beginning of the fuel irradiation cycle (BOC). The PWR lattice was loaded with neptunium targets in two water channels to facilitate their insertion/withdrawal and the separation of the Pu-238 vector from the arrangement. The conversion efficiency of Np-237 to Pu-238 is analyzed in the last section of the next chapter after carrying out a 3D core-wide analysis.

As was done for the BWR lattice, Am-241 was loaded at BOC in the PWR lattices, but even though the maximum power peaking factor for the PWR lattices could be maintained very low, these designs did not facilitate adding a high amount of planted americium. This is because when MAs are loaded at BOC, additional U-235 needs to be added to compensate for the loss of excess reactivity. Meanwhile, the U-235 enrichment is presently constrained to 5.0 w/o, therefore, it limits the amount of MA that can be added. In fact, the assemblies loaded with a low americium content show a high initial reactivity and carry forward reasonable power distributions in 3D core simulations. Furthermore, even though the optimized lattices generated with FORMOSA-L may have used PHOENIX-4 during the optimization, all the final calculations (optimized lattices) herein reported were re-generated with the TRITON/NEWT depletion sequence of the SCALE package before being ported to NESTLE.

4.1 The BWR Lattice Optimization with Americium Recycling

Figure 4.1 shows the initial lattice loading pattern where the green locations represent UO_2 lattices with wt. % of U-235 enrichment loaded with wt. % of gadolinium (*), the blue locations are for saturated water rod channels that help for neutron moderation at the center of the assembly. The remaining pin locations show UO_2 pins with different wt. % of U-235 enrichment.

	A	B	C	D	E	F	G	H	I	J
10	2.00	2.80	3.60	3.95	4.40	4.40	4.40	3.60	2.80	2.00
9	2.80	4.40	3.95	4.90	3.95	3.95	4.90	3.95	4.40	2.80
8	3.95	3.95	4.40 *4.00	4.40	4.90	4.40 *5.00	3.95	4.40 *5.00	3.95	3.60
7	4.40	4.90	4.40	-	WR	4.90	4.40 *2.00	3.95	4.90	4.40
6	4.40	4.40	4.40 *5.00	-	-	4.40	4.90	4.40 *5.00	3.95	4.40
5	4.40	4.40 *4.00	4.40	4.40	4.40	-	WR	4.90	3.95	4.40
4	4.40	4.90	4.40 *4.00	4.40	4.40	-	-	4.40	4.90	3.95
3	3.95	3.95 *4.00	4.40	4.40 *4.00	4.40	4.40 *5.00	4.40	4.40 *4.00	3.95	3.60
2	3.60	4.40	3.95 *4.00	4.90	4.40 *4.00	4.40	4.90	3.95	4.40	2.80
1	2.00	3.60	3.95	4.40	4.40	4.40	4.40	3.95	2.80	2.00

Figure 4:1 Reference BWR lattice pattern

The optimization engine of FORMOSA-L was modified to include minor actinide loadings, such as americium or neptunium, alongside other standard parameters already in the code. In one test, gadolinium loadings of a 10x10 reference bundle were substituted with variable concentrations of americium in 14 of the 92 available pin positions. The optimization algorithm adjusted the concentration and location of all material loading, pursuing objectives (e.g., power peaking minimization) while satisfying constraints (e.g., k_∞ trajectory). The algorithm was forced to pursue higher concentrations of americium loading by modifying the lower constraint of americium in each optimization cycle. Table 4.1 shows the americium isotopic vector used as a reference in the optimization analysis. The vector is based on spent nuclear fuel with a discharge exposure of 50 GWd/MTU, initial U-235 enrichment of 4.26% and a storage time (cooling time) of 30 years. Figure 4.2 shows the optimized lattice loading pattern with americium pins averaging approximately 6.30 wt. % of americium content (*) in 14 pin locations and distributed toward the center of the assembly following a ½ symmetry.

Table 4:1 Mass fraction of the americium vector at the BOC

Radioisotope	Mass fraction
Am-241	0.8578
Am-242m	0.1877×10^{-2}
Am-243	0.1403

	A	B	C	D	E	F	G	H	I	J
1	3.36	2.91 *6.01	4.21	2.70 *6.51	5.00	4.98	4.98	4.98	2.91 *6.01	3.50
2	2.91 *6.01	5.00	3.49	3.49	4.98	5.00	5.00	5.00	2.80 *6.96	2.91 *6.01
3	4.12	5.00	4.98	4.98	5,00	4.97	4.98	5.00	5.00	4.98
4	2.70 *6.51	5.00	4.97	-	WR	4.97	5.00	4.98	5.00	4.98
5	4.97	4.97	5.00	-	-	3.36	4.97	4.97	5.00	4.98
6	4.98	4.97	5.00	5.00	3.36	-	WR	5.00	4.98	5.00
7	4.97	5.00	5.00	5.00	5.00	-	-	4.98	3.49	2.70 *6.51
8	2.70 *6.51	4.97	5.00	5.00	5.00	5.00	4.97	4.98	3.49	4.21
9	3.00 *6.10	2.70 *6.51	4.97	4.98	4.97	4.97	5.00	5.00	5.00	2.91 *6.01
10	3.50	3.00 *6.10	4.98	4.97	5.00	4.97	2.70 *6.51	4.12	2.91 *6.01	3.36

Figure 4:2 The optimized BWR lattice for americium recycling

The maximum power peaking was constrained to a level comparable or lower than that of reference bundle. The lattice's reactivity trajectory (k-infinity profile versus exposure) was constrained particularly at EOC to remain viable. Figure 8 shows graphically the path of the FORMOSA-L optimization engine with its ability to reduce the power peaking reduction as an objective function when the lattice is loaded with americium and with the k_∞ meeting the reactivity requirements during the fuel burnup. It should be noted that when the simulated annealing cooling schedule is "reheated," the objective function changes peak, and as the algorithm cools down, the objective function stabilizes to a near optimum result. Figure 4.3 illustrates 6 cooling schedules on this particular example.

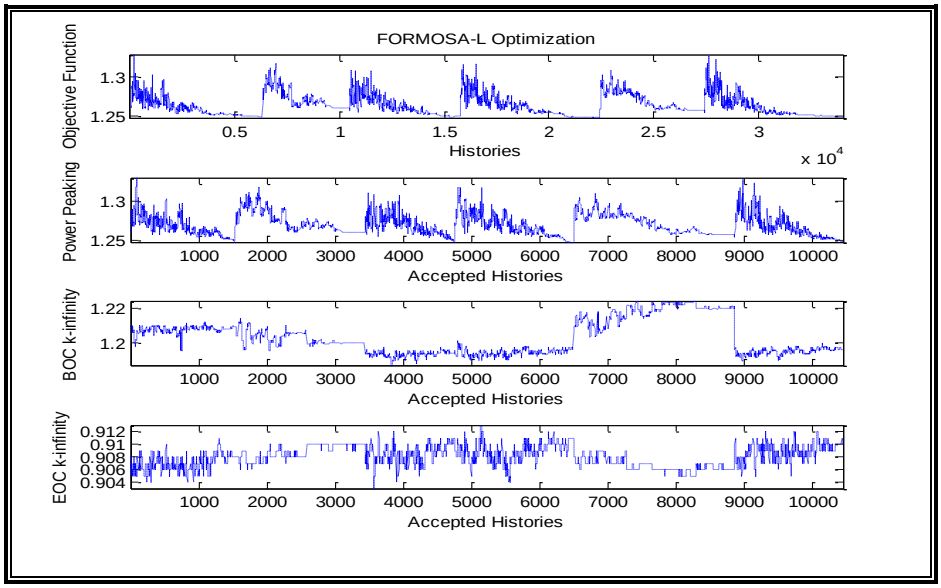

Figure 4:3 BWR lattice optimization with americium recycling

A general tendency observed was the reduction of the BOC U-235 content within the spiked pins in order to maintain the reactivity at the first burn up steps with added americium. In general, the requirements of U-235 enrichment are low in the americium pins, 2.70 to 3.00 wt. %, to maintain BOC reactivity. This low U-235 enrichment requirement enabled the americium content to increase to an average of around 6.3 w/o and up to 6.96 wt. % in one pin location. Important to point out is the fact that the optimized lattice without gadolinium shows higher reactivity at BOC and, ultimately, later in life. The smoother overall "reactivity swing" exhibited by the spiked lattices could ultimately translate into simpler and less stringent control blade pattern requirements, as show in Figure 4.4. Figure 4.5 shows the increment of the power peaking factor at approximately 30 GWd/MTHM mainly attributed to a significant formation of Pu-239, a fissile isotope that directly enhances the heat load.

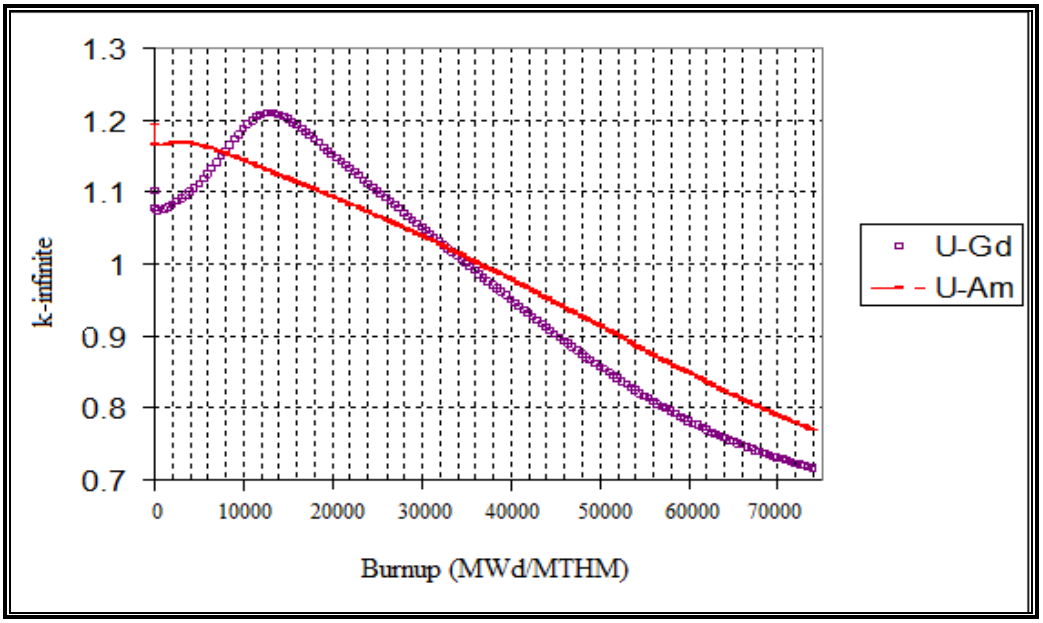

Figure 4:4: Contrast of k_∞ profile for lattice with americium or gadolinium

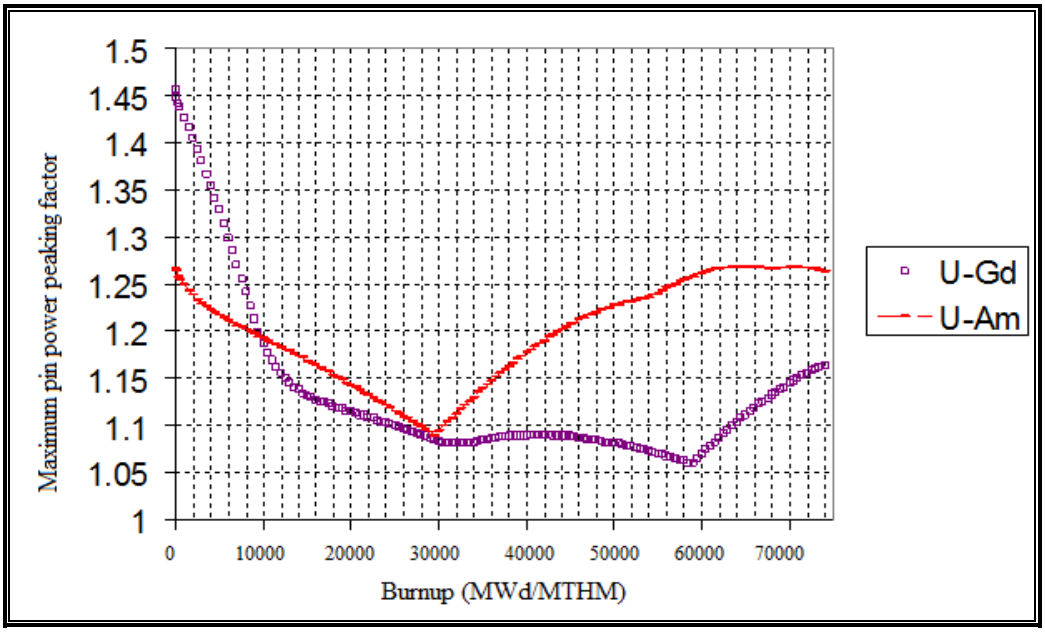

Figure 4:5 Maximum power peaking factor for UO2 lattices with Am or Gd

Analyzing one UO_2 pin with 4.90 wt. % U-235 enrichment from the reference assembly and one UO_2 pin with 2.80 wt. % U-235 enrichment and AmO_2 with 6.96 wt. % of Am, the data extracted from PHOENIX illustrates an overall americium reduction of about 88% at 50 GWd/MTHM. At this burnup the more significant transuranics found in the spent fuel are shown in Table 4.2 with their percentage respect to the total amount they represent; plutonium is the most abundant vector with 72.47 a/o. In particular, Pu-238, the most predominant MA and the most abundant after U-238 in the spent fuel, the table shows 27.35 a/o for this transuranic. Cm-242 is formed by the most common transmutation of Am-241 in Am-242 and contributes considerably to the creation of Pu-238 by alpha decay, Cm-242 is the second more abundant radioisotope of the curium vector after Cm-244.

Table 4:2 Transuranic vector with relative percentages obtained using PHOENIX

Radioisotope	UO2 pin, relative (a/o)	UO2 pin with Am, relative (a/o)
Np-237	5.06	0.73
Np-238	0.01	0.00
Np-239	0.55	0.12
Pu-238	**2.15**	**27.35**
Pu-239	43.01	15.53
Pu-240	27.05	11.83
Pu-241	12.16	4.16
Pu-242	7.17	13.61
Am-241	0.59	2.68
Am-242	0.00	0.01
Am-242 m	0.01	0.05
Am-243	1.49	8.68
Cm-242	0.20	1.98
Cm-243	0.00	0.14
Cm-244	0.52	12.15
Cm-245	0.02	0.65
Cm-246	0.00	0.35

Figure 4.6 illustrates the process of producing pure Pu-238 by loading a light water reactor assembly with americium (*Sasahara et al. 2004*).

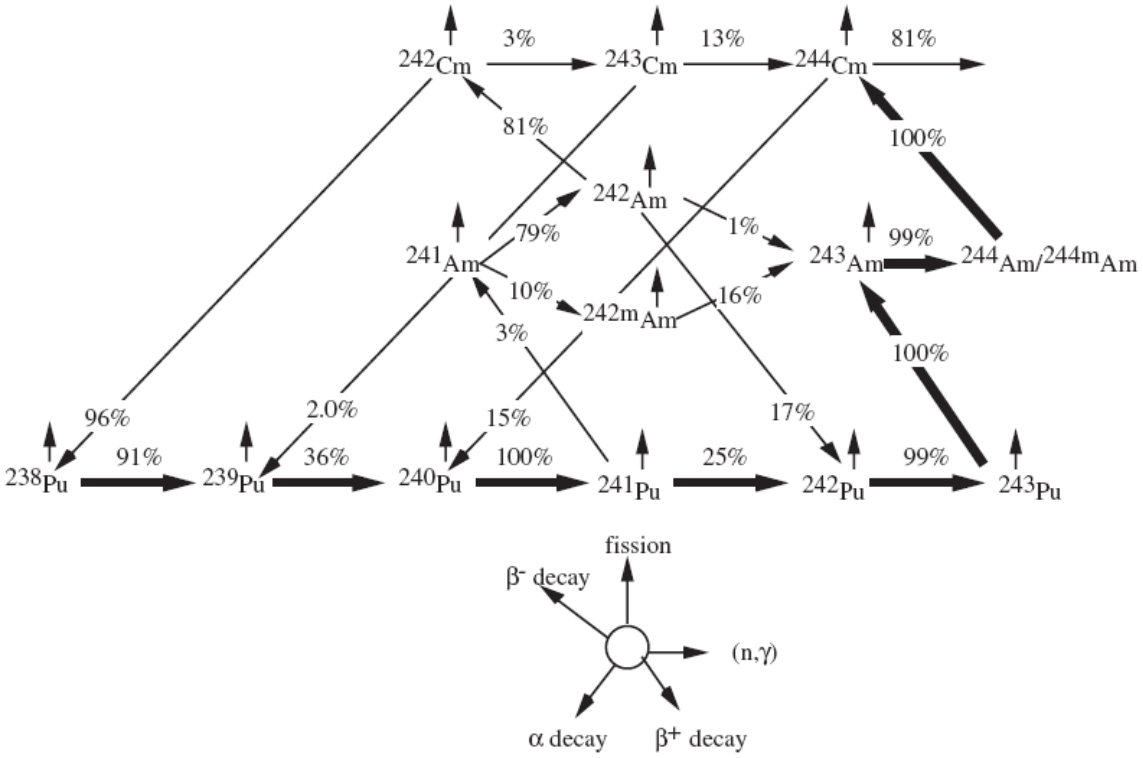

Figure 4:6 Americium transmutation chain in a thermal reactor (Sashara et al. 2004)

The amount of Np-237 is relative low and directly correlated to the U-235 amount at the BOC; low enrichments of U-235 imply less production of Np-237. Thus, a reactor with high U-235 enrichment is more suitable for the production of this radioisotope.

4.2 PWR Lattice Optimization

A UO_2 PWR lattice was chosen to carry out optimization studies with FORMOSA-L. This lattice was selected by carefully analyzing the UO_2 loading pattern used in the PWR MOX/UO_2 core transient numerical benchmark (*Kozlowski, 2006*), from which the core analysis is based. All the assembly simulations were carried out using the lattice deterministic depletion code TRITON from the SCALE package (*DeHart M. 2008*) in order to characterize the lattices with reactivity and pin power as a function of burnup. The UO_2 lattices were arbitrary loaded with 4 and 24 NpO_2+ZrO_2 rods in symmetrical positions; the strategy was to insert these rods in the guide tubes in order to have a better manipulation of the actinides that are initially loaded, such that the targets could be withdrawn after a specific fuel irradiation according to the isotopic vector produced, as Np-237 is depleted. This would be done to achieve a reasonable concentration of Pu-238 while minimizing the production of other undesirable minor actinides.

The UO_2 assembly with 4.5 wt% of U-235 enrichment was chosen to be optimized by using the FORMOSA-L code coupled to the lattice physics code simulator PHOENIX. These results were then validated with TRITON.

An important observation was that the burnup-dependent reactivity of the 4.5 wt % U-235 assembly with 4 NpZr rods was similar to the UO_2 assembly with 4.2 wt % U-235 enrichment. The evaluation in the 3D core environment is based on the substitution of UO_2 assemblies with

4.2 wt % U-235 in core locations where there are not control rods. This is because the guide tubes would be occupied with lattices that are loaded with Minor Actinides as Np-237 and/or americium. As observed, the insertion of neptunium in a lattice configuration has a penalty in excess reactivity, which was analyzed by increasing the number of NpO_2+ZrO_2 rods or by increasing the volume concentration of neptunium with respect to zirconium in each rod, which causes a k-infinite reduction as a function of burnup. A simple spatial lattice optimization of the Np-237 loading produced a minimization in the maximum pin power peaking factor by symmetrically relocating the 4 NpO_2+ZrO_2 rods in the 24 available positions of the water rod channels.

For the analysis with americium loadings, a 17x17 PWR UO_2 lattice designed by Siemens with gadolinium bearing rods was modified by substituting americium in the gadolinium locations using the already optimized lattice configuration loaded with 4 NpO_2+ZrO_2 rods and without the use of IFBA rods. Three different optimized lattices with low, medium and high content of americium were obtained. In general, a higher concentration of americium gives a minor initial reactivity jump, but the maximum pin power peaking factor increases to a value comparable to that obtained with a MOX fuel assembly, or even more for the results obtained with the lattice with higher americium contents.

4.2.1 Depletion Capabilities of the SCALE Code Using TRITON

The use of the generalized-geometry discrete-ordinates transport code NEWT can help model the behavior of Light Water Reactor fuel containing weapons-grade mixed-oxide (MOX) fuel with a high level of accuracy. The TRITON sequence, based on the NEWT transport solver can perform two-dimensional lattice calculations for non traditional lattice designs, including hexagonal arrays. The neutron transport solution available within NEWT, coupled with the accuracy of ORIGEN-S depletion capabilities within TRITION, provides a rigorous first-principle approach for the calculation of few group collapsed and lattice homogenized cross sections for fuel designs. The TRITON sequence starts with cross-section processing operations according to the mixtures and a cell structure defined in the input, and uses the Bondarenko method (BONAMI) to calculate resonance self-shielding in the unresolved resonance evaluation. CENTRM/PMC modules are used for resolved resonance evaluation. The produced cross-section library is used in the NEWT calculation and the transport solution is followed by COUPLE and ORIGEN-S calculations. NEWT creates a three-group weighted library based on calculated and volume-averaged fluxes for each mixture. COUPLE updates the ORIGEN-S cross-section library with cross-section data read from the weighted library. Three-group fluxes calculated by NEWT are supplied to ORIGEN-S for depletion calculations. COUPLE/ORIGEN calculations are repeated for each mixture being depleted, as specified in input, using mixture-specific cross-section data and fluxes. Used in conjunction with TRITON, NEWT can generate a library of cross sections as a function of burnup, with a branch capability that provides cross sections at each burnup step for perturbations in moderator density, fuel and moderator temperatures, boron concentration, and control-rod insertion or removal (*De Hart Mark D., 2007*)

4.2.2 Specifications of the Reference PWR Lattices

Based in the NEACRP L-335 Pressurized Water Reactor benchmark proposed by Finneman in 1991 (*Finneman, 1991*), a nuclear reactor core loaded partially with weapons-grade MOX is modeled with four types of assemblies: two assemblies loaded with UO_2 with uniform U-235 enrichment of 4.2 and 4.5 wt. % in a 17 x 17 pin loading pattern and 104 integral fuel burnable absorbers (IFBA) rods, and two MOX assemblies loaded with fissile plutonium to 4.0 and 4.3 wt. %. On the average, each assembly has 24 wet annular burnable absorber (WABA) rods located in the control rod tubes of the 17x17 pin loading pattern. IFBA consists of a thin zirconium diboride (ZrB_2) coating applied on the outer surface of the UO_2 pellet and does not reduce the core heavy metal inventory because does not displace the uranium from the fuel matrix. Also, B-10 is used as a burnable absorber does not produce any residual absorber isotopes following its depletion, having an intermediate thermal absorption cross-section between erbium and gadolinium. IFBA does not need to be concentrated in a few rod locations favoring a smoother intra-assembly power distribution (*Franceschini et al, 2009*). The IFBA are located in the highest worth regions: the vicinity of guide tubes and corners of the assembly where they provide reactivity control over a short burnup period. WABA consists of an annular pellet of Al_2O_3-B_4C with a wet (water-filled) central region and Zircaloy cladding. In contrast to IFBA, WABA provides relatively long-term reactivity control (*Kozlowski,et at, 2006*). Table 4.3 shows the pin material composition for the different assemblies' configuration. Other materials included in the UO_2 assemblies are the control rods inserted in 24 symmetrical locations. The MOX assemblies do not have reactivity insertion instead the WABA rods are inserted in the guide tubes. Table 4.4 shows the physical characteristics of other materials used in the assembly

configuration for its consequent numerical simulation. Table 4.5 shows the geometrical dimensions for the pin configurations and table 4.6 shows the material composition for each pin type. The pin pitch is 1.26 cm and the design radial pin peaking (F_H) is 1.528 with a maximum pin burnup of 62,000 MWd/MTHM.

Table 4:3 Pin material composition specifications

Pin type	**Density (g/cm^3)**	**Composition**
UO_2	10.24	U-235 4.2 or 4.5 wt. % U-238 95.8 or 95.5 wt. %
UO_2 / IFBA	10.24 1.69	U-235 4.2 or 4.5 wt. % U-238 95.8 or 95.5 wt. % ZrB_2 (B-10/B-11= 19.9/80.1 wt. %)
MOX	10.41	Uranium vector: 234/235/236/238 0.002/0.2/0.001/99.797 wt. % Plutonium vector 239/240/241/242 93.6/5.9/0.4/0.1 wt. %
WABA	3.5635	AlO_2-B_4C, 10.0 wt. % B_4C

Table 4:4 Other assembly material specifications

Material type	**Density (g/cm^3)**	**Composition**
Control rod	1.84	B_4C (B-10/B-11= 19.9/80.1 wt. %)
Gap	0.001	O-16
Pin clad	6.504	Zircaloy -2
Coolant	0.71187	Water at 580 K and 15.5 MPa

Table 4:5 Pin cell dimensions in cm

Cell type/radius	Fuel	IFBA	Guide tube	Control rod	WABA
r_1	0.3951	0.3951	0.5624	0.4331	0.2858
r_2	0.4010	0.3991	0.6032	0.4839	0.3531
r_3	0.4583	0.4010		0.5624	0.4039
r_4		0.4583		0.6032	0.4839
r_5					0.5624
r_6					0.6032

Table 4:6 Pin cell material regions

Cell type/ region	Fuel	IFBA	Guide tube	Control rod	WABA
$r_1 - 0$	Fuel	Fuel	Water	Control rod	Water
$r_2 - r_1$	Gap	IFBA	Clad	Clad	Clad
$r_3 - r_2$	Clad	Gap		Water	WABA
$r_4 - r_3$		Clad		Clad	Clad
$r_5 - r_4$					Water
$r_6 - r_5$					Clad

Figure 4.7 and figure 4.8 show the top right of the UO_2 and MOX lattice configuration, respectively, (1/4 symmetry) simulated in TRITON. Under hot full power (HFP) conditions, each pin is surrounded by water with density=0.71187 g/cm^3 and temperature=580 K. The pin pitch = 1.26 cm, while the assembly pitch = 21.42 cm. The water rod channels are used for the insertion of control rods banks in the UO_2 assemblies. For the MOX assemblies, WABA pins substitute the control rods during the entire lattice burnup as a long-term reactivity control. The two different MOX fuel assemblies contain average military-weapon fissile plutonium of 4.0 and 4.3 wt. % respectively. The MOX assemblies do not have IFBA rods, and the periphery fuel rods

contain less fissile plutonium compared to the centered pins, being the less reactive elements located at the corner of the assembly.

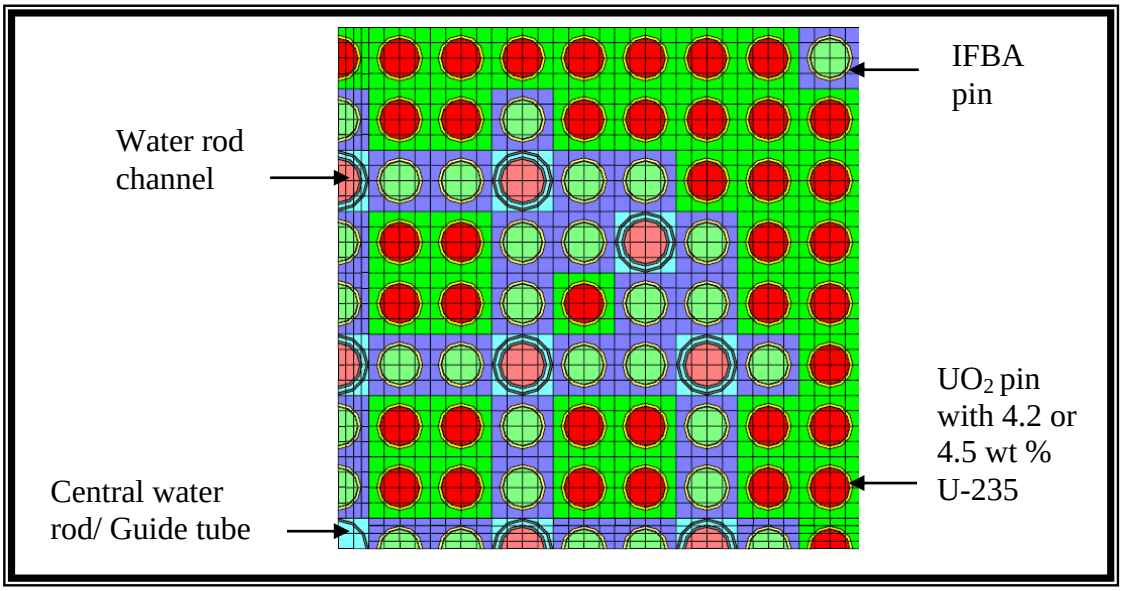

Figure 4:7 UO_2 assembly configuration (1/4 symmetry)

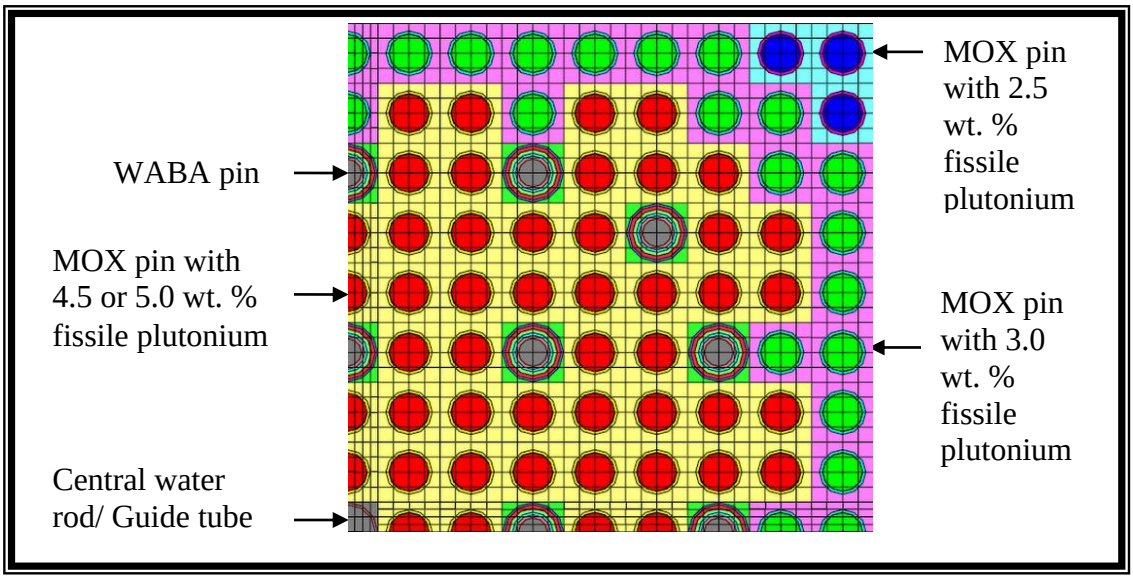

Figure 4:8 MOX assembly configuration (1/4 symmetry)

4.3 $NpO_2 + ZrO_2$ pins loaded in water channel rods of UO_2 PWR assemblies

The standard UO_2 PWR assembly was loaded with 4 $NpO_2 + ZrO_2$ targets placed in symmetric locations in the guide tubes. The material cladding and the rod diameter for the Np-Zr rods are the same used for a UO_2 pin pellet. The initial composition of NpO_2 in the mixture is 20% vol. The NpO_2 density = 11.16 g/cm^3 (*Nishi Tsuyosi, et.al. 2008*) and the ZrO_2 density = 6 g/cm^3. Figure 4.9 shows the pin placement of the $NpO_2 + ZrO_2$ rods for a ¼ symmetrical lattice configured in TRITON.

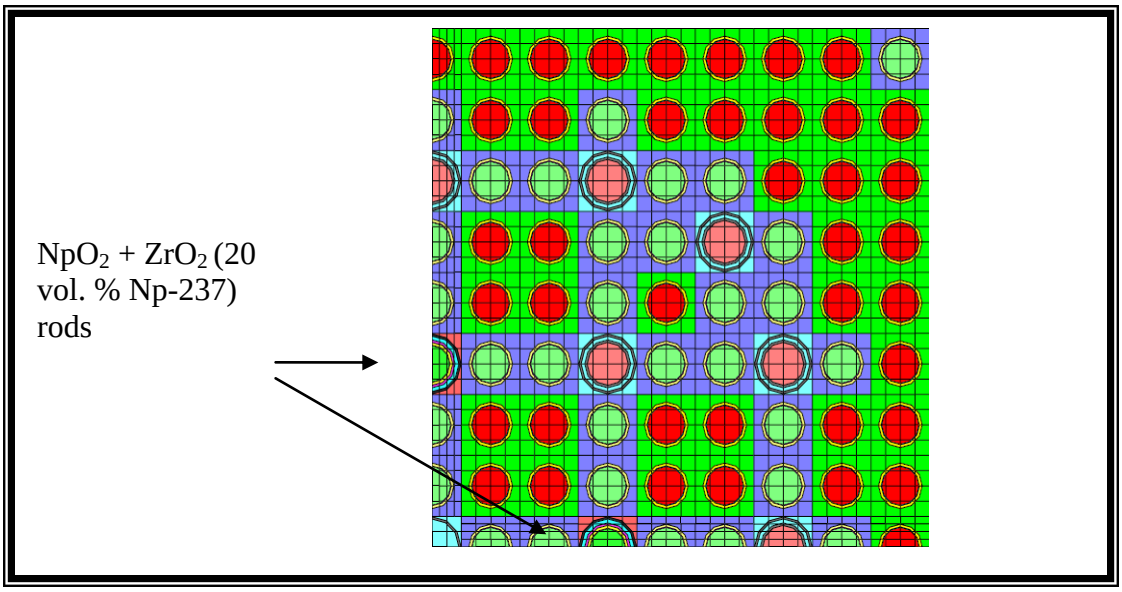

Figure 4:9 UO_2 assembly with four NpO2 + ZrO_2 rods (1/4 symmetry)

The UO_2 assemblies with and without NpO_2 + ZrO_2 rods were simulated under standard hot full power conditions: density=0.71187 g/cm^3, fuel temperature=900 K, and boron concentration=0 ppm. Figure 4.10 shows the reactivity behavior as a function of burnup. The assembly loaded with 4.2 wt. % of U-235 enrichment (UO4.2) shows a similar behavior with respect to the UO_2 assembly loaded with 4.5 wt. % of U-235 enrichment with 4 NpO_2 + ZrO_2 rods (UO24.5 with 4 Np-Zr rods). An extra 0.3 wt. % of U-235 is required to compensate the penalty in reactivity of inserting Np-237 in the assembly. The k-infinite behavior of the of U-235 enrichment with 4 NpO_2 + ZrO_2 rods assembly focused our analysis to carry out an optimization analysis with minor actinides loading and utilize this assembly instead of the UO_2 assembly loaded with 4.2 wt. % of U-235 enrichment in the 3D core configuration.

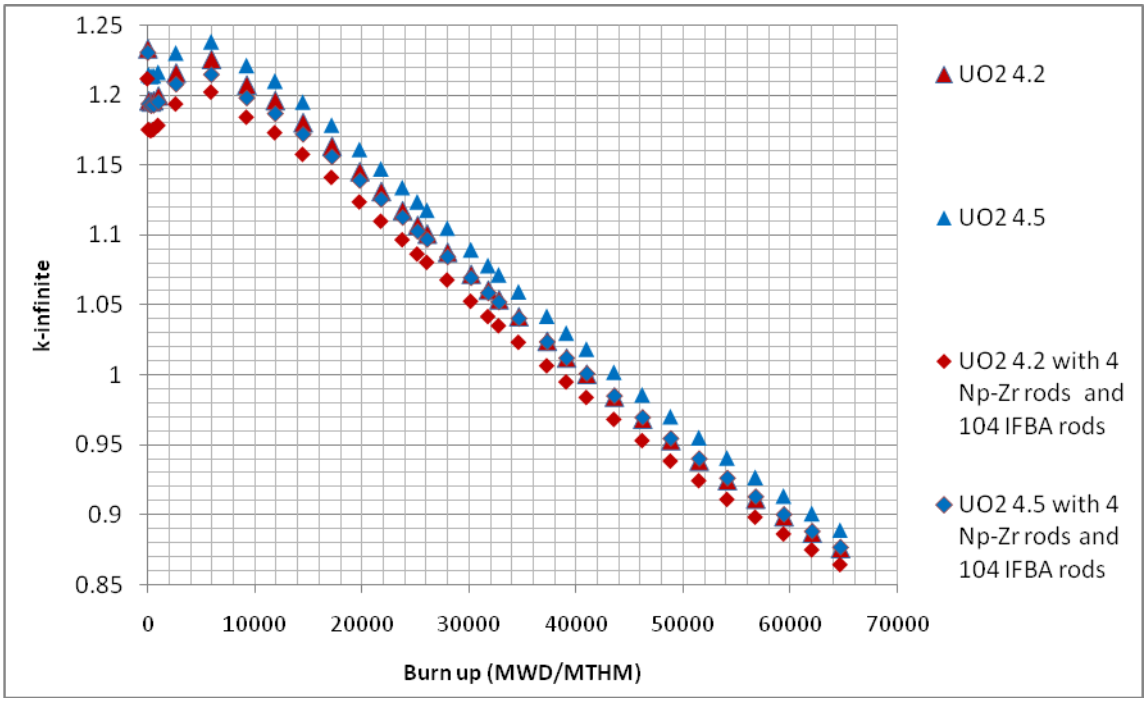

Figure 4:10 k_∞ for 4.2% and 4.5% UO_2 assemblies and four NpO_2+ZrO_2 rods

The UO_2 lattices loaded with 4 Np-Zr rods were also simulated with PHOENIX, but it was not possible to simulate the IFBA rods effects in the assemblies for lack of information. Although the initial reactivity behavior cannot be correctly captured, the k-infinite profile for upper burn ups is very similar for the lattices simulated in TRITON, as shown in figure 4.11, especially for the UO_2 assemblies with 4.5 wt. % of U-235 enrichment. Figure 4.12 shows that PHOENIX can accurately reproduce this reactivity behavior with UO_2 assemblies without IFBA rods. This feature is in some sense useful for a spatial lattice optimization. In Figure 4.12, it can also be observed the reactivity penalty of inserting 24 NpO_2 + ZrO_2 in the assembly.

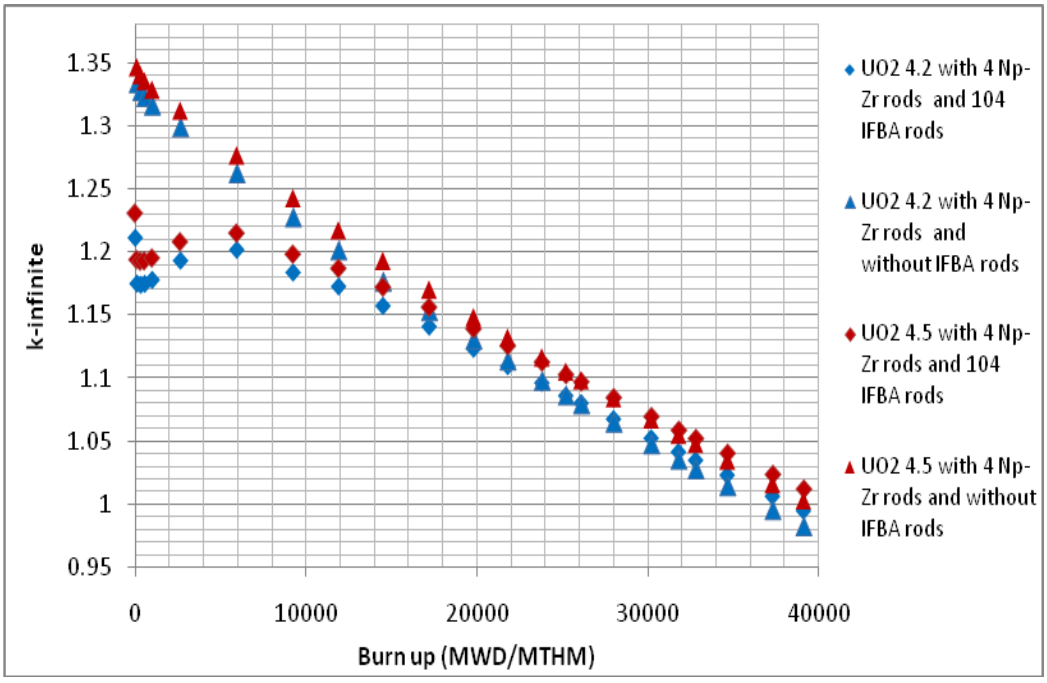

Figure 4:11 Simulating UO_2 lattices in TRITON without IFBA rods

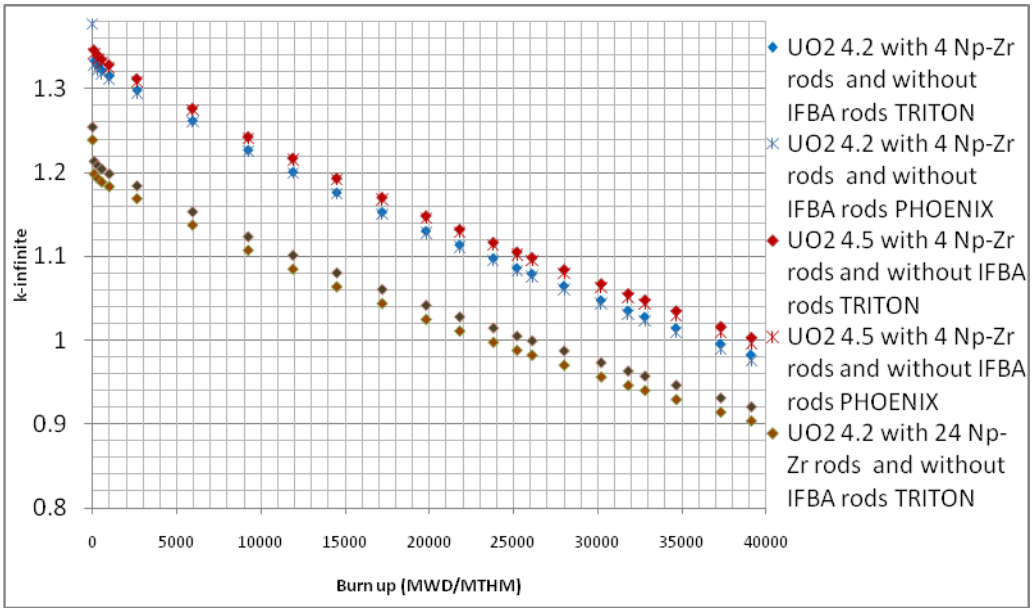

Figure 4:12 UO2 assembly simulation with PHOENIX without IFBA rods

4.4 Optimized lattice with 4.5 wt. % of U-235 and four NpO_2 + AmO_2 rods

A single spatial assembly optimization with respect to the pins with NpO_2 + AmO_2 placed symmetrically in 4 of 24 locations occupied by the water channel tubes was carried out to minimize the maximum pin power peaking factor. A better assembly was obtained by placing the Np-Zr at the corners of a centered 8x8 pin configuration, as shown in figure 4.13.

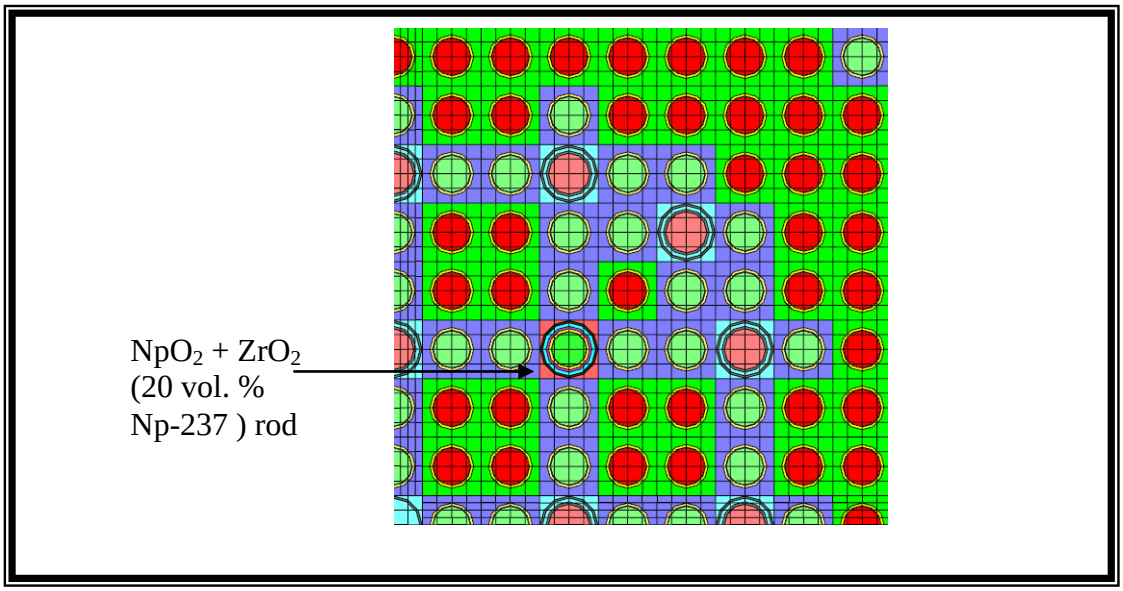

Figure 4:13 Optimized lattice with 4.5 w/o U-235 and four NpO_2+AmO_2 rods

Figure 4.14 shows the maximum pin power peaking factor reduction obtained by simulating the initial and optimized assemblies in TRITON. The optimized assembly loaded with Np-237 can also even aproach the same maximum power peaking factor with respect to the UO_2 lattice with 4.2 wt. % of U-235 enrichment toward the end of cycle. Figure 4.15 shows that the optimized lattice conserves the same k-infinite profile as a function of burnup with respect to the reference assembly.

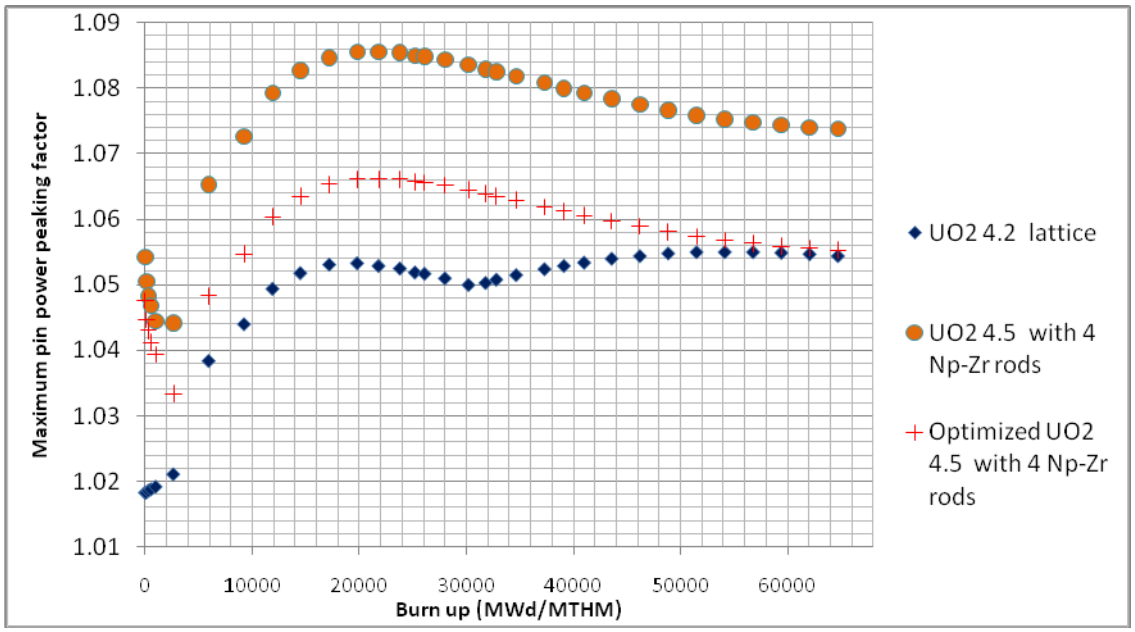

Figure 4:14 FORMOSA-L power peaking minimization for 4.5 w/o U-235 lattice with four NpO_2+AmO_2 rods

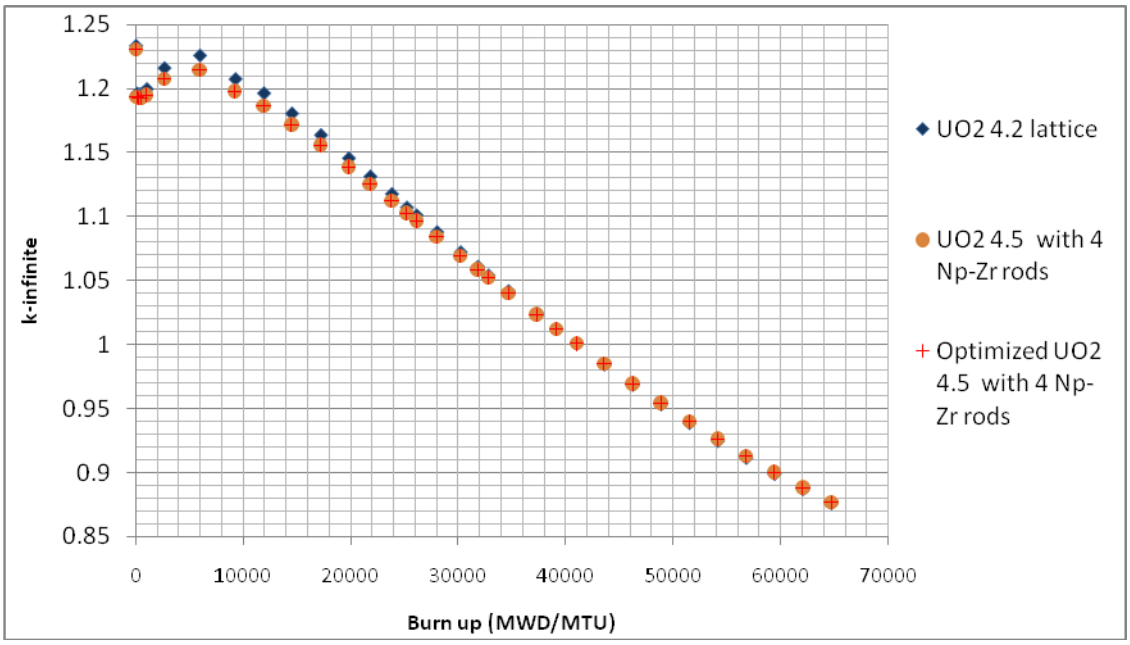

Figure 4:15 k-infinite profile for optimized UO2 lattice with four NpO_2 + AmO_2 rods

An increased amount of Np-237 with respect to zirconium was explored with FORMOSA-L, as well, but as it can be observed in figure 4.13, a higher percentage in Np-237 with respect to zirconium decreases the k-infinite value.

4.5 Optimized lattices with blended americium and four NpO_2 + ZrO_2 rods

Figure 4.16 shows a 17x17 PWR Siemens design with gadolinium bearing rods. There are 6 rods with 4 wt. % and16 rods with 8 wt% of Gd_2O_3 (*Sanders et al. 2002*). These rods are placed strategically by forming rings close to the water rod channels to shape the assembly's power.

As table 4.2 shows for the BWR optimized lattice, Pu-238 is the most abundant radioisotope in the transuranic vector of the BWR americium recycling case. Thus, the possibility of recycling americium and neptunium in a PWR lattice was also explored. Similar to the analysis carried out with the BWR assembly, the gadolinium pins were substituted by spiked pins with minor actinides, forming a set of 3 different assemblies; configurations with low, medium and high americium content and by placing the 4 NpO_2 + ZrO_2 rods with 20 vol. % of zirconium in the corner of an 8x8 pin array around the assembly' instrumentation tube.

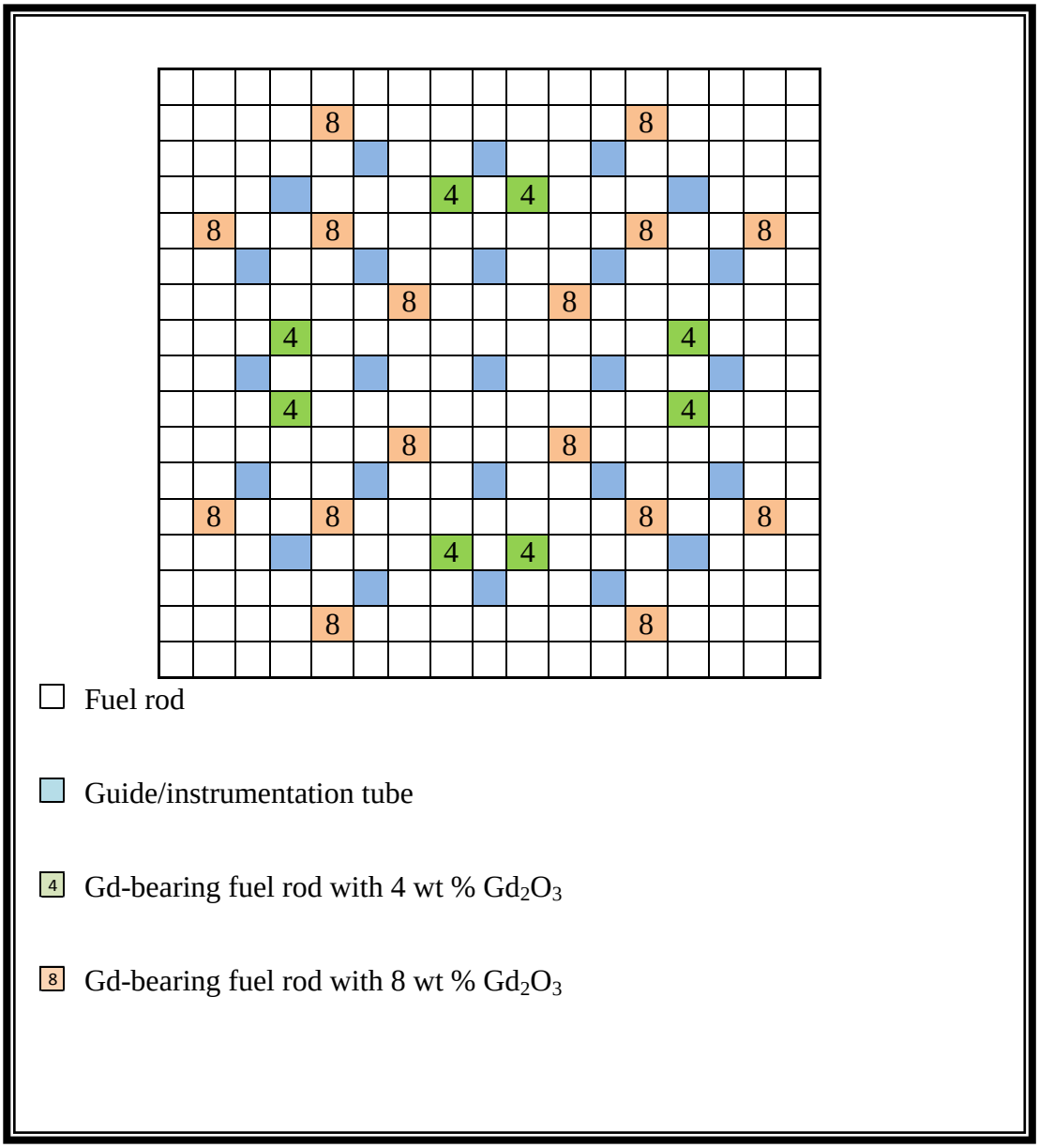

Figure 4:16 PWR lattice loading pattern with gadolinium loadings (17x17)

Table 4.7 shows the set the pin material composition of the 3 optimized lattices resulted of FORMOSA-L, while figures 4.17 to 4.19 show the geometrical pin placement using quarter-assembly symmetry.

Table 4:7 Initial isotopic composition UO_2 optimized lattices with Am-Np (wt. %)

Assembly type	# of rods	Mixture	U-235	Am	Am-241	Np-237	Zr
UO2/Np-Zr & low Am content	244	UO_2	4.8	0	0	0	0
	16	UO_2+AmO_2	4.93	1.7	1.46	0	0
	4	UO_2+AmO_2	5	1.8	1.54	0	0
	4	NpO_2+ZrO_2	0	0	0	27.28	50.7
UO2/Np-Zr & medium Am content	244	UO_2	4.95	0	0	0	0
	20	UO_2+AmO_2	4.7	3	2.57	0	0
	4	NpO_2+ZrO_2	0	0	0	27.28	50.7
UO2/Np-Zr & high Am content	244	UO_2	5	0	0	0	0
	16	UO_2+AmO_2	4.9	4	3.43	0	0
	4	UO_2+AmO_2	4	4.8	4.12	0	0
	4	NpO_2+ZrO_2	0	0	0	27.28	50.7

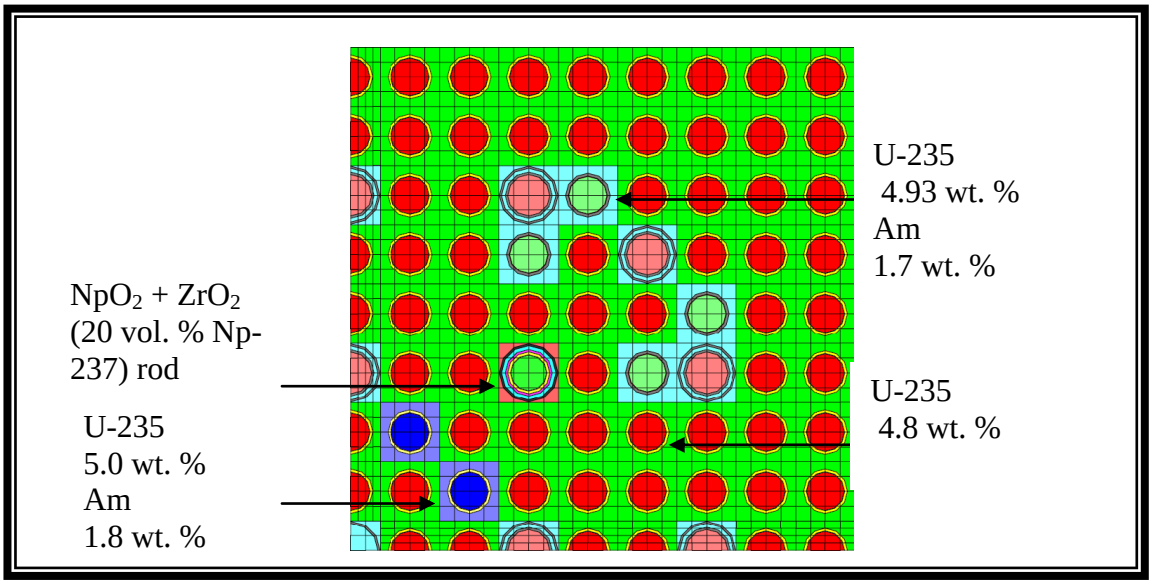

Figure 4:17 Optimized lattice with NpO_2 and low Am content

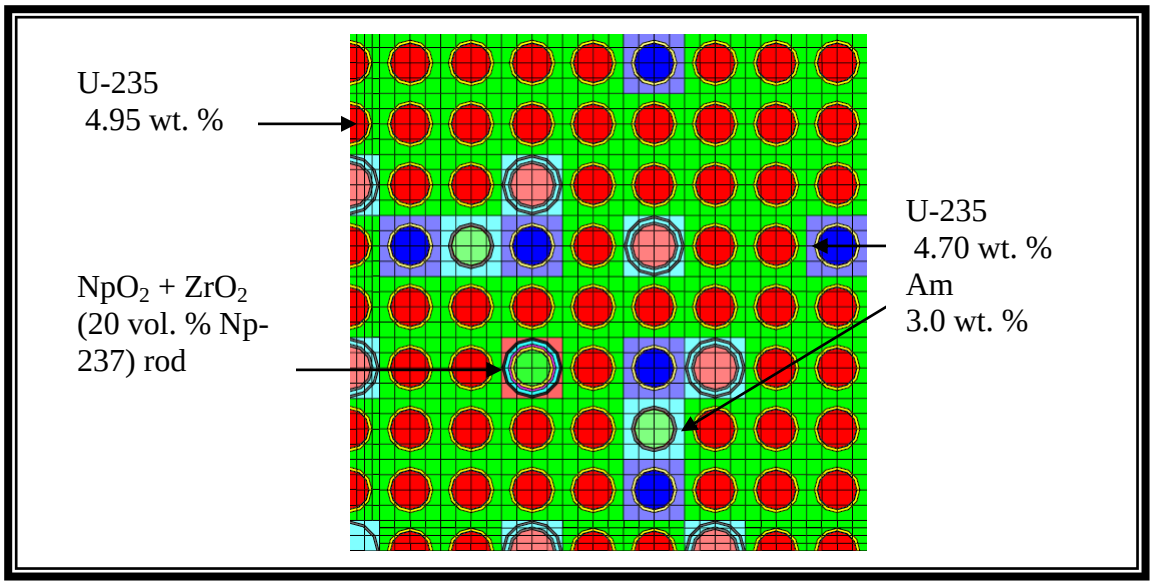

Figure 4:18 Optimized lattice with NpO_2 and medium Am content

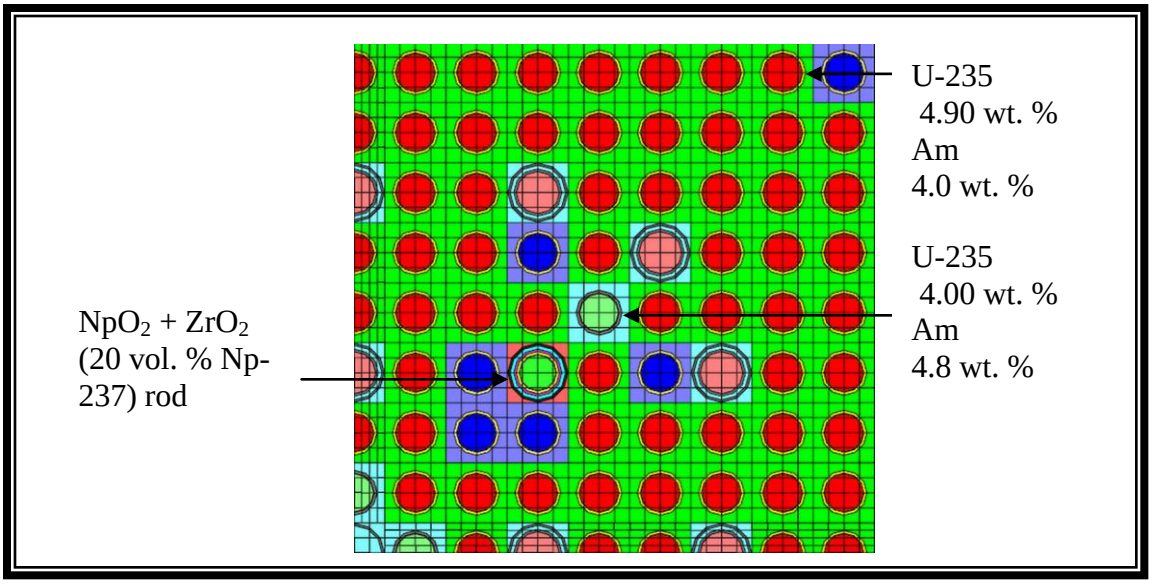

Figure 4:19 Optimized lattice with NpO_2 and high Am content

4.5.1 Evaluation of k_∞ profiles

The k-infinite profile as a function of burnup was forced to follow the same profile as that of the UO_2 lattice with 4.2 wt. % of U-235 enrichment. In general, all the optimized lattices configurations follow the same k-infinite behavior as a function of burnup, with the exception of the lattices loaded with americium, where low loading amounts of this minor actinide at the BOC give a higher k-infinite jump that can be diminished by increasing the pin's americium content. This behavior ultimately can be translated in higher power relative values during a 3D core simulation. The higher americium loading, however, is constrained to a maximum of 5.0 wt. % of U-235 enrichment (current legal limit for commercial fuel manufacturing facilities). Figure 4.20 shows the k-infinite profile for these various assembly configurations.

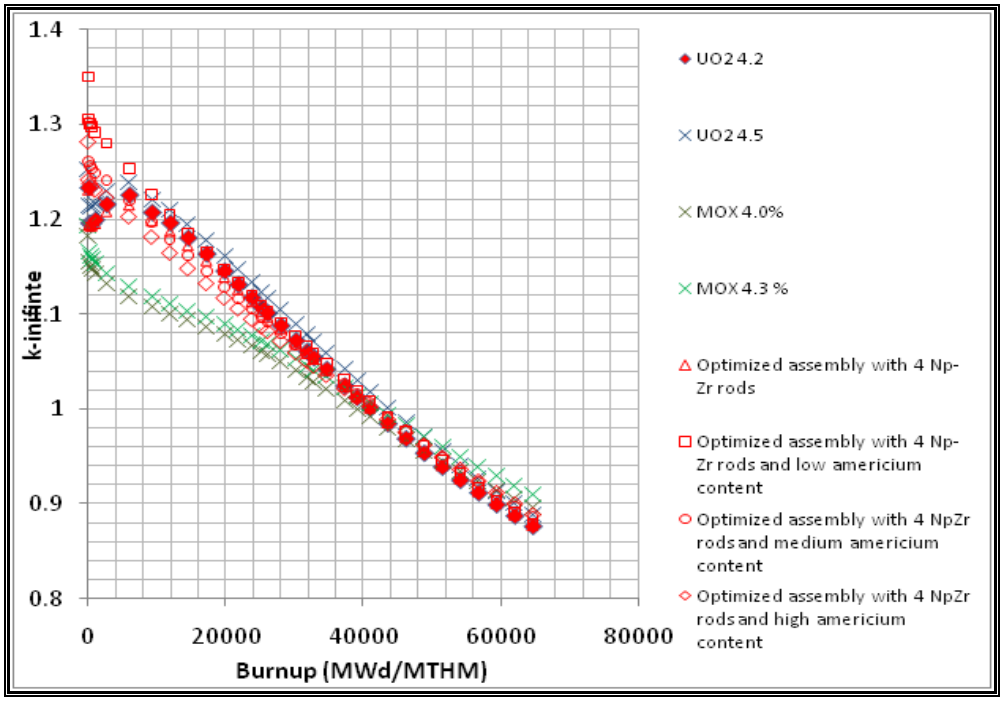

Figure 4:20 k_∞ profile for the different lattice configurations

4.5.2 Maximum pin power peaking factor

The constraint in maximum pin power peaking factor for a PWR lattice is equal to 1.550 (*Alim Fatih et al. 2008*). For the optimization scheme this parameter was minimized to be below the limit while trying to keep it as low as possible, especially toward the EOC where the fuel pellet has been under more mechanical stress. The lattices with americium-spiked pins show higher maximum pin power peaking factors that are due mainly to Pu buildup. The optimized lattice with high americium content is the one with the greatest power peaking value even above the MOX fuel values, with a maximum peak of 1.25 at the EOC as shown in Figure 4.21. Note that this lattice also has pins capped at 5.0 wt. % of U-235 enrichment.

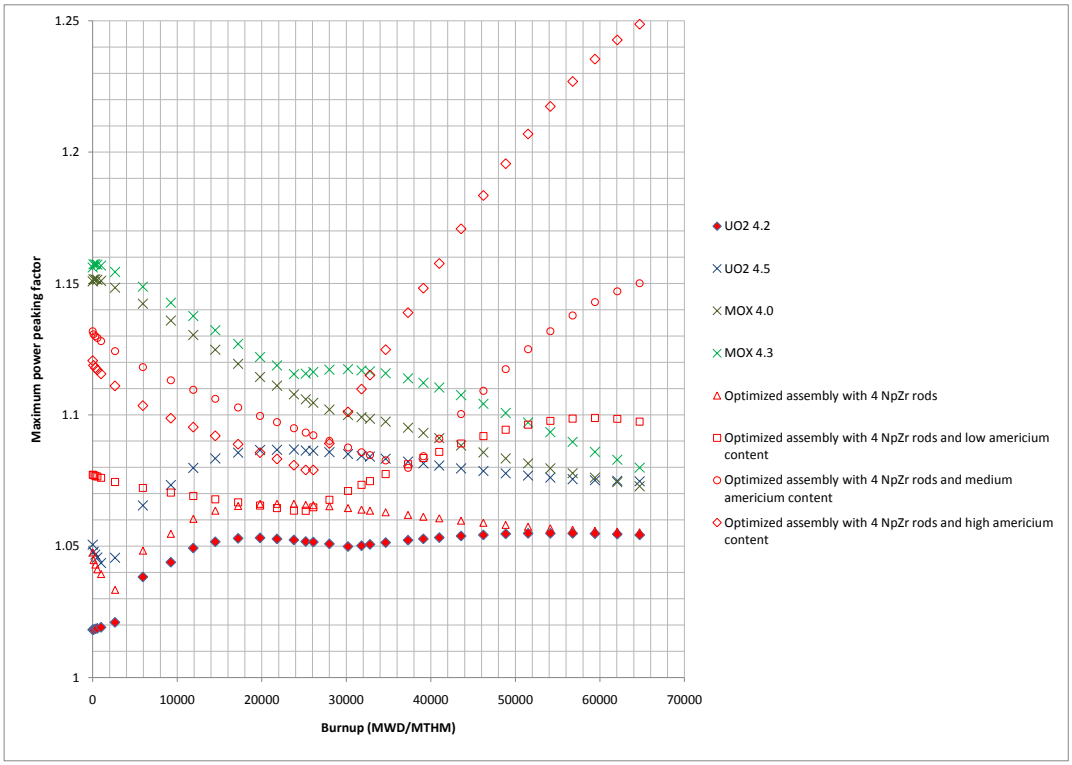

Figure 4:21 Maximum power peaking profile for various lattice configurations

5 Lattice to Core Coupling with the NESTLE Full Core Simulator

Via collaboration between NCSU, ORNL, and UT, the NESTLE three-dimensional simulator code (*Electric Power Research Center, 2003*) has been adopted at ORNL and is now being maintained and upgraded to develop an end-to-end capability for three dimensional LWR and CANDU analysis (Maldonado, 2009a, 2009b). Two main adaptations were performed to this diffusion-based nodal expansion method code to accurately benchmark a well-known and modern OECD reference PWR core with 1/3 MOX loading: first, the development of an interface for coupling the results from the TRITON lattice physics code to a format required for NESTLE to simulate the arrangement of these lattices in a family of bundles for a three-dimensional simulation. This utility code developed for the coupling is named TRITON-TO-NESTLE, or T2N for short. The second modification was the implementation of thermodynamic tables to substitute the original polynomials that represent equations of state in the NESTLE code in order to have a better radial and axial water density map as a function of the coolant temperature distribution for this specific case simulated in steady-state conditions.

5.1 The Triton to Nestle Interface

The TRITON to NESTLE "T2N" interface code links the two-dimensional TRITON lattice physics output binary file: xfile016 to the cross section data file of the three-dimensional reactor core simulator NESTLE. In this process, the lattice simulation is carried out with TRITON with the appropriate perturbation branches, and two-group (energy) collapsed and (spatial) homogenized cross sections are transferred for the core-wide diffusion equation and nodal

expansion method based numerical solution.

The branches in TRITON account for cross sectional changes due to:

1. Fuel temperature
2. Moderator temperature
3. Moderator density
4. Boron concentration
5. Control rods (in/out)

The macroscopic model represents macroscopic cross-section for a given fuel color (fuel type), burnup (exposure), and rod insertion condition as a Taylor's Series expansion in terms of coolant density, coolant temperature, effective fuel temperature and soluble poison number density as follows:

$$\Sigma_{xg} = a_{1xg} + \sum_{n=1}^{2} a_{(n+1)xg}(\Delta\rho^n) + a_{4xg}\Delta T_C + a_{5xg}\Delta\sqrt{T_{Feff}} + \sum_{n=1}^{3} a_{(n+5)xg}\left(\Delta N_{sp}\right)^n \qquad (6.1)$$

where:

Σ_{xg}	**Macroscopic cross-section for reaction type *x* and energy group *g* without transient fission products corrected to local conditions**
$a_{j_{xg}}$	**Expansion coefficients**
$\Delta\rho = \rho_C - \rho_C^0$	**Change in coolant density from reference condition**
$\Delta T_C = T_C - T_C^0$	**Change in coolant temperature from reference condition**
$\Delta\sqrt{T_{F_{eff}}} = \sqrt{T_{F_{eff}}} - \sqrt{T_{F_{eff}}^{(0)}}$	**Change in square root of effective fuel temperature from reference condition**
$\Delta N_{sp} = N_{sp} - N_{sp}^0$	**Change in soluble poison number density from reference condition**

The soluble poison number density increment accounts for both: soluble poison concentration (ppm) and coolant density (ρc). The reference boron concentration is given in (ppm) and the coefficients for the cross section file are calculated with equation 6.2.

$$\Delta solp = \frac{N_A(a/o)\left[NSP - XS\%REFB\right]}{A_{sol}\rho_{ppm}} * 1\times10^{-24}\times1x10^{-6} \qquad (6.2)$$

where

$\Delta solp$ = incremental value in boron from reference

N_A = Avogadro's number

(a/o)= abundance in soluble poison

A_{SOL} = soluble poison atomic weight

NSP =specific boron concentration (ppm)

XS%REFB = reference boron concentration (ppm)

ρ_{ppm} = moderator density (g/cm^3)

After 0.15 MWd/MTHM an equilibrium level of xenon and samarium is assumed. For this purpose, NESTLE uses the effective yield from the TRITON binary file (xfile016) for the yields of I-135 and Xe-135. The T2N subroutine performs the calculation of the macroscopic cross sections coefficients, which corresponds to an over-determined system of equations (more branches are available than the polynomial approximation for a specific physical property). The subroutine finds the values of the coefficients that give the minimum reduced chi-square value with the data points that are supplied from the lattice physics calculation. The nonlinear parameters are obtained by an optimally combined gradient search and linearization procedure

(the Marquardt algorithm). The linear parameters are then determined by the standard multiple linear regression approach with the previously fixed nonlinear parameters (*Bevington, P.R., 1969*).

5.1.1 Lattices Simulated in TRITON and NESTLE with Boron Feedback

The k-effective comparisons was carried out by simulating 2D assemblies in NESTLE with the use of TRITON cross sections (2 group energy collapsing, cutoff energy of 0.625 eV) against the results obtained by simulating the lattices with TRITON at Hot Full Power (HFP) conditions: coolant density = 0.71187 g/cm3, fuel temperature=900 K and coolant temperature=580 K. The PCM differences are all negative after 0 days of burn up referenced to TRITON cross sections and can be attributed to a mismatch in Xe and Sm strategies between the two codes.

The boron feedback was validated in NESTLE by simulating the assemblies at HFP conditions with reference boron at 1000 ppm and with thermo-hydraulic feedback on, maintaining the other physical properties approximately unchanged. The boron concentrations were changed in the NESTLE control parameters input to compare with those performed with the branches of TRITON. For TRITON the physical properties considered are for coolant density = 711.87kg/m^3, fuel temperature = 900 K, coolant temperature=580 K and for NESTLE the physical properties are: coolant density = 711.87 kg/m^3, average fuel temperature = 904.934 K, average coolant temperature= 579.97 K. Tables 5.1 to 5.4 shows the similarities in k_∞ for each assembly simulated in NESTLE compared to the reference values in TRITON.

Table 5:1 k_∞ results for 4.2 % U-235 UO_2 lattice at HFP for a range of boron letdown

	k-infinite Lattice simulated in TRITON			k-infinite NESTLE simulation			PCM difference TRITON/T2N		
Burnup	Boron Concentration (ppm)								
(MWd/MTHM)	0	1000	2000	0	1000	2000	0	1000	2000
99	1.19611	1.11043	1.03799	1.198144	1.11141	1.03838	-203.4	-98	-39
17200	1.16362	1.07653	1.00381	1.16661	1.077829	1.004048	-299	-129.9	-23.8
19800	1.14551	1.05913	0.98714	1.148587	1.060681	0.987438	-307.7	-155.1	-29.8
23800	1.11758	1.03228	0.9614	1.120232	1.033404	0.961367	-265.2	-112.4	3.3
32800	1.05393	0.97102	0.90262	1.056729	0.972296	0.902912	-279.9	-127.6	-29.2
34655	1.04169	0.95922	0.8913	1.044254	0.960245	0.891351	-256.4	-102.5	-5.1
37300	1.02421	0.94239	0.87515	1.026658	0.943359	0.875	-244.8	-96.9	15

Table 5:2 k_∞ results for 4.5 % U-235 UO2 lattice at HFP for a range of boron letdown

	k-infinite Lattice simulated in TRITON			k-infinite NESTLE simulation			PCM difference TRITON/T2N		
Burnup	Boron Concentration (ppm)								
(MWd/MTHM)	0	1000	2000	0	1000	2000	0	1000	2000
99	1.21453	1.13113	1.06019	1.216597	1.132304	1.060585	-206.7	-117.4	-39.5
17200	1.17857	1.09392	1.02275	1.181668	1.09535	1.023083	-309.8	-143	-33.3
19800	1.16109	1.07702	1.00647	1.164244	1.078664	1.00688	-315.4	-164.4	-41
23800	1.13394	1.05079	0.98121	1.136778	1.051953	0.981335	-283.8	-116.3	-12.5
32800	1.07145	0.99034	0.92295	1.074474	0.991791	0.923258	-302.4	-145.1	-30.8
34655	1.05932	0.97859	0.91162	1.061977	0.979769	0.911733	-265.7	-117.9	-11.3
37300	1.04191	0.96173	0.89537	1.044548	0.962832	0.895393	-263.8	-110.2	-2.3

Table 5:3 k_∞ results for 4.0 % MOX lattice at HFP for a range of boron letdown

	k-infinite Lattice simulated in TRITON			k-infinite NESTLE simulation			PCM difference TRITON/T2N		
Burnup	Boron Concentration (ppm)								
(MWd/MTHM)	0	1000	2000	0	1000	2000	0	1000	2000
99	1.15476	1.10814	1.07349	1.156727	1.110121	1.074526	-196.7	-198.1	-103.6
17200	1.08678	1.0306	0.9968	1.089541	1.032417	0.997684	-276.1	-181.7	-88.4
19800	1.07934	1.02284	0.98729	1.082109	1.024444	0.98826	-276.9	-160.4	-97
23800	1.06616	1.00926	0.97127	1.06876	1.010772	0.971802	-260	-151.2	-53.2
32800	1.0285	0.96681	0.92874	1.031082	0.968035	0.929306	-258.2	-122.5	-56.6
34655	1.02053	0.95411	0.92	1.02298	0.955306	0.920281	-245	-119.6	-28.1
37300	1.00842	0.94492	0.90694	1.010739	0.946022	0.907167	-231.9	-110.2	-22.7

Table 5:4 k_∞ results for 4.3 % MOX lattice at HFP for a range of boron letdown

	k-infinite Lattice simulated in TRITON			k-infinite NESTLE simulation			PCM difference TRITON/T2N		
Burnup	Boron Concentration (ppm)								
(MWd/MTHM)	0	1000	2000	0	1000	2000	0	1000	2000
99	1.1652	1.12319	1.08611	1.167137	1.124652	1.087091	-193.7	-146.2	-98.1
17200	1.09668	1.05066	1.01052	1.099424	1.052422	1.011552	-274.4	-176.2	-103.2
19800	1.0894	1.04237	1.00144	1.092282	1.044243	1.002473	-288.2	-187.3	-103.3
23800	1.07687	1.0284	0.98639	1.079481	1.029936	0.987168	-261.1	-153.6	-77.8
32800	1.04153	0.99045	0.94656	1.044172	0.992016	0.947289	-264.2	-156.6	-72.9
34655	1.03401	0.98249	0.9383	1.036494	0.983873	0.938847	-248.4	-138.3	-54.7
37300	1.02247	0.97041	0.92586	1.024886	0.971652	0.926284	-241.6	-124.2	-42.4

5.2 Using Sub-cooled Water Thermodynamic Tables in NESTLE

The hydrodynamic model for a PWR used in NESTLE is based in the mass and energy continuity equations assuming constant pressure and modeled as a single phase coolant flow up closed coolant channels (*Electric Power Research Center, 2003*). The one-dimensional, mass continuity equation along a specified homogeneous channel for a radial node *ij* is:

$$A_C^{ij}(z)\frac{\partial \rho_C^{ij}(z,t)}{\partial t} = -\frac{\partial}{\partial z} G_C^{ij}(z,t) A_C^{ij}(z) \tag{6.1}$$

Similarly, the energy conservation equation assuming constant pressure is given by

$$A_C^{ij}(z)\frac{\partial}{\partial t}\left(\rho_C^{ij}(z,t)U_C^{ij}(z,t)\right) = -\frac{\partial}{\partial z}\left(G_C^{ij}(z,t)A_C^{ij}(z)U_C^{ij}(z,t)\right)$$

$$-P\frac{\partial}{\partial z}\left(\frac{G_C^{ij}(z,t)A_C^{ij}(z)}{\rho_C^{ij}(z,t)}\right) + q_S^{ij}(z,t)S_F^{ij} + q_C^{ij}(z,t)A_C^{ij}(z) \tag{6.2}$$

Where;

ρ_C^{ij} = coolant density

G_C^{ij} = coolant mass velocity

U_C^{ij} = coolant internal energy

q_C^{ij} = volumetric power density from heat deposited directly in the coolant

q_S^{ij} = fuel rod surface heat flux into the coolant

A_C^{ij} = total cross-sectional area for coolant flow within the node

S_F^{ij} = total fuel rod surface area per unit axial length within node

P = coolant pressure

The heat flux q_S is obtained using Newton's Law of Cooling:

$$q_S^{ij}(z,t) = h_{eff}^{ij}(z,t)\left(T_F^{ij}(z,t) - T_C^{ij}(z,t)\right) \tag{6.3}$$

where

T_C^{ij} = coolant temperature

T_F^{ij} = lumped (*i.e.* radial averaged temperature) fuel temperature

h_{eff}^{ij} = effective heat transfer coefficient

For steady-state conditions, the governing equations used to solve for the coolant and fuel conditions are obtained by setting the temporal derivative equal to zero and integrating along z over mesh products:

$$U_C^{l+1/2} = U_C^{l-1/2} - PA_{C_{In}}^{ij} G_{C_{In}}^{ij}\left(\frac{1}{\rho_C^{l+1/2}} - \frac{1}{\rho_C^{l-1/2}}\right) + \bar{q}_C^l V_C^l + \bar{q}_F^l V_F^l \tag{6.4}$$

where:

V_C^l and V_F^l are the coolant and fuel volume respectively.

This equation is solved for U_C^{l+n+1} at each radial node by sweeping in the direction of coolant flow.

Having obtained values for the coolant internal energy at the new time-step, the coolant densities are evaluated at the new time-step using a thermodynamic table for constant pressure because a thermodynamic state is defined by at least two thermodynamic properties. So, having predicted values of coolant internal energy, they are then utilized to update the coolant density, as noted previously. Also, the coolant temperature is determined based upon coolant internal energy,

using a thermodynamic table for sub-cooled fluid and the saturation temperature for saturated fluid.

Similarly the fuel energy conservation equation is

$$\bar{T}_F^l = \bar{T}_C^l + \left(\frac{V_F^l}{h_{eff}^l S_F^l \Delta z^l}\right) q_F^l \tag{6.5}$$

These equations are iteratively solved as new estimates of the flux become available, providing new estimates of the surface heat flux and volumetric heat densities. During these iterations the effective heat transfer coefficient is also updated, producing consistent values for the effective heat transfer coefficient and lumped fuel temperature.

For the lumped fuel temperature model to be utilized, the effective heat transfer coefficient must be evaluated. For steady-state conditions we can select the effective heat transfer coefficient such that the correct values of the lumped fuel temperature result, these temperatures determined utilizing a more detailed fuel pellet model. This implies the following:

$$\bar{q}_F A_F = h_{eff} S_F (\bar{T}_F - T_{C_{Ref}}) \tag{6.6}$$

One can now solve for h_{eff} given the values of $\bar{T}_F$and $\bar{q}_F$ for a fixed coolant temperature as follows.

$$h_{eff} = \frac{\bar{q}_F A_F}{S_F (\bar{T}_F - T_{C_{Ref}})} \tag{6.7}$$

Note that h_{eff} has been characterized as a function of $\bar{T}_F$since the fuel thermal conductivity and gap closure, both functions of fuel temperature, are the main reasons why h_{eff} changes. This characterization is captured using a polynomial representation as follows:

$$h_{eff} = 0.1578\,\bar{T}_F{}^2 - 2.92x10^{-5}\bar{T}_F + 7.37x10^{-9} \tag{6.8}$$

with the effective heat transfer coefficient in kW/ft^{2}F and average fuel temperature in F.

For steady-state calculations, an initial estimate of fuel temperature (F) is obtained by characterizing it as a function of linear power density (kW/ft) in terms of the following polynomial:

$$T_F = 569.56\, q^2 + 169.64\, q - 2.917 \tag{6.9}$$

Given this initial lumped fuel temperature estimate, the effective heat transfer coefficient can be evaluated. Then *Equation 6.6* can be used to calculate a new estimate of the lumped fuel temperature once the node average coolant temperature and volumetric heat density have been evaluated. As the flux solution is iterated, this sequence of calculations is repeated. The iteration of the thermal-hydraulic equations not only addresses feedback between its solution and the neutronic solution, but also addresses the nonlinearities in calculating the lumped fuel temperature due to effective heat transfer coefficient dependency on fuel temperature.

6 Three-Dimensional Full Core Numerical Simulation

A three-dimensional simulation was carried out using the TRITON assembly simulation parameters coupled to NESTLE. The results for hot full power calculations (HFP) and critical boron search were benchmarked against those obtained with a numerical benchmark of several participant institutions (*Kozlowski and Downar, 2006*). The required operational and safety parameters were calculated for different core configurations loaded with AmO_2 and/or NpO_2 and selected core refueling patterns that met these criteria to carry out a material balance with the use of TRITON. The results at the end of cycle (50 GWd/MTHM) show a Np-237 to Pu-238 conversion rate of about 33% and an Am-241 incineration rate of roughly 96 % at the end of cycle.

6.1 Simulation of the OECD benchmark with a third load of MOX fuel

The Pressurized Water Reactor (PWR) core herein employed to test the various tools involved in this thesis work is based upon a numerical benchmark designed to assess the ability of modern reactor kinetics codes to predict the transient response of a core partially loaded with mixed oxide (MOX) fuel to a control rod ejection transient (*Kozlowski and Downar, 2006)*. The benchmark employs many of the characteristics of the NEACRP L-335 PWR benchmark proposed by Finnemann in 1991 (*Finneman, 1991*). The benchmark participants used the latest versions of nuclear data sets and the most advanced core simulators. The methods varied from few-group nodal diffusion and multi-group heterogeneous transport calculations to continuous-energy Monte Carlo calculations of the heterogeneous core's configuration.

Computational benchmarks based on a well defined problem with a complete set of input and a

unique solution is often used as a mean of verifying the reliability of numerical solutions. The Nuclear Science Committee of the OECD Nuclear Energy Agency (NEA) has in the past organized a series of numerical and experimental benchmarks to verify the current level of accuracy in pin-power calculations and to identify the relative merits of various calculation methods. It is essential to accurately calculate the pin-power of a reactor core with a high degree of accuracy in order to make the correct decisions regarding the core design, burnup cycle and safety margins. In the numerical benchmark nine participating groups provided twelve solutions using the latest versions of nuclear data sets and various advanced core simulation methods. Most solutions were submitted with the two-group nodal diffusion methods (the codes CORETRAN, EPISODE, NUREC, PARCS and SKETCH-INS). An additional multi-group nodal diffusion calculation was performed with PARCS and multi-group cell homogeneous transport solutions were performed with BARS and DORT. Cell heterogeneous transport calculations were performed with De-CART and MCNP using deterministic and stochastic solutions, respectively.

The core is based in a simplified 3D geometry with uniform fuel in axial direction and axial reflector of the same width as the fuel assembly pitch. The axial reflector has fixed moderator at the same condition as the core inlet and outlet for the bottom and top respectively. The axial boundary condition is zero flux. The core is surrounded by a single row of reflector assemblies of the same width as the fuel assembly pitch. The outer radial boundary condition is zero flux. General rules are applied to the partial MOX assemblies loading as no placing fresh MOX on the core periphery, no MOX assemblies facing each other, no MOX assemblies in control rod position, maximum 1/3 of the core loaded with MOX fuel and no IFBA rods in MOX

assemblies. Table 6.1 shows the assembly loading scheme for a three batch equilibrium cycle of approximately 18 months and figure 6.1 shows the radial core configuration for ¼ symmetry.

Table 6:1 OECD benchmark core loading distribution (Kozlowski et al. 2006)

Assembly type	Fresh fuel 0 GWd/MTHM	Once-burned 20 GWd/MTHM	Twice-burned 35 GWd/MTHM
UO_2 4.2%	28	28	17
UO_2 4.5%	24	24	20
MOX 4.0%	8	8	4
MOX 4.3%	12	12	8
Total	72	72	49

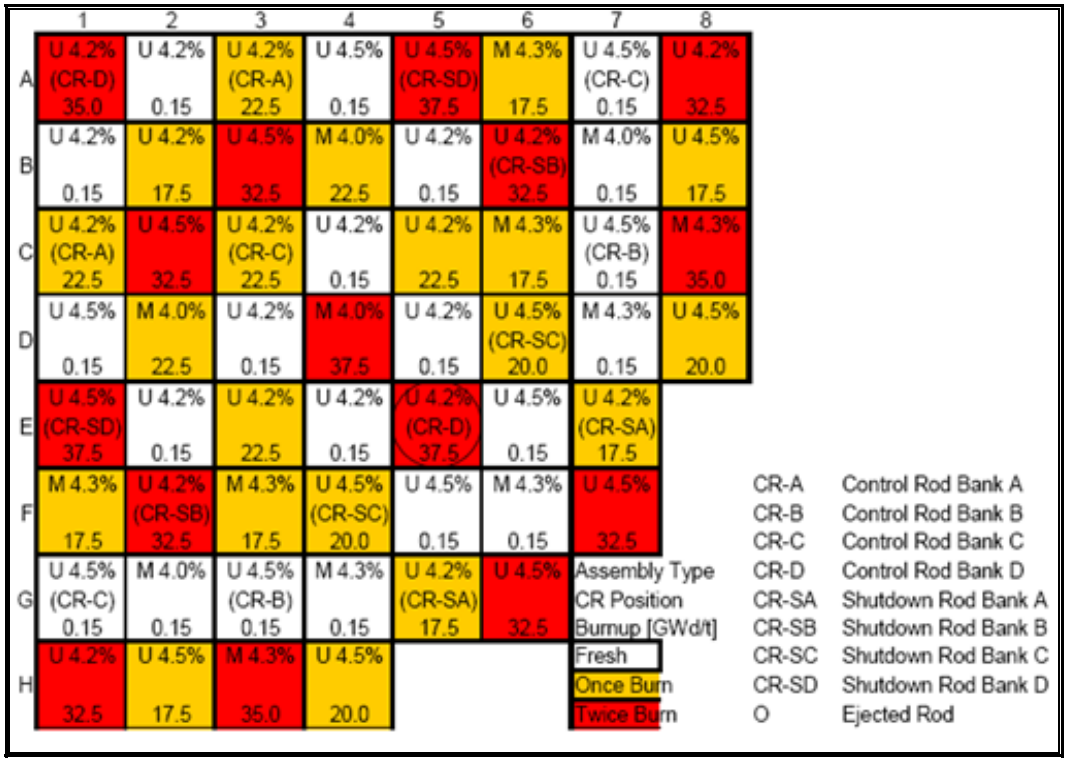

Figure 6:1 OECD benchmark core radial loading pattern (Kozlowski et al. 2006)

The typical parameters of Westinghouse fuel assemblies in which the core simulation was based are shown in table 6.2 (Kozlowski Tomas et al. 2006).

Table 6:2 Typical parameters of the PWR fuel assemblies

Number of fuel assemblies	193
Power level (MW_{th})	3565
Core inlet pressure (MPa)	15.5
Hot full power (HFP) core average moderator temperature (K)	580
Hot zero power (HZP) core average moderator temperature (K)	560
Hot full power (HFP) core average fuel temperature (K)	900
Fuel lattice, fuel rods per assembly	17x17, 264
Number of control rod guide tubes	24
Number of instrumentation guide tubes	1
Total active core flow (kg/sec)	15849.4
Active fuel length (cm)	365.76
Assembly pitch (cm)	21.42
Pin pitch (cm)	1.26
Design radial pin-peaking (F_H)	1.528
Design point-wise peaking (F_Q)	2.5
Core loading (tHM)	81.6
Capacity factor (%)	90
Target discharge burn-up (GWd/tHM)	40 to 50
Maximum pin burn-up (GWd/tHM)	62

6.2 3D Core Benchmark

The assemblies were simulated with TRITON with branches for the different physical parameters from the reference condition and by following the simulation points of the 3D diagram, as shown in figure 6.2. The polynomial fit results were coupled to NESTLE by the T2N subroutine. A 3D numerical simulation was carried out with a critical boron search at hot full power conditions (HFP): core power of 100.00% rated power (3,565 MWth), inlet coolant temperature of 560 K, inlet pressure of 15.5 MPa and equilibrium Xenon-Samarium.

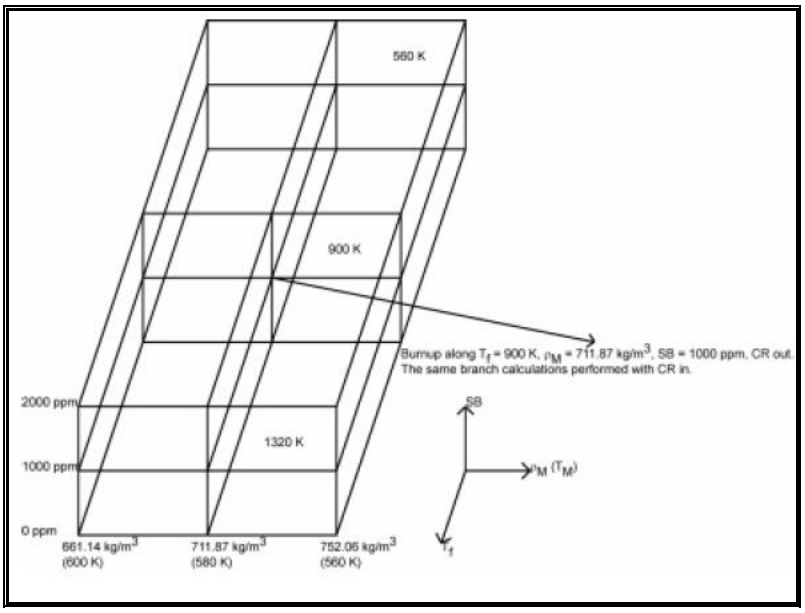

Figure 6:2 3D diagram of lattice physics branches (Kozlozwki et al. 2007)

The results show a good agreement compared to other heterogeneous codes, as shown in table 6.3, for the mean physical parameters, while table 6.4 shows the error distribution for the radial relative power, Doppler temperature, coolant temperature and coolant density radial maps.

Table 6:3 Critical boron and mean physical parameters for HFP 3D benchmark

Code	Critical boron concentration (ppm)	Doppler temperature (K)	Moderator density (kg/m^3)	Moderator temperature (K)
NESTLE	1674	836	705	580.5
PARCS	1679	836	706	581.3
SKETCHS-INS	1675	837	705.5	580.9
CORETRAN 1	1647	908	706	581.0

Table 6:4 Radial core error distributions for three-dimensional benchmark at HFP

Parameter	%PWE	%EWE
Power relative	1.04	1.09
Doppler temperature	1.42	0.00
Coolant temperature	0.12	0.00
Coolant density	0.15	0.00

Figure 6.3 to 6.6 show the power relative, Doppler temperature (F), coolant temperature (F) and coolant density (kg/m3) maps in a ¼ symmetry for the numerical results of the core simulated with TRITON/NESTLE against the results of HELIOS/PARCS.

1.0923 1.096	1.3702 1.397	1.1873 1.191	1.3674 1.403	1.0139 1.020	1.1172 1.113	1.1176 1.1344	0.4861 0.485
1.3702 1.397	1.2521 1.257	1.0696 1.071	1.1966 1.193	1.3011 1.326	0.973 0.968	1.1149 1.1056	0.5795 0.58
1.1873 1.191	1.0696 1.071	1.1685 1.171	1.3344 1.359	1.209 1.201	1.1924 1.168	1.1124 1.1167	0.4846 0.4785
1.3674 1.403	1.1966 1.193	1.3344 1.359	1.0656 1.057	1.2893 1.303	1.1796 1.159	1.0056 0.9855	0.4015 0.3985
1.0139 1.020	1.3011 1.326	1.209 1.201	1.2893 1.303	0.9316 0.925	1.1229 1.128	0.6446 0.6349	
1.1172 1.113	0.9729 0.968	1.1924 1.168	1.1796 1.159	1.1229 1.128	0.8409 0.839	0.3185 0.3189	
1.1176 1.134	1.1149 1.106	1.1123 1.117	1.0056 0.986	0.6445 0.635	0.3185 0.319		
0.4861 0.485	0.5795 0.580	0.4846 0.479	0.4015 0.399				

HELIOS/PARCS
TRITON/NESTLE

Figure 6:3 Assembly relative power map comparisons at HFP conditions

860.96 870.43	953.14 960.09	891.96 898.48	952.55 962.15	836.42 848.04	869.67 844.98	870.06 882.21	681.64 693.49
953.14 960.09	913.33 918.21	853.83 862.87	895.26 866.21	930.23 938.93	823.78 832.87	869.18 843.21	707.38 720.54
891.96 898.48	853.83 862.87	885.88 892.71	941.36 948.76	899.55 901.71	894.34 859.76	868.4 876.98	681.23 679.18
952.55 962.15	895.25 866.21	941.36 948.76	852.84 829.87	926.35 932.15	890.14 889.48	834.25 811.26	659 669.16
836.41 848.04	930.22 938.93	899.54 901.71	926.35 932.15	810.84 820.09	871.62 880.32	725.7 736.22	
869.66 844.98	823.77 832.87	894.33 859.76	890.13 889.48	871.61 880.32	783.33 772.50	637.36 646.91	
870.06 882.21	869.17 843.21	868.4 876.98	834.25 811.26	725.7 736.22	637.35 646.91		
681.64 693.49	707.37 720.54	681.23 679.18	658.99 669.16				

HELIOS/PARCS
TRITON/NESTLE

Figure 6:4 Doppler temperature (F) map comparisons at HFP conditions

582.89 582.30	588.14 587.84	584.81 584.13	588.31 588.11	581.63 581.02	583.81 582.93	583.94 583.39	570.84 570.35
588.14 587.84	585.98 585.31	582.56 581.87	585.15 584.29	587.18 586.77	580.95 580.12	583.91 582.88	572.86 572.33
584.81 584.13	582.56 581.87	584.51 583.79	587.73 587.32	585.48 584.49	585.33 584.01	583.86 583.07	570.82 570.23
588.31 588.11	585.15 584.29	587.73 587.32	582.65 581.74	587 586.37	585.07 583.82	581.74 580.53	569 568.54
581.63 581.02	587.18 586.77	585.48 584.49	587 586.37	580.04 579.21	583.92 583.19	574.21 573.43	
583.81 582.93	580.95 580.12	585.33 584.01	585.07 583.82	583.92 583.19	578.31 577.57	567.15 566.84	
583.94 583.39	583.91 582.88	583.86 583.07	581.73 580.53	574.21 573.43	567.15 566.84	HELIOS/PARCS	
570.84 570.35	572.86 572.33	570.82 570.23	569 568.54			TRITON/NESTLE	

Figure 6:5 Coolant temperature (F) map comparisons at HFP conditions

702.76 685.70	687.99 685.70	697.61 696.70	687.58 684.90	706.13 705.30	700.45 700.20	700.16 698.90	731.07 730.90
687.99 696.70	694.32 693.30	703.68 703.00	696.74 696.30	690.99 689.10	707.88 707.70	700.25 700.30	726.75 726.40
697.61 684.90	703.68 703.00	698.47 697.70	689.34 687.40	695.86 695.80	696.34 697.20	700.38 699.70	731.11 731.20
687.58 705.30	696.74 696.30	689.34 687.40	703.48 703.40	691.53 690.30	697.06 697.70	705.93 706.50	734.88 734.90
706.13 700.20	691 689.10	695.86 695.80	691.53 690.30	710.13 710.00	700.15 699.40	723.79 723.90	
700.45 698.90	707.88 707.70	696.34 697.20	697.06 697.70	700.15 699.40	714.37 714.00	738.63 738.50	
700.16 730.90	700.25 700.30	700.38 699.70	705.93 706.50	723.79 723.90	738.63 738.50	HELIOS/PARCS	
731.07 730.90	726.75 726.40	731.11 731.20	734.88 734.90			TRITON/NESTLE	

Figure 6:6 Coolant density (kg/m^3) map comparisons at HFP conditions

The relative axial power profile obtained was compared against PARCS. The results are very similar, as shown in figure 6.7. The top and bottom zones show the greater differences and could be attributed to the differences in the reflector simulation.

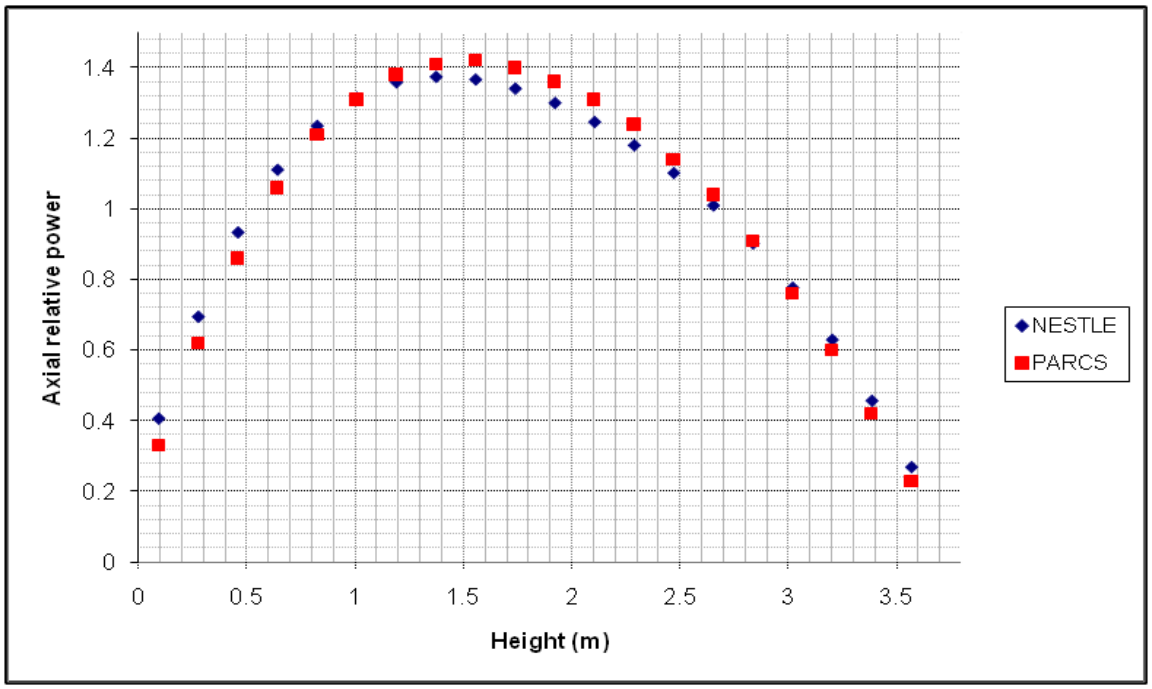

Figure 6:7 Benchmark results of axial relative power at BOC

6.3 Pressurized Water Reactor Constraints

For this particular PWR core, 8 constraints were analyzed for a correct and safe core operation (Turinsky Paul J., et al. 1999):

1. Maximum soluble boron concentration: This limit is imposed to limit the pH of the coolant which affects the clad corrosion rate. The critical boron is higher in the MOX core due to reduced effectiveness of neutron absorber in harder spectrum (Franceschini Fausto et al. 2008).
2. Maximum moderator temperature coefficient (MTC) is an operational parameter with safety considerations and is defined as the change of reactivity per degree change of the core-averaged moderator temperature. As a rule, MTC should be negative, as this ensures that negative feedback will be provided in the event of a power excursion. However, the value of MTC should not be too negative because during certain cool-down accident analyses in PWRs, limits are established based on how negative MTC may become during the fuel cycle. As a consequence, surveillance tests are performed at the plants during the fuel cycle to determine if the MTC complies with the specifications (Housaiads, C., et al. 2001). Numerically MTC is defined as:

$$MTC = \frac{\delta\rho}{\delta T_M} \tag{7.1}$$

where the change in reactivity is a function of the k-effective values:

$$\delta\rho = \frac{k_2 - k_1}{k_2 k_1} \tag{7.2}$$

and the change in moderator temperature coefficient between these two states is

$$\delta T_M = T_2 - T_1 \tag{7.3}$$

The overall MTC effect is determined by the interplay of competing trends. An increase in water temperature leads to a decrease in density, which in turn leads to a loss of moderation and introducing a negative reactivity. At the same time, the reactivity tends to become more positive since a decrease in density will cause a reduction in the absorption. The latter trend is particularly favored when an appreciable chemical shim, as soluble boron, is used since a decrease in density is translated directly to a proportional decrease in poison concentration and hence in absorption. The nuclear standard (ANS, 1997) recommends carrying out MTC measures in the range of $3 \leq \delta T_M \leq 5$ K. The cycle length of a full MOX core can be extended more easily than for a uranium core because of the more negative moderator temperature coefficient at BOC and the flatter power distribution, both (Tochihara et al. 1998).

3. Target end of cycle (EOC) soluble boron concentration: a way of stating the cycle energy production requirement.
4. Maximum feed enrichment limited to less than 5.0 wt. % U-235 in the rod design.
5. Maximum pellet, pin and node power densities.
6. Maximum pin, assembly, batch and region average discharge burnup limits to maintain pin integrity.
7. For assemblies with burnable absorbers content there is a maximum wt. % loading.
8. Doppler temperature coefficient: defined as the change in reactivity for change in fuel temperature. For the Doppler coefficient (C_D) calculation there are considered two fuel temperatures corresponding to hot zero power (HZP) and hot full power (HFP) conditions (Erradi L., et al. 2001) with the following formula used:

$$C_D = \frac{k_{eff}^{HFP} - k_{eff}^{HZP}}{k_{eff}^{HFP}\, k_{eff}^{HZP}\, \Delta T} \tag{7.4}$$

With $\Delta T = T^{HFP} - T^{HZP}$ and k_{eff} as the effective multiplication factor. The values are taken at a constant moderator temperature and coolant density (Ali Khan, 2000).

In a MOX core compared to UO_2 fuel larger negative MTC coefficients occur requiring additional shutdown capacity and the moderator void coefficient can become positive at plutonium contents of around 10 to 15 wt. % of heavy metal (*Koo et. Al., 1997*).

6.4 Numerical simulation of 3D core loaded with minor actinides

The strategy to replace the UO_2 with 4.2 wt. % of U-235 enrichment with bundles loaded with MAs is limited to few locations in the core. This is due to the limited number of UO_2 bundles with 4.2 wt. % of U-235 and because the bundles with MAs do not have to occupy sites with control rod banks. Two different core configurations were used; the central loading (CL) is specified in table 6.5 with 4 fresh and 4 once-burned bundles loaded with MAs and placed at the center of the core as shown in figure 6.8 with the bundles marked by the sign (*); these bundles are grouping each other and possibly could cause power relative peaking concerns, while the 4 twice-burned bundles were placed at the core periphery.

The second core configuration is the “ring of fire” (RF) loading which has bundles placed in a more distributed manner (figure 6.9). Note that the number of fresh and once-burned bundles increased to 8 with 4 twice-burned bundles, as specified in table 6.6.

The central loading core configuration with 4 fresh bundles (CL4), as well as the ring of fire core configuration with 8 fresh bundles (RF8), were each analyzed with four different core configurations corresponded to the type of MA content in the replaced bundles: Namely, with Np-237 (Np), with low Am and Np-237 (L), with medium Am and Np-237 (M), and with high Am and Np-237 (H). The first calculation for these two refueling strategies was a critical boron search 3D simulation with HFP conditions to obtain a power relative radial shape and maximum power relative values.

Table 6:5 Refueling strategy for 4 fresh fuel bundles with MAs

Assembly type	Fresh fuel 0 GWd/MTHM	Once-burned 20 GWd/MTHM	Twice-burned 35 GWd/MTHM
UO_2 4.2%	24	24	13
UO_2 4.5%	24	24	20
MOX 4.0%	8	8	4
MOX 4.3%	12	12	8
MAs	4	4	4
Total	72	72	49

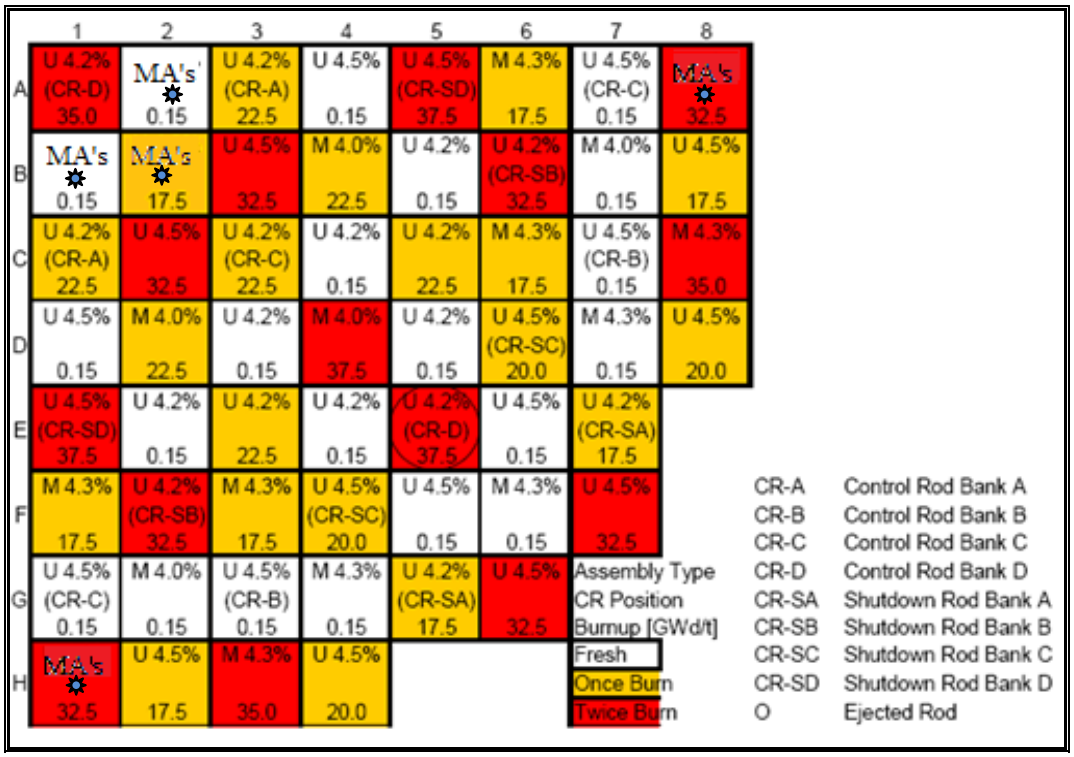

Figure 6:8 Central loading strategy with 4 fresh bundles with MAs

Table 6:6: Refueling strategy for 8 fresh fuel bundles with MAs

Assembly type	Fresh fuel 0 GWd/MTHM	Once-burned 20 GWd/MTHM	Twice-burned 35 GWd/MTHM
UO_2 4.2%	20	20	13
UO_2 4.5%	24	24	20
MOX 4.0%	8	8	4
MOX 4.3%	12	12	8
MAs	8	8	4
Total	72	72	49

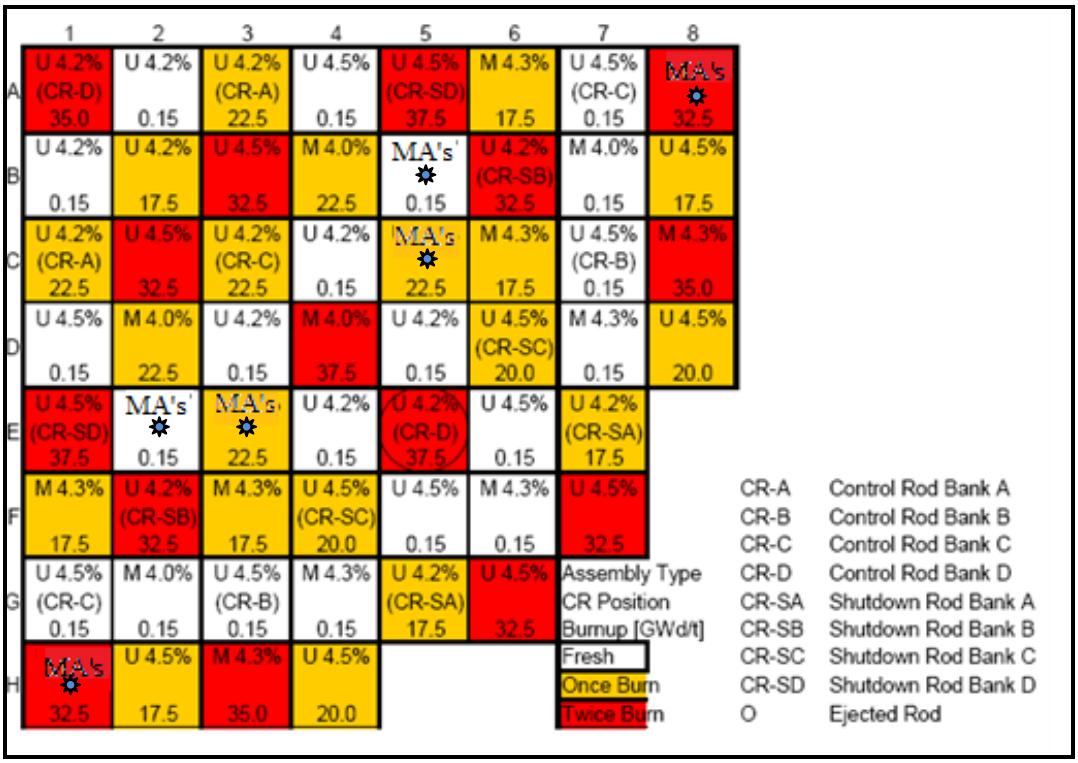

Figure 6:9 Ring of fire loading strategy with 4 fresh bundles with MAs

6.4.1 Critical boron search for a 3D core loaded with MAs

The PWR assemblies loaded with NpO_2 and the others with spiked pins of low, medium and high concentrations of AmO_2 were coupled each one to the core simulator by following the CL4 and 8RF refueling strategies. A 3D numerical simulation under HFP conditions was carried out following a depletion model to show that each core configuration should meet the relative power constraints. Table 6.7 shows the results for the different core configurations

Table 6:7 F_H and F_Q calculated at the BOC for the different core configurations

Core	F_Q	F_Q<1.7	F_H	F_H<2.6
Reference	**1.4**	**yes**	**2.02**	**yes**
CL4 Np	1.46	yes	2.04	yes
CL4 L	2.11	no	3.5	no
CL4 M	1.84	no	2.66	no
CL4 H	1.58	yes	2.38	yes
RF8 Np	1.41	yes	2.01	yes
RF8 L	1.7	no	2.41	yes
RF8 M	1.55	yes	2.21	yes
RF8 H	1.48	yes	2.1	yes

With the CL4 strategy, not unexpectedly, the results showed very high relative power peaks at the center of the core. Thus, the bundles with medium and high AmO_2 pins loaded in the bundles don't meet the constraint of radial pin-peaking (F_Q=1.70; *Ozer et al. 2006*). Only the core with NpO_2 and the core with NpO_2 and AmO_2 met this criteria with F_H = 1.46 and 1.58, respectively. The same criteria applies for the point-wise peaking constraint (F_Q=2.6). The cores with low and medium americium content don't meet this criterion. Figure 6.10 shows the radial relative power distribution at the BOC for the different core configurations, where it can be noted that the loading strategy with MA-spiked bundles near the center of the core is not very good, particularly for the cases in which Am-spiked bundles are included, being worst for the low-Am case.

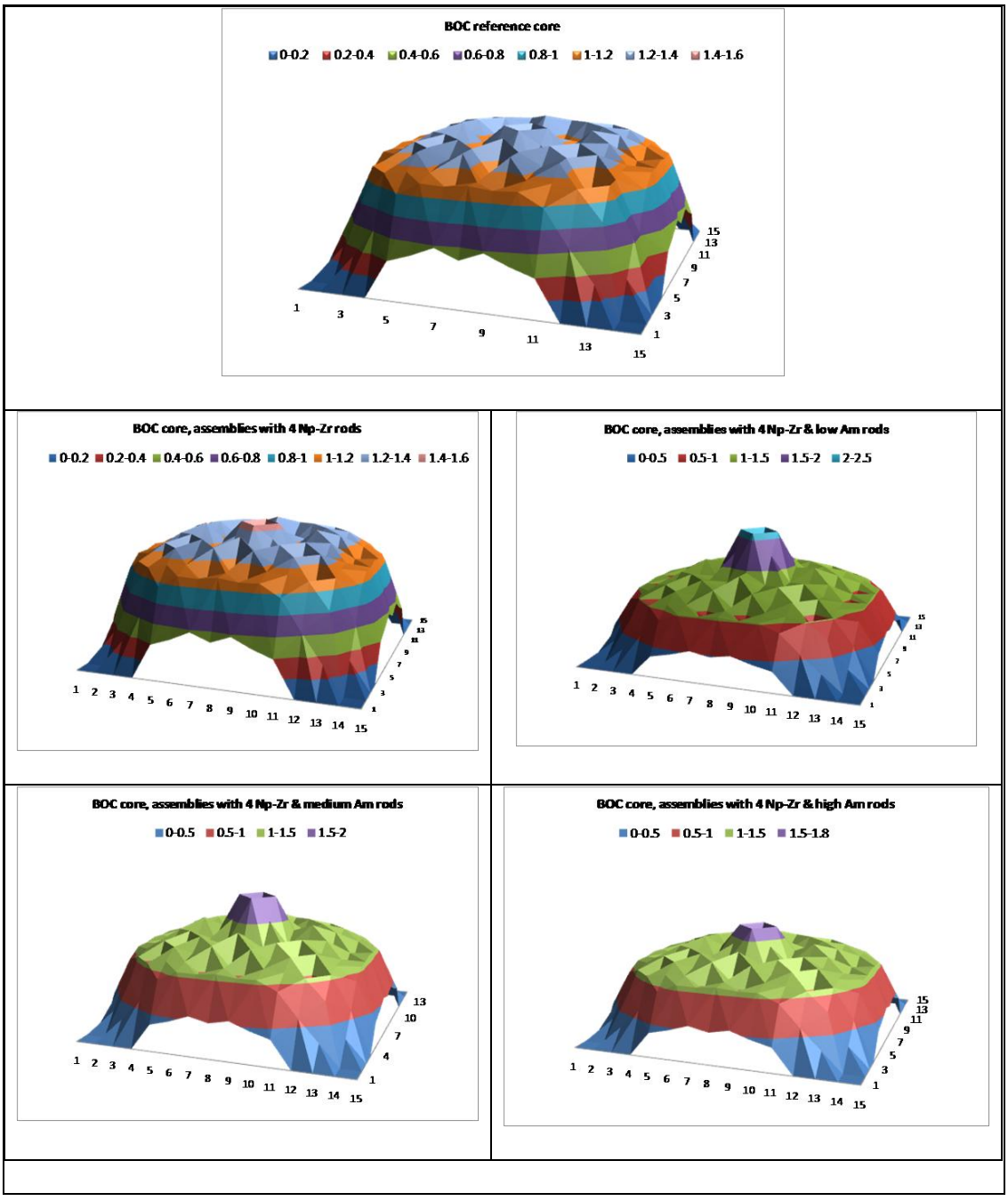

Figure 6:10 EOC 3D power distribution for 4 MA bundles centrally loaded

Figure 6.11 shows the radial relative power distribution at the BOC for the different core configurations for the second “ring of fire” strategy (RF8). In this case, the core with high Am content shows a better power relative distribution but the U-235 enrichment is at the upper constraint limit of 5 wt. % for the UO_2 pins. Overall, the most acceptable core loading strategy was RF8 because it has more bundles with MAs and a better power distribution. Three different core configurations were selected for further analysis: bundles loaded with NpO_2, with no, medium, or high AmO_2 content as described in figures 4.13, 4.18 and 4.19, respectively. Figure 6.12 shows the critical boron letdown curves as a function of effective full power days. In general, the different core configurations show a similar behavior and all met the criteria of soluble boron at the BOC and the excess reactivity is sufficient to sustain an 18-month fuel cycle with a capacity factor of 90%.

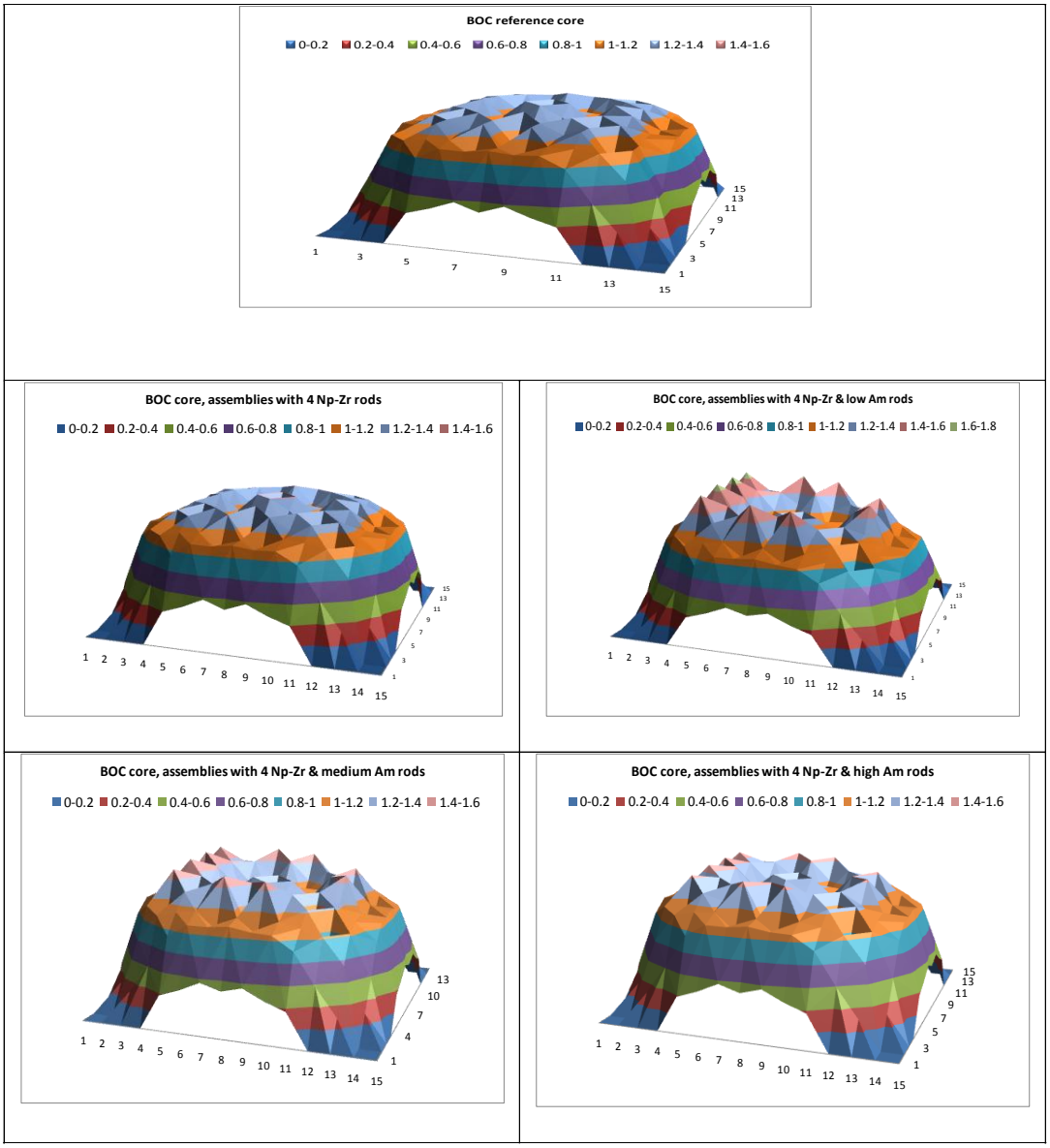

Figure 6:11 EOC 3D power distribution for 8 MA bundles with ring of fire load

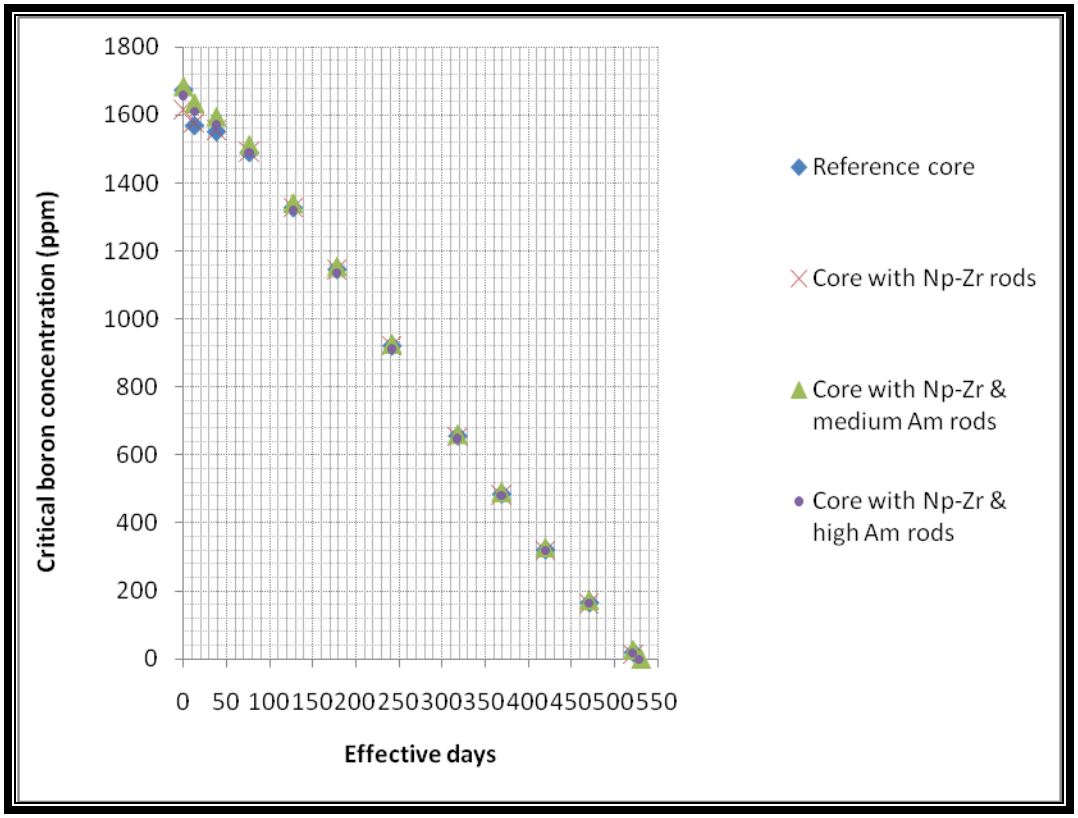

Figure 6:12 Critical boron concentration at HFP for spiked and reference cores

6.4.2 Moderator temperature coefficient (MTC)

The value of k-effective was calculated at seven moderator temperature points with an interval of 5K and a reference temperature of 580K. The 3D core simulation was performed at hot zero power conditions (HZP), corresponding to a core power of 10^{-4} % rated power and inlet pressure of 15.5 MPa with an inlet coolant temperature of 560K. The mean MTC value was calculated as function of boron concentration and the results in percent mil per degree Kelvin (pcm/K) are shown in figure 6.13 for the reference core and the three different core configurations with MAs loading. As expected, the values are negative and very similar between them, with the core with higher minor actinides concentration having the most negative MTC. The magnitude MTC is

higher for cores loaded with plutonium than for pure UO_2 cores, with typical values of around -34.4 pcm/K (*Jiwei Wang, 2008, Hussain A. et al. 2009*). The results shown in Table 6.8 are well within an expected and acceptable range.

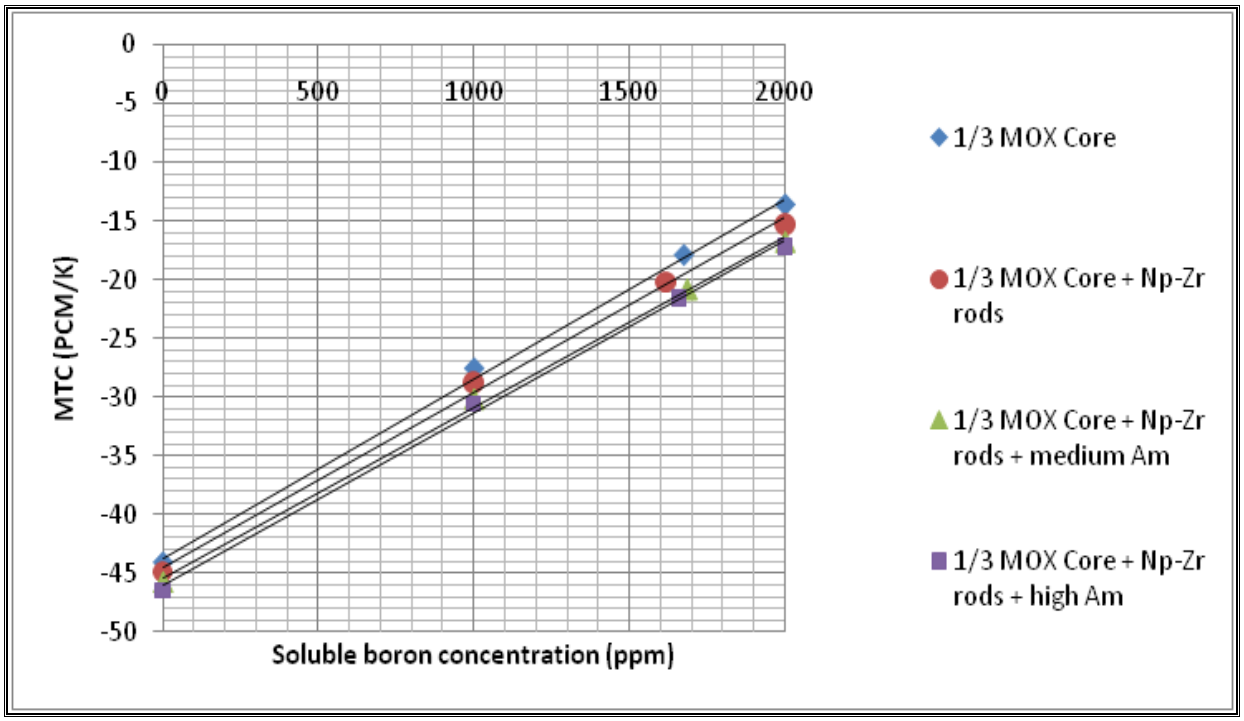

Figure 6:13 MTC versus soluble boron concentration for spiked and reference cores

6.4.3 Doppler temperature coefficient (C_D)

The Doppler temperature coefficient (C_D) was calculated using the k-effective values of the core simulation at HFP conditions with a Doppler temperature ~840 K and at HZP conditions with a Doppler temperature ~583 K with free Xenon and Samarium. The results are shown in Table 6.8 with all the simulations giving negative results. As expected, the least negative C_D is that for the pins with higher americium concentrations.

Table 6:8 MTC and C_D calculation for the PWR core

Core	MTC(pcm/K) @ critical boron	C_D (pcm/K)
1/3 MOX	-17.96	-4.12
1/3 MOX + Np-Zr rods	-20.22	-3.81
1/3 MOX Core + Np-Zr rods + medium Am	-20.78	-3.72
1/3 MOX Core + Np-Zr rods + high Am	-21.58	-3.52

6.5 Summary of PWR constraints and performance of core designs

Three different core configurations following a refueling strategy of 8 fresh, 8 once-burned and 4 twice-burned bundles loaded with Am and/or Np-237 met the core design and safety criteria with values comparable to the reference 1/3 MOX benchmarked core. Table 6.9 summarizes these results.

Table 6:9 Summary of the PWR constraints for spiked configurations

PWR constraints	1/3 MOX Core	1/3 MOX Core + Np-Zr rods	1/3 MOX Core + Np-Zr rods and medium Am	1/3 MOX Core + Np-Zr rods and high Am
Maximum wt. % U-235 enrichment = 5.00	4.50	4.50	4.95	5.00
Maximum rod relative power Fdelta H = 1.70	1.403	1.412	1.552	1.478
Maximum local relative power FO(z) = 2.60	2.024	2.015	2.211	2.100
Critical boron concentration (ppm)	1674.00	1615.00	1685.00	1650.00
Effective operation days	475	474	477	478
Full power days	528	527	530	531

7 Minor Actinide Loading Results

7.1 Assembly MA characterization

The assembly minor actinide characterization was carried out by simulating the lattices in TRITON and taking advantage of the time table feature which permits a variation in boron concentration as a function of time during the assembly's depletion simulation. The approach for boron was set to follow the boron concentration, as shown in figure 7.1, and the MAs amount were obtained by using the OPUS module. In general, the Pu-238 production is approximately the same for all the lattices analyzed, and the comparison of results can be observed in figure 7.2.

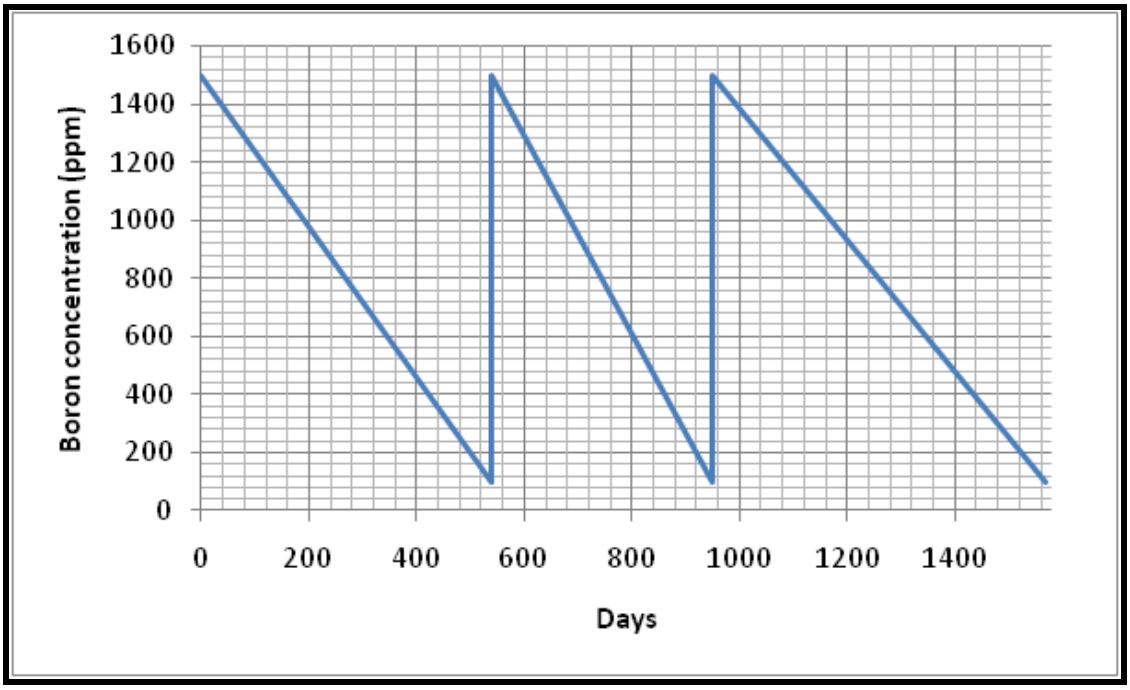

Figure 7:1 Reference boron letdown curve for assembly simulation

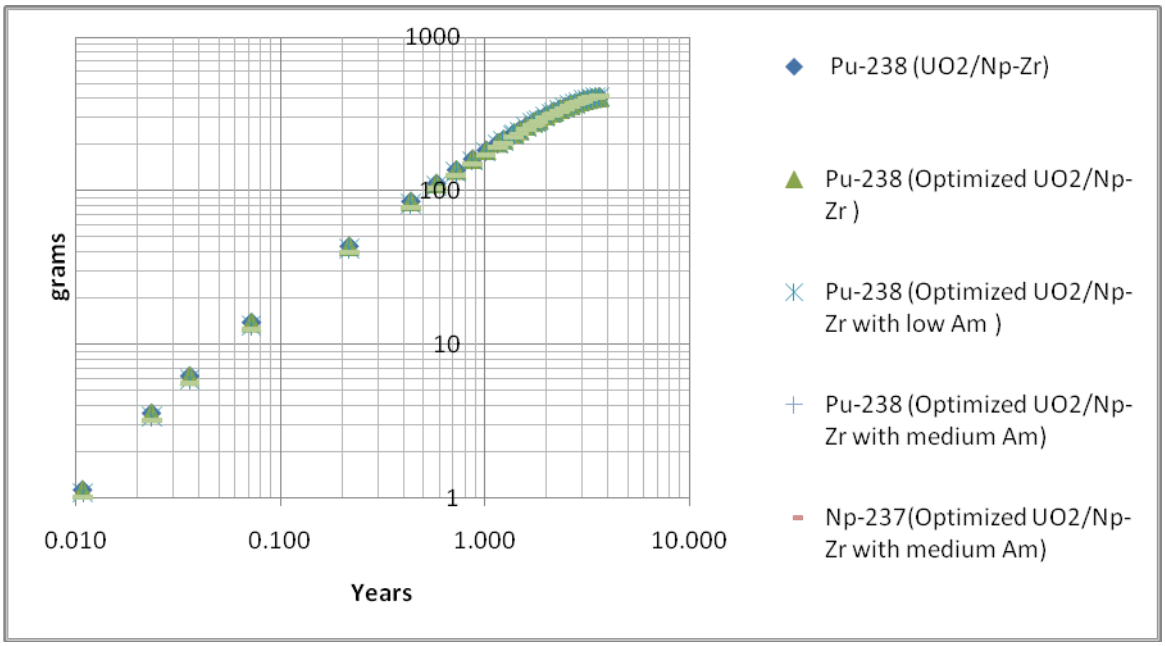

Figure 7:2 Pu-238 production in the various spiked configurations.

By analyzing the isotopic vector for the 4 pins with Np-Zr in the lattice, it can be observed in figure 7.3 that Pu-239 is the most abundant radioisotope after Zr and Np-237; following in less proportion are Pu-242, U-234, and Np-238 (figure 7.4). The remaining MAs are in small amounts and are presented in figure 7.5. The pins with Am-241 have similar behavior for all pins with Am in the three different lattice configurations of this analysis, and the incineration rate is shown in figure 7.6.

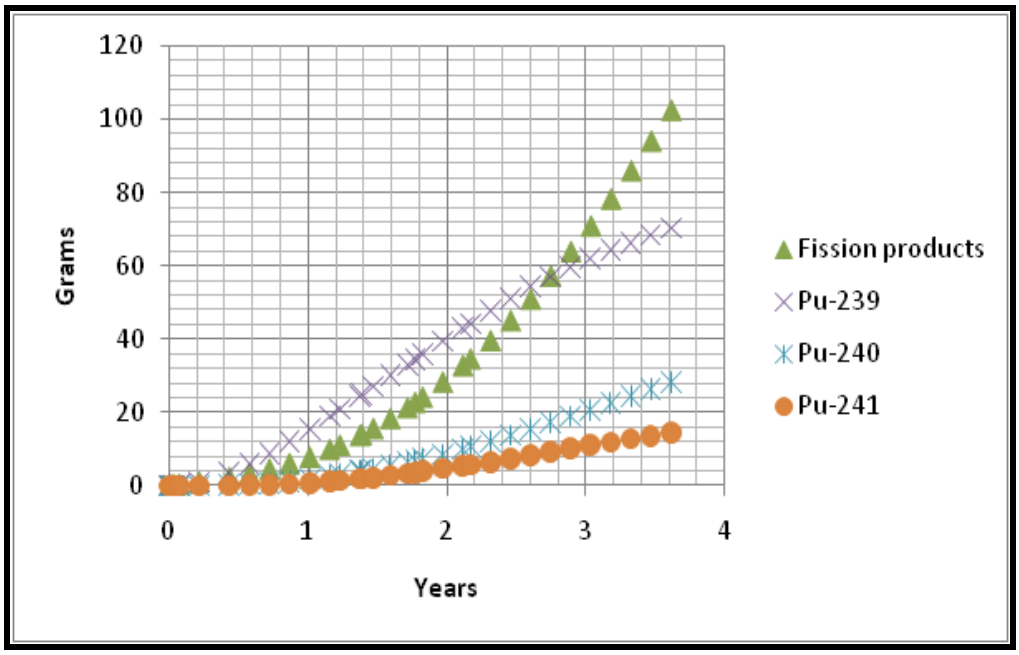

Figure 7:3 Dominant radioisotope accumulation in NpO_2 pins versus burnup

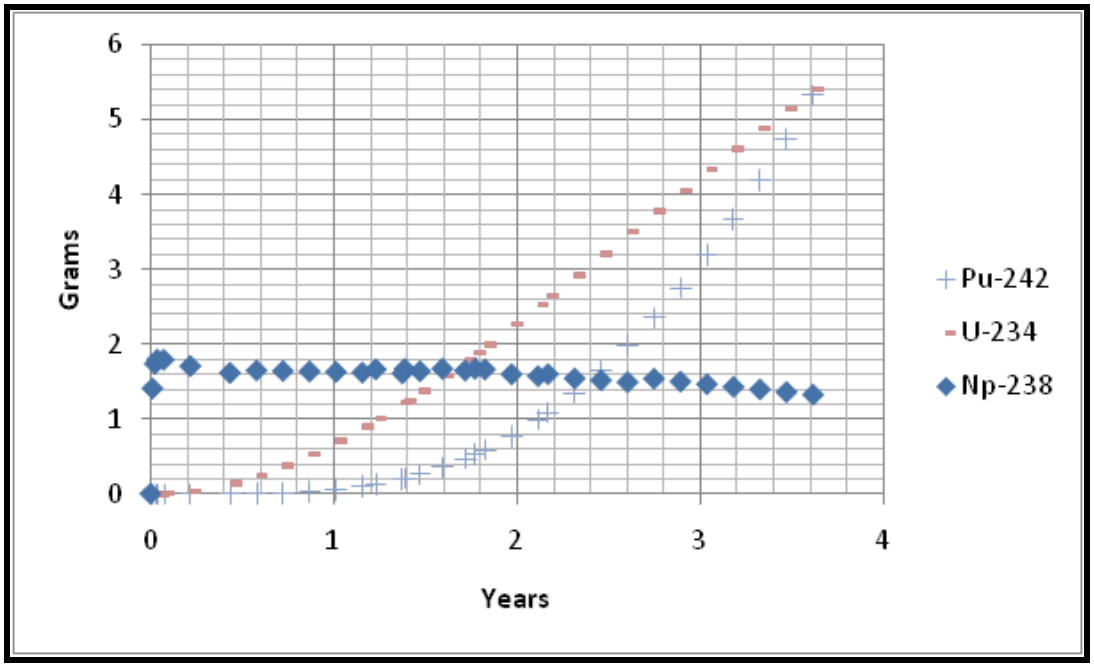

Figure 7:4 Small amount radioisotopes present in NpO_2 pins versus burnup

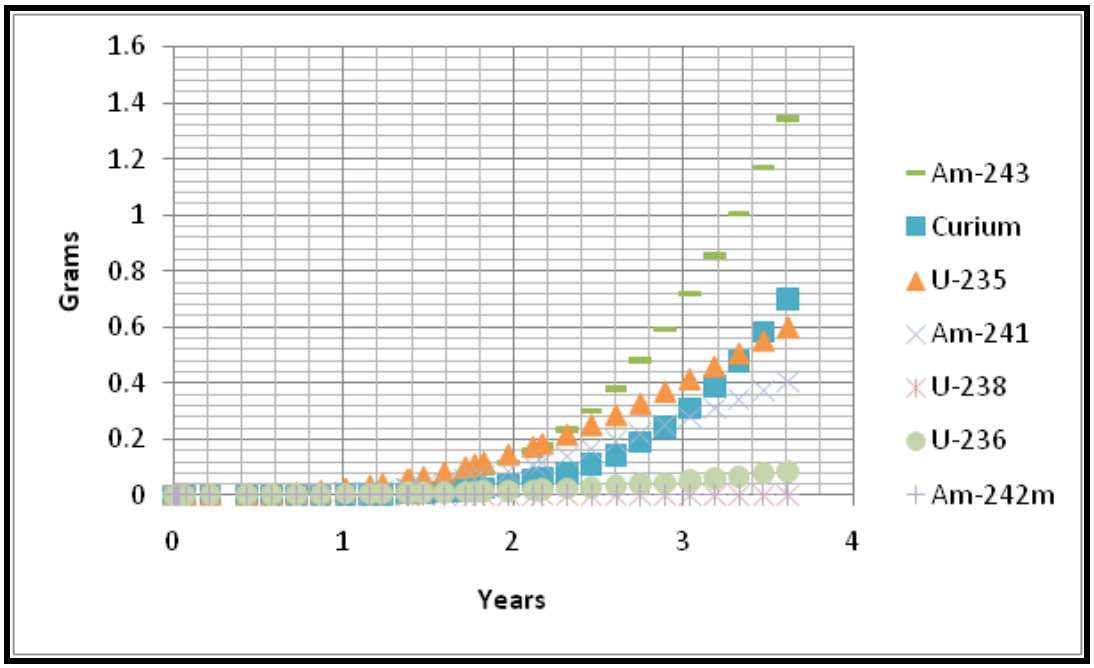

Figure 7:5 Near negligible radioisotopes in NpO_2 pins versus burnup

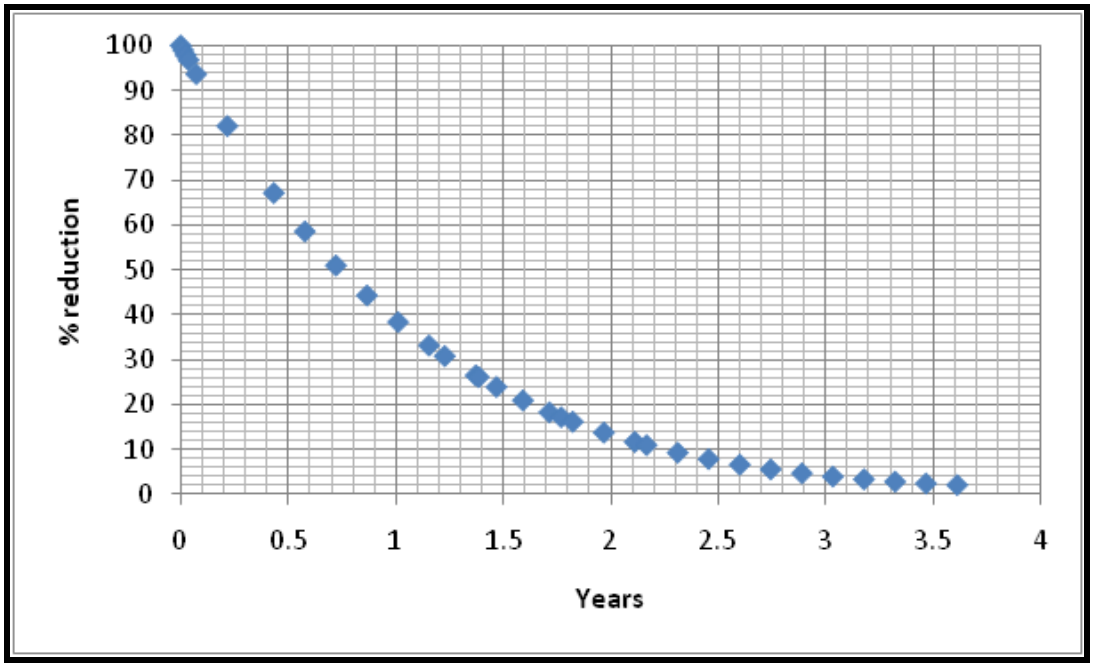

Figure 7:6 PWR-based Am-241 incineration in spiked pins

7.2 Material balance for the accepted core configurations loaded with MAs

Tables 7.1 to 7.3 show the material balance for the three different core configurations of assemblies loaded with Np-237, Np-237 with medium Am, and Np-237 with high Am content, respectively. Np-237, Pu-238 and Cm-242, whose daughter is Pu-238 with a $t_{1/2}$ of 162.8 days are quantified as a function of time. The overall efficiency is calculated for Np-237 transmutation to Pu-238, with a conversion rate of approximately 33% reached near EOC (50 GWd/MTHM), while the americium pins exhibit an incineration rate of 96% and 97 % for high and medium Am content, respectively. The initial loading of Np-237 is of approximately 1.237 kg/assembly.

Table 7:1 Material balance for the 3D core loaded with NpO_2

Bundle type	# bundles	Np-237 (kg)	Pu-238 (kg)	Np/Pu conversion rate (%)	Cm-242 (kg)
Fresh (1.41 years)	8	29.863	7.724	19.517	0.000
Once- burned (2.47 years)	8	22.890	11.339	28.652	0.001
Twice-burned (3.53 years)	4	8.286	6.508	32.890	0.002

Table 7:2 Material balance for the 3D core loaded with NpO_2 + medium AmO_2

		Pins with NpZrO2				Pins with medium Am (initial loading ~1.230 kg of Am-241/assembly)					
Bundle type	**# bundles**	**Np-237 (kg)**	**Pu-238 (kg)**	**Np/Pu conversion rate (%)**	**Cm-242 (kg)**	**Am-241 (kg)**	**% Am incineration**	**Pu-238 (kg)**	**Cm-242 (kg)**	**total Pu-238 (kg)**	**total Cm-242 (kg)**
Fresh (1.41 years)	8	30.222	7.532	**19.03**	0.000	11.921	**70.661**	11.583	7.070	**19.115**	**7.070**
Once-burned (2.47 years)	8	23.543	11.205	**28.31**	0.001	3.926	**90.338**	15.473	3.817	**26.677**	**3.818**
Twice-burned (3.53 years)	4	8.736	6.566	**33.18**	0.002	0.577	**97.159**	6.863	0.794	**13.429**	**0.796**

Table 7:3 : Material balance for the 3D core loaded with NpO_2+ high AmO_2

		Pins with NpZrO2				Pins with high Am (initial loading ~ 1.780 kg of Am-241)					
Bundle type	**# bundles**	**Np-237 (kg)**	**Pu-238 (kg)**	**Np/Pu conversion rate (%)**	**Cm-242 (kg)**	**Am-241 (kg)**	**% Am incineration**	**Pu-238 (kg)**	**Cm-242 (kg)**	**total Pu-238 (kg)**	**total Cm-242 (kg)**
Fresh (1.41 years)	8	30.662	7.266	**18.36**	0.000	19.040	**66.576**	15.280	9.608	**22.546**	**9.608**
Once-burned (2.47 years)	8	24.158	11.013	**27.83**	0.001	6.884	**87.916**	21.519	5.641	**32.532**	**5.642**
Twice-burned (3.53 years)	4	9.087	6.578	**33.24**	0.002	1.083	**96.198**	10.021	1.267	**16.598**	**1.269**

8 Summary and Conclusions

The results of this project are various. Firstly, a generalized software capability has been developed for the pin-wise loading optimization of light water reactor (LWR) fuel lattices with the enhanced flexibility of control variables that characterize heterogeneous or blended target pins loaded with non-standard compositions, such as minor actinides (MAs). Furthermore, this study has developed the software coupling to evaluate the performance of optimized lattices outside their reflective boundary conditions and within the realistic three-dimensional core-wide environment of a LWR. These evaluations have been done thanks to upgrades and modifications to help couple the TRITON code to the NESTLE 3D nodal simulator.

The practical applications employed to illustrate the benefits of the new methodologies developed included the evaluation of the recycling (destruction) of "undesirable" minor actinides from spent nuclear fuel such as Am-241 in a thermal reactor environment, as well as the timely study of planting Np-237 (blended NpO2 + UO2) targets in the guide tubes of typical commercial pressurized water reactor (PWR) bundles for the production of Pu-238, a highly "desirable" radioisotope used as a heat source in radioisotope thermoelectric generators (RTGs). Both of these applications creatively stretch the potential utility of existing commercial nuclear reactors into areas historically reserved to research or hypothetical next-generation facilities. To help confirm the viability of the core designs herein studied, key assessments of core-wide safety parameters were performed for the reference benchmark as well as for the cores loaded with minor actinides to ensure that these studies are as realistic as possible.

Aspects of the optimization, lattice-to-core coupling, and tools herein developed were tested in a concurrently developed Ph.D. project (Galloway, 2010) in which heterogeneous lattices

developed by this study were coupled to three-dimensional boiling water reactor (BWR) core simulations and showed incineration rates of Am-241 targets of around 90%, while this study focused primarily upon PWR demonstrations.

For PWR demonstrations a benchmarked reference equilibrium core was used as a test bed for MA-spiked lattices and was shown to satisfy standard PWR reactivity and thermal operational margins while exhibiting consistently high destruction rates of Am-241 and Np to Pu conversion rates of approximately 30% for the production of Pu-238.

The work in this thesis includes important advances to the lattice optimization code named FORMOSA-L and to the infrastructure that couples TRITON to NESTLE.

Of importance to note, the developed software and modifications have been carried out in an open and collaborative environment that has included contributions from NCSU, ORNL, and UT, with the aim to ultimately release a validated and first of its kind open-source end-to-end lattice to core LWR design capability to support research and education.

9 List of References

ABB Atom AB. “PHOENIX version 4 User’s Guide”, UR 85-149, Rev. 5 (1985).

Aldama, D.L., Trkov, A.“Analysis of the burnup credit benchmark with an updated WIMS-D library”. Annals of Nuclear Energy. 27(5), 169 174 (2000).

Alim Fatih, Ivanov Kostadin, Levine Samuel H. “New genetic algorithms (GA) to optimize PWR reactors: Part III: The Haling power depletion method for in-core fuel management analysis”. Annals of Nuclear Energy 35(1), 121-131. January (2008).

ANS. “Calculation and measurement of the moderator temperature coefficient of reactivity for water moderated power reactors”. American National Standard ANSI/ANS-19.11 (1007)

Bevington, P.R. “Data reduction and error analysis for the Physical sciences”, McGraw-Hill Book Company, New York (1969).

Bringer O., Letourneau A., Dupont E. “Impact of nuclear data uncertainties on the incineration of 237Np and 241Am targets”. Annals of Nuclear Energy, 35(8), 1535-1549 (2007).

DeHart M. “TRITON: A Two-Dimensional Transport and Depletion Module for Characterization of Spent Nuclear Fuel”, ORNL-TM-2005/39, Rev. 6. September (2008).

Duderstadt James J. and Hamilton Louis J. “Nuclear Reactor Analysis. John Wiley Sons, Inc. Pp. 480 (1976).

Electric Power Research Center, North Carolina State University, NESTLE , "Few-Group Neutron Diffusion Equation Solver Utilizing The Nodal Expansion Method for Eigenvalue, Adjoint, Fixed Source Steady-State and Transient Problems", Version 5.2.1 User's manual., Raleigh, NC (2003).

Erighin M., Yin C., Galloway J., Maldonado G.I., "Analysis of BWR Lattices to Recycle Americium". PHYSOR, Vancouver, BC, Canada, D063, 1-10/10, Sept. 10-14 (2006).

Finnemann, H., A. Galati. "NEACRP 3D LWR Core Transient Benchmark, NEACRP-L-335". October (1991).

Franceschini Fausto and Petrovic Bojan. "Core physics analysis of 100 % MOX core in IRIS". Annals of Nuclear Energy, 35, 1587-1597 (2008).

Francois J.L., Guzman R. BWR Fuel Design Using Minor Actinides as Burnable Absorber. ANS Annual Meeting, Boston, MA, USA. June 24-27 (2001).

Galloway J.D., "Boiling Water Reactor Core Simulation with Generalized Isotopic Inventory Tracking for Actinide Management," Ph.D. Thesis, University of Tennessee (2010).

Galloway J.D., Maldonado G.I., "Three-dimensional Core Simulations of BWR Bundles with Americium Target Pins," Trans. Am. Nucl. Soc., 97, 400-401 (2007)

Gropp William, Ewing Lusk, Skjellum Anthony. "Using MPI: portable parallel programming with the message-passing interface". William Gropp. Cambridge, Mass.: MIT Press, 2nd edition, 371 p. (1999).

Hernandez H., Maldonado G.I., “Application of Simulated Annealing Optimization to Recycle Minor Actinides in a BWR Lattice,” Trans. Am. Nucl. Soc., 96, 771-773 (2007).

Hernandez H., Maldonado G.I., “Added Features and MPI-based Parallelization of the FORMOSA-L Lattice Loading Optimization Code,” Proc. Advances in Nuclear Fuel Management IV, Hilton Head Island, SC (2009).

Hussain A., and Xinrong C. “Core Optimization Simulation for a Pressurized Water Reactor”. Information Technology Journal., 8(2), 250-255, (2009).

Jiwei Wang. “Developing a high thermal conductivity nuclear fuel with silicon carbide additives”. PhD dissertation, University of Florida, 132 pp. (2008).

Jong-Chae Kim, Myung-Hyun Kim, Un-Chul Lee. “Nuclear Design Feasibility of the Soluble Boron Free PWR Core”. Journal of the Korean Nuclear Society 30 (4), 342-342. August (1998).

Koo Y., Sohn D., Volkov B. “A comparative analysis of UO_2 and MOX fuel behavior under reactivity initiated accidents”. Annals of Nuclear Energy 24 (11), 859-870 (1997).

Kimhy S., and Galperin A. “Simple model of thermal-hydraulic feedback for the neutronic analysis of PWR cores”. Annals of Nuclear Energy 5(2), 95-100 (1988).

Kozlowski Tomasz and Downar Thomas J. Pressurized Water Reactor MOX/UO2 Core Transient Benchmark. Final Report. OECD,NEA No. 6084, December (2006).

Kropaczek, D.J., and Turinsky, P.J., “In-core nuclear fuel management optimization for PWRs utilizing Simulated Annealing,” *Nuclear Technology,* **95**:9 (1991).

Liu X.J., and Cheng X. “Coupled thermal-hydraulics and neutron-physics analysis of SCWR with mixed spectrum core”. Progress in Nuclear Energy 52, 640-647 (2010).

Maldonado G.I., T. Guo, and P. Engrand "Dual-Objective Simulated Annealing Applied to Within-Lattice Loading Optimization." *Trans. Am. Nucl. Soc*., **78**, 236-237 (1998a)

Maldonado G.I. and T. Guo "Penalty-Based Constraints Applied to Within-Bundle Loading Optimization." *Trans. Am. Nucl. Soc.*, **78**, 235-236 (1998b)

Maldonado G.I., and J. Zheng, "Approximation of Lattice-Physics Parameters via Linear Superposition.” *Trans. Am. Nucl. Soc.*, **79**, 317-318 (1998c)

Maldonado G.I., J. Zheng, and T. Guo, "Separability of Perturbations Within a Superposition-Based Lattice Physics Model.” *Trans. Am. Nucl. Soc.*, **80**, 234-238 (1999)

Maldonado G.I., Galloway J.D., Hernandez H. “Recycling Heterogeneous Americium Targets in a Boiling Water Reactor,” Accepted In Press, Annals of Nuclear Energy (2009 a).

Maldonado G.I., Galloway J.D., Hernandez H., Clarno K.T., Popov E., Jessee M.A. “Integration of the NESTLE Core Simulator with SCALE,” Trans. Am. Nucl. Soc., 100, 619-620 (2009b).

Metropolis, N.; Rosenbluth, A.W.; Rosenbluth, M.N.; Teller, A.H.; Teller, E. "Equations of State Calculations by Fast Computing Machines". *Journal of Chemical Physics* 21 (6): 1087–1092 (1953).

Mourtzanos K., Housiadas C., and Antonopoulos-Domis M. "Calculation of the moderator temperature coefficient of reactivity for water moderator reactors". Annals of Nuclear Energy 28, 1773-1782. (2001).

Ozer O., Edsinger K. "Optimum Cycle Length and Discharge Burnup for Nucler Fuel-A Comprehensive Sutdy for BWRs and PWRs". EPRI US DOE. Nuclear Energy Plant Optimization (2006).

Rankin D. Thomas, Kanne William R. Jr., Louthan McIntyre R. Jr., Bickford Dennis F. Congdon James W. " Production of Pu-238 Oxide Fuel for Space Exploration" (2000).

Roggenkamp Paul L., "Production of Pu-238 at the Savannah River Plant". E.I. du Pont de Nemours and Company. Savannah River Laboratory, Aiken, SC. 29808. ANS 1987 Winter Meeting, Los Angeles, CA. November 15-19 (1987).

Sanders C.E. and Wagner J.C., "Study of the Effect of Integral Burnable Absorbers for PWR Burnup Credit". U.S. Nuclear Regulatory Commission. Washington, DC. March (2002).

Santos, A.C.F. "Implantation and validation of the code WIMSTRACA (Portuguese translation)", IEN-60 (1994).

Sasahara Akihiro, Matsumura Tetsuo, Nicolaour Giorgos and Papaioannou Dimitri. "Neutron and Gamma Ray Source Evaluation of LWR High Burn-up UO_2 and MOX Spent Fuels". Nuclear Science and Technology, 41 (4) 448-456. (2004).

Shimzau Yoichiro. "A new method of estimation for MTC using Fourier-Transform". Journal of Nuclear Science and Technology 32(7), 622-628, July (1995).

Taiwo T.A., Kim T.K., Sillman J.A., Hill R.N., Salvatores M. and Finck P.J. "Assessment of a Heterogeneous PWR Assembly for Plutonium and Minor Actinide Recycle". Nuclear Technology,155(1),34-54 (2006).

Takeda, T., Yokoyama, K. Study on neutron spectrum for effective transmutation of minor actinides in thermal reactors. Annals of Nuclear. Energy 24(9), 705-719 (1997).

Trellue Holly R. "Safety and neutronics: A comparison of MOX vs UO_2 fuel". Progress in Nuclear Energy 48, 135-145 (2006).

Tochihara H., Komano Y., Ishida M., Narukawa K., Uneno M."Nuclear design for mixed moderator PWR". Progress in Nuclear Energy 32(374), 533-537 (1998).

Turinsky Paul J., and Parks Geoffrey T. "Advances in Nuclear Fuel Management for Light Water Reactors". Advances in Nuclear Science and Technology 26. New York (1999).

Yin C., J. Galloway, G. Ivan Maldonado, E. Fuentes, J. Casal, "University of Cincinnati and Westinghouse Collaboration: PHOENIX-4 Lattice Physics Studies," Trans. Am. Nucl. Soc., 94, 483-485 (2006).

Zheng Jie. “Application of Linear Superposition Methods to Within-lattice Loading Design Optimization of Light Water Reactor Nuclear Fuel Assemblies”, Ph.D. Thesis Iowa State University, 72 p (1999).

10 Vita

Hermilo Hernandez-Noyola obtained a BS degree in Electrical and Electronics and a MS of Energy Engineering from the Universidad Nacional Autónoma de México, in 2003 and 2005 respectively. He subsequently joined the University of Cincinnati, where he obtained an MS degree in nuclear engineering in 2006. In 2007, Hermilo joined the University of Tennessee department of nuclear engineering as a Ph.D. candidate. While at UT, he has been a research assistant under sponsorship from a DOE NERI project and also as an intern at Oak Ridge National Laboratory. Some of the awards he has received include the 2008 Graduate Student Award by the American Nuclear Society in the "Student Design Competition," for the project "Internal Instrumentation for a Spent Nuclear Dry Storage Cask (together with Nick Luciano)". Also, his BS thesis titled "Development of a Multi-cycle Analysis Methodology for the Physical and Economical Optimization of the Nuclear Fuel in the Mexican Nuclear Power Plant Laguna Verde (Spanish translation)", received the following three awards: "Best Thesis in Science and Nuclear Technology" by the Mexican Nuclear Society and Radiological Protection Mexican Society (2004), Second place in the "XII National Thesis Competition 2003-2004" by the Mexican Electrical Research Institute (IIE) and National Electricity Company (CFE), and Second place: "First Competition in Electro Mechanics Theses" by the Mechanical Electrical Association of Engineers (AIUME) and National Council of Science and Technology (CONACYT).